From Pattern Formation to Morphogenesis

Multicellular Coordination in *Dictyostelium discoideum*

Aan dit proefschrift is een CD-ROM toegevoegd. Op deze CD-ROM staat niet alleen het proefschrift zelf, maar ook de filmpjes die van de simulaties gemaakt zijn (in MPEG formaat). De informatie op de CD-ROM kan worden bekeken met met een Internet-browser naar keuze. Bovendien bevat de CD-ROM het proefschrift als PDF-bestand. Dit bestand kan bekeken en geprint worden met Acrobat Reader.

A CD-ROM is enclosed in this thesis. The CD-ROM contains the thesis itself, combined with MPEG movies of the simulations. The information can be viewed by using a default web-browser. The CD-ROM also contains a PDF-file of the thesis, which can be viewed with Acrobat Reader.

OMSLAG Leonoor Ruigrok
DRUK Optima Grafische Communicatie, Rotterdam
ISBN 90-393-2520-0

From Pattern Formation to Morphogenesis
Multicellular Coordination in *Dictyostelium discoideum*

Van Patroonvorming naar Morfogenese
Meercellige Coördinatie in *Dictyostelium discoideum*
(met een samenvatting in het Nederlands)

Proefschrift

ter verkrijging van de graad van doctor aan de Universiteit Utrecht
op gezag van de Rector Magnificus, Prof. Dr. H. O. Voorma,
ingevolge het besluit van het College voor Promoties
in het openbaar te verdedigen op
maandag 16 oktober 2000 des middags te 14.30 uur

door

Athanasius Franciscus Maria Marée

geboren op 7 mei 1971
te Renkum.

Promotor:
Prof. Dr. P. Hogeweg
Faculteit Biologie
Universiteit Utrecht.

Co-Promotor:
Dr. A. V. Panfilov
Faculteit Biologie
Universiteit Utrecht.

The studies described in this thesis were performed at the department of Theoretical Biology and Bioinformatics at Utrecht University. The investigations were financially supported by the Priority Program Nonlinear Systems of the Netherlands Organization for Scientific Research (NWO).

Ter nagedachtenis aan mijn vader

Contents

1 General Introduction **1**
1.1 From Pattern Formation to Morphogenesis 2
1.2 Excitable Media and Oscillatory Systems 4
1.3 A Two-Scale CA with Differential Adhesion 6
1.4 The Cellular Slime Mould 8
1.4.1 The life cycle 8
1.4.2 Key elements of morphogenesis 10
1.4.3 Model history 13
1.5 This Thesis 17

I Pattern Formation in Homogeneous Excitable Media **21**

2 Spiral Breakup in Excitable Tissue due to Lateral Instability **23**
2.1 Introduction 24
2.2 The Model 25
2.3 Results 25
2.4 Discussion 30

II Morphogenesis of *Dictyostelium discoideum* **33**

3 Migration and Thermotaxis of *Dictyostelium discoideum* Slugs, a Model Study **35**
3.1 Introduction 36
3.2 The Model 37
3.2.1 Description of the amoebae 37
3.2.2 cAMP dynamics 38
3.2.3 Chemotaxis 40
3.3 Slug Migration 40
3.3.1 Stability of the slug shape 40
3.3.2 Motion velocity 42
3.3.3 Cell sorting 43
3.4 Thermotaxis 44
3.4.1 Mechanism of thermosensitivity 44
3.4.2 Thermosensitivity and the influence of stochastic noise . . . 46
3.4.3 A partially thermosensitive slug 49
3.5 Discussion 50
3.5.1 Slug motion and cell sorting 50
3.5.2 Thermotaxis 51

4 Phototaxis during the Slug Stage of *Dictyostelium discoideum*: a Model Study **55**
4.1 Introduction 56
4.2 The Model 57
4.3 Phototaxis 60
4.4 Discussion 67
4.5 Conclusions and Predictions 69

Colour Plates **71**

5 How Slime Moulds Self-Organise into a Fruiting Body: the "Reverse Fountain" Explained **79**
5.1 Introduction 80
5.2 The Model 80
5.3 Results 81
5.4 Discussion 84
Appendix 85
5.5 Methods 85

6 Modelling *Dictyostelium discoideum* Morphogenesis: the Culmination **87**
6.1 Introduction 88
6.1.1 Stalk formation 88
6.1.2 Cell differentiation 89
6.1.3 Cell movements 89
6.2 The Model 90
6.2.1 Adhesion 91
6.2.2 Cell differentiation 92
6.2.3 cAMP signalling 93
6.2.4 Initial condition 94
6.3 The Culmination of *Dictyostelium discoideum* 94
6.3.1 Tube formation 96
6.3.2 Stalk elongation 96
6.3.3 The role of cAMP and pathfinder cells in stalk elongation . . 98
6.3.4 Correction of orientation 99
6.3.5 Anchoring 100
6.3.6 Final configuration 100
6.3.7 Cell adhesion 102
6.4 Discussion 103
6.4.1 Stalk formation 103
6.4.2 cAMP signalling 104
6.4.3 Model considerations 105
6.4.4 Side-effects 107
6.4.5 Conclusions 108

7 Summarising Discussion **109**
7.1 A Short Review 109
7.2 From Local Interactions towards Global Coordination 111
7.3 Model Complexity 112
7.3.1 From simple to simpler, to a little more complex 113
7.3.2 Interaction of generic modules
and interesting new observables 114
7.3.3 Gene regulation and morphogenesis 115
7.3.4 Evolving complexity 117
7.4 Future Directions 118
7.5 Conclusion 119

Bibliography **121**

Samenvatting **131**

Curriculum Vitæ **137**

List of Publications **139**

Dankwoord **141**

1
General Introduction

The emergence of multicellular organisms is regarded as one of the major transitions in evolution (Maynard Smith & Szathmáry, 1995). During this evolutionary transition some individual cells 'gave up' part of their autonomy to become differentiated functional units of multicellular assemblages. In so doing, the organisms had to develop ways of organising themselves and communicating with each other over long distances. This thesis focuses on the process of multicellular coordination.

The three main types of multicellularity evolved independently from different kinds of unicellular Protista. An explosion of metazoan morphotypes took place some 540 million years ago, during the early Cambrian. This was followed about 40 million years later by the appearance of large numbers of multicellular plants and fungi. Multicellular organisms, however, are even older. Ediacaran faunas date back at least 565 million years, and there are even indications of pre-Ediacaran multicelled creatures (Conway Morris, 2000). A transition from unicellularity to a simple type of multicellularity is still occurring today and can be studied in the cellular slime mould *Dictyostelium discoideum*, which is the 'model' organism investigated in this thesis.

Dictyostelium is a unicellular eukaryote, and therefore belongs to the kingdom of Protista. Nevertheless, once in many generations this unicellular amoeboid suddenly turns into a multicellular creature, a transition which is triggered by food shortage. After the transition, the organism is able to sense new cues from the external world, such as light, temperature- and pH-gradients and air-currents, and the behaviour of the whole organism adjusts to these signals in a coordinated way. Many other species of unicellular organisms can also convert to cooperative behaviour. This usually occurs when they are subjected to harsh conditions, and is often attended by complex pattern formation. Collective behaviour can for example be observed in the bacteria *Escherichia coli* (Budrene & Berg, 1991, 1995), *Bacillus subtilis* (Kawasaki *et al.*, 1997) and *Proteus mirabilis* (Matsuyama *et al.*, 2000), and the yeast *Saccharomyces cerevisiae* (Palková *et al.*, 1997). Nevertheless, the cellular slime moulds are considered to be the most primitive organisms which have all the basic elements of multicellular development (Maeda, 2000).

Because in *Dictyostelium* the transition from unicellularity to multicellularity can easily be triggered in experimental settings and is not accompanied by cell divisions, a detailed study of this organism gives us the opportunity to find out how multicellularity can develop and how a 'fresh' multicellular 'organism' can sense the environment and form a collective and appropriate response. This opportunity has been embraced by scientists with research interests in fields such as gene regulation, signal transduction, pattern formation and morphogenesis (Maeda *et al.*, 1997). As a consequence, *Dictyostelium* has been the subject of many detailed studies, and large amounts of information have been and still are being produced. However, to understand how these processes work, it is important to combine all this information. This can be done using a method of modular modelling. In the second part of this thesis we present a comprehensive model which describes the multicellular coordination and development of *Dictyostelium*.

A great challenge for those engaged in biological modelling is to find simplifications without taking interesting biological details for granted. Both experimental observations and theoretical evolutionary studies have shown that in general organisms do not evolve minimal solutions. This means that it is important to retain enough biology in the model. In this thesis our strategy is to develop the model in terms of a low level coupling between a few modules. The two main modules in the model are a description of cell signalling in the form of an excitable medium, and a description of cell rearrangement by means of differential adhesion. The two modules have been well established experimentally in isolation and have also been well studied theoretically. Our modelling approach allows us to tightly integrate physical aspects of morphogenesis with cell signalling and cell differentiation; this integration seems to be essential if the model is to reproduce the intricate patterns, forms and dynamics that we observe in nature.

The model can describe how *Dictyostelium discoideum* morphogenesis unfolds: previously, Savill & Hogeweg (1997) described how single cells develop into a crawling slug; in this thesis we describe how the slug then orientates towards the light and/or responds to very shallow and very noisy temperature gradients, and how it finally transforms itself into a fruiting body, i.e. a globule of spores on a slender stalk. By means of our model we can explain the mechanisms which lead to the normal morphogenesis as well as to aberrant phenotypes. And although in the course of this thesis we increase the complexity of the model, extensions never invalidate previous results; instead we show that self-organisation continues and drives the global dynamics.

In this Introduction we will first explain the title ‘from pattern formation to morphogenesis’; next we will present a detailed background for the two main modules we use; we continue with an extensive survey of *Dictyostelium*; and finally we give an overview of the whole thesis.

1.1 From Pattern Formation to Morphogenesis

The formation of intricate patterns ‘from almost nothing’ is a fascinating area of scientific studies. It is known that several generic mechanisms can generate complex patterns via simple rules. The prime examples of these are excitable media (see, e.g. Murray, 1993) and Turing patterns (Turing, 1952). The striking resemblance between patterns produced by such mechanisms and patterns observed in nature, combined with the fact that the underlying dynamics could be very general, has tempted theoreticians to explain biological development in terms of such patterns.

Turing (1952) was the first to study the problem of pattern formation relating to development. He showed how periodic stationary patterns can emerge spontaneously in a homogeneous system, and pointed out that this could be important for the breaking of symmetry during morphogenesis (see also Chaplain *et al.*, 1999). Turing patterns are used to explain many patterns, including the coats of animals, e.g. zebra stripes. Initial variations in the size and shape of the medium, as well as in the saturation-levels of the reaction-part of the model, literally lead to a whole 'zoo' of patterns (Murray, 1993).

Note, however, that explanations for early segmentation in the fruitfly *Drosophila* based on this minimal model (Kauffman *et al.*, 1978; Kauffman, 1981) have been falsified: the formation of each segment is regulated differently (Akam, 1987; Nusslein-Volhard, 1991). Thus, it is important to look at other features besides spots and stripes. In fact, in no biological system have the morphogens involved in this type of pattern formation been identified[1].

The other prime pattern formation mechanism is excitable media, which is the main pattern-generating mechanism studied in this thesis. Fortunately, the situation here is entirely different: for many systems the underlying physiology or chemistry of excitability has been well established. This is also the case for *Dictyostelium* cAMP signalling. In section 1.4 we describe the mechanism of excitability, and we elucidate some examples of models which represent *Dictyostelium* as an excitable medium.

The 'classical' view of development by pattern formation is based on the assumption that a (more or less) static prepattern is established and 'read out' by the cells, which respond to it by differentiating, migrating or changing their shape. That is, once the morphogen prepattern is defined, morphogenesis is a slave process (Murray & Swanson, 1999). Not only Turing patterns, but also gradient models for 'positional information' (Wolpert, 1969), are classic examples of such chemical prepattern models. In this thesis we do not decouple pattern formation and morphogenesis. Instead, we use the word morphogenesis in a wide sense involving all aspects of development. To understand how the morphogenesis of *Dictyostelium* is coordinated, we need to know about: (i) the formation and dynamic changes not only of patterns, but also of shapes; (ii) morphogenetic movements on different scales; and (iii) the interplay of the organism with the environment.

We consider morphogenesis as an inherently multilevel process, involving processes on different time and space scales. Here we focus on the entanglement between these levels: we consider not only how microlevel 'rules' give rise (via a self-structuring process) to macrolevel behaviour (as in pattern formation models), but also how the macrolevel behaviour determines the microlevel behaviour. This reciprocal influence between the levels can be considered as an essential characteristic of living systems (Hogeweg, 2000b). Thus, in our model morpho-

[1]Surprisingly, it was almost 40 years until Turing patterns were irrefutably established experimentally; the medium was a chemical system, called the chlorite-iodide-malonic acid starch (CIMA) reaction (Castets *et al.*, 1990).

genesis is no longer a slave process, but unfolds by the interactions between pattern formation, the collective behaviour of the cells, and its feedback to the pattern formation process. We observe new features on many different scales. As a result, our model leads to explanations of morphogenesis in terms of mechanisms not directly included in the model formulation, but which emerge from the model at an intermediate level (e.g. the pressure waves and peristalsis, which drive the stalk downwards during culmination, see chapters 5 and 6).

In conclusion, we will develop a comprehensive model which is not restricted to explaining pattern formation but incorporates many aspects of *Dictyostelium* morphogenesis. This means that we move one step beyond 'equating' a Turing pattern with a zebra. When asked if his theory of morphogenesis could account for the stripes on a zebra, Turing allegedly responded: "The stripes are easy, it's the horse part that troubles me!".

1.2 Excitable Media and Oscillatory Systems

Pattern formations in excitable media are important examples of self-organisation phenomena in spatially distributed biological and chemical systems. Excitable media have been studied for a long time, in for example heart tissue (Allessie *et al.*, 1973), the Belousov-Zhabotinsky (BZ) reaction (Winfree, 1972) and cellular slime moulds (Durston, 1973).

An excitable medium is a medium which has two main properties, namely the ability to conduct pulses of excitation, and the ability to recover its properties after some period of time, called the refractory period. Excitable media can be regarded as a generic concept for pattern formation: it consists of a whole class of systems, which have to possess these few basic properties in order to produce the same common generic behaviour. It is a form of abstraction at the process level, i.e. it defines a generic class of interactions. Obviously, such interactions can be realized in many different ways. For example, Martiel & Goldbeter (1987) have worked out in some detail the receptor kinetics in *Dictyostelium*, which lead it to behave as an excitable medium (see section 1.4.3).

There are two main classes of excitable media, namely relaying excitable media and oscillatory excitable media. Examples of systems that behave like relaying excitable media include waves of electrical stimulation propagating through cardiac tissue (Panfilov & Holden, 1997) and reverberating cortical depression waves in the brain cortex (Shibata & Bures, 1972); many typical examples of oscillatory excitable media can be found in more ecological contexts, e.g. in the spruce budworm dynamics (Ludwig *et al.*, 1979), hypercycles during pre-biotic evolution (Boerlijst & Hogeweg, 1991), and predator-prey waves (Savill & Hogeweg, 1999). Some examples in which both types of dynamics can be observed are the two- and three-dimensional waves in the BZ-reaction (Winfree & Strogatz, 1984; Jahnke *et al.*, 1988), spiral calcium waves propagating on the surface of an amphibian's egg (Lechleiter *et al.*, 1991; Vaessen, 1999) and the cAMP waves which organise *Dictyostelium* development (Tyson & Murray, 1989; Siegert & Weijer, 1992).

In a relaying excitable medium there is a local rest state, which can be excited by pushing the state away from equilibrium, over a certain threshold. When this occurs, the state makes a wide detour through state space before returning to the rest state. Because of the influx of an activator into the nearby medium (usually by diffusion), a wave of excitation can form: when the medium is in the so-called excited state, it is able to push the nearby region over the threshold, which creates a propagating pattern of medium that is triggered into the excited state. Because the excited state is followed by a recovering state, during which the medium cannot be excited, such waves of excitation can only propagate forwards. In two-dimensional (2D) excitable media patterns are often organised in the form of spiral waves. Usually, spiral waves originate either because of inherent heterogeneity in the excitable tissue, or because of some special initial conditions. Sometimes, however, spiral waves spontaneously break up (and/or new ones appear) in a homogeneous medium, without any special initial conditions, a topic which has received a great deal of attention during the last few years.

The other class of excitable media consists of oscillatory excitable media. In these systems, there is no stable rest state; instead the local dynamics are in a limit cycle regime, called relaxation oscillation. Both classes, however, share many features, such as wave propagation, spiral waves, some types of breakup, and curvature-effects. Nevertheless, there are also differences. For example, in oscillatory systems target waves can form. These are waves that originate from a point source and spread out in an ever larger circle. Both classes of systems are closely related; in many models the behaviour can switch from one regime to the other as a result of only small parameter changes. In our module of *Dictyostelium* cAMP signalling we incorporate both types of systems in the one model, simply by making a small parameter change.

Many models converge to excitable media, and therefore one expects to find excitable media in many different biological settings. Note, however, that whereas many different models can behave as excitable media, the size of parameter regions, for which different types of behaviour can be found, varies between models. Hence, the behaviour that we observe in only a very small parameter region of one model can be the prime behaviour in another model. Hence, it can be a good heuristic method to zoom in on interesting parameter regions of models that are easier to study.

A well-known mathematical caricature for excitable media is the partial differential equation (PDE) model that is based on the FitzHugh-Nagumo (FHN) system (FitzHugh, 1960, 1961; Nagumo *et al.*, 1962). The FHN equations were originally developed as a simplification of the classical model for action potentials (Hodgkin & Huxley, 1952), but they have been widely used elsewhere. The model has two variables; one variable describes the excitation, and the other is the recovery variable. The equations exist in many variations; in this thesis we use the piecewise linear 'Pushchino' version (Panfilov & Pertsov, 1984). Figure 3.1 on page 39 shows the phase plane and dynamics of this model for both the excitable and the oscillatory regime. Because this model is a qualitative generalisation of excitable media, it can be used to describe waves in the BZ-reaction (see chapter 2), in the heart muscle, (Panfilov & Hogeweg, 1993), as well as in *Dictyostelium* (Savill & Hogeweg, 1997).

In this thesis we use excitable media in two different ways. In part I of this thesis we study a homogeneous excitable medium. We explore the parameter space of the above model in our search for spiral breakup and other interesting behaviour. We find several new types of patterns, hitherto unknown. The study illustrates that excitable media is a rich mechanism for pattern formation.

In part II of this thesis we apply the concept of excitable media to the process of *Dictyostelium discoideum* morphogenesis. Because we couple the excitable and motile properties of *Dictyostelium* cells, the pattern formation is now able to change both the shape and the excitability of the medium itself.

1.3 A Two-Scale CA with Differential Adhesion

In order to describe the individual amoebae in our model we use the Glazier & Graner-model formalism, which is a two-scale cellular automata (CA) with differential adhesion. Steinberg (1963) first proposed the so-called differential adhesion hypothesis, asserting that differential intercellular adhesion is one of the most important factors in cell sorting. Differential adhesion, however, is not as clear a generic concept for pattern formation as is the concept of excitable media. This is mainly due to the fact that it is only recently that models have been developed that are really able to describe the basic elements of cell sorting arising from differential adhesion.

Many of the attempts to model cell sorting using standard CA models succeeded only when special tricks were used (for a thorough overview of such early model work on cell sorting, see Mostow, 1975). The main problem was that no ways could be found to overcome the local optima in the CA, which consist of many small clumps of cells, and arrive at global cell sorting.

The problem was finally solved by Graner & Glazier (1992); Glazier & Graner (1993). They presented a two-scale stochastic CA which is indeed able to generate complete cell sorting. Their model is called the extended large-Q Potts-model, or simply the Glazier & Graner-model. The precursor of the model dates from 1925, when Ising proposed a simple lattice model in which individual elements modify their behaviour so as to conform to the behaviour of other individuals in their vicinity. The Ising-model was proposed to explain certain empirically observed facts about ferromagnetic materials. In the Ising-model, each lattice site can be in one of two different states. Potts (1952) extended the Ising-model by assuming that each lattice site can be in one of q different states (where $q > 2$; for $q = 2$ both models are equivalent). The Potts-model was originally developed to simulate order-disorder transformations and surface-energy-driven diffusion in non-biological patterns. Initially, the focus was mainly on the statistical dynamics of the $q = 3$ and $q = 4$ Potts-model. It is only recently that researchers have begun to look at the spatial dynamics of the large-Q Potts-model, which has a much higher number of states, and in which a group of the same state refers to an individual soap bubble or 'cell' (Glazier *et al.*, 1990).

To be more concrete, the large-Q Potts-model is embedded in a 2D lattice, but can easily be extended to three dimensions (3D). It describes a collection of Q

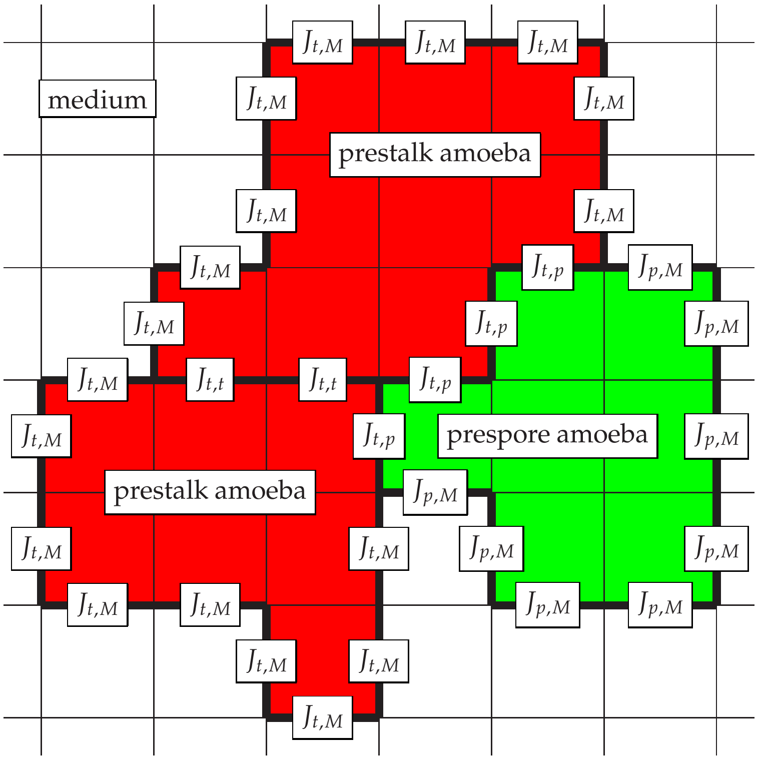

Figure 1.1. Sketch of the Glazier & Graner-model formalism. Indicated are the medium and three different cells ($\sigma \in \{1, 2, 3, 4\}$), which belong to two different cell types ($\tau \in$ {medium, prespore, prestalk}). All the surface contact energies are also drawn (J_{τ_1,τ_2}). See also the colour plate on page 71.

'cells' in that each cell is given a unique identification number, $\sigma = 1, 2, \ldots, Q$. A cell σ consists of all sites in the lattice that have value σ. Bonds between different cells are given an energy of 1 and bonds within one cell an energy of 0, and then the total free energy is calculated. At each step a lattice site is chosen at random and the chance that the state of one of its neighbours will be copied into it is either 1 if $\Delta H \leq 0$ or $e^{\left(-\frac{\Delta H}{kT}\right)}$ if $\Delta H > 0$, where ΔH is the change in energy *if* the copying were to occur. The pattern which evolves minimises surface area. Hence, large compact cells are formed, while many others completely disappear. The dynamics and statistics can, for example, describe accurately surface-energy-driven grain growth, e.g. in soap froth (from Graner & Glazier, 1992).

Nevertheless, significant applications of this model-formalism in biology only became possible after Glazier & Graner had made two important extensions to the Potts-model. These extensions were made to describe cell sorting resulting from differential adhesion in biological systems. First, Glazier & Graner introduced a second scale in the model. They understood that biological cells have a more or less fixed size, and they added to the free energy function an extra term, to describe the area constraint for each individual cell (except for the surrounding medium, of course). Secondly, they introduced different contact energies between cells of different types by introducing a second label, τ, which indicates to which cell type each cell belongs, and by defining J_{τ_1,τ_2}, the surface energy between two lattice sites occupied by cell types τ_1 and τ_2.

Figure 1.1 shows the model in a schematic way. Three different cells from two different cell types are shown, with their boundaries and contact energies. When the above extensions are taken into account, the Hamiltonian energy function becomes:

$$H_\sigma = \sum_{\text{all } \sigma,\sigma' \text{ neighbours}} \frac{J_{\tau_\sigma,\tau_{\sigma'}}}{2} + \sum_{\text{all } \sigma, \text{medium neighbours}} J_{\tau_\sigma,\tau_{\text{medium}}} + \lambda(v_\sigma - V)^2, \quad (1.1)$$

where v_σ is the volume of the cell, V the target volume, and λ the inelasticity. The term $\lambda(v_\sigma - V)^2$ ensures that the volume of a cell remains close to V. These dynamics allow cells to move slowly by gradually adjusting their boundary positions, instead of jumping abruptly. As a result, the model-formalism is able to create neutral paths around the local optima. By using these neutral paths, i.e. by a slow diffusion of cell clumps in their entirety, complete cell sorting can be achieved. The time-scales of cell sorting, however, still increase exponentially when the domain sizes grow.

In part II of this thesis we use the Glazier & Graner-model to describe the individual cells of *Dictyostelium*. However, we again extend the model-formalism by adding dissipation costs to cell deformations and by including chemotaxis in the energy function. In last two chapters we make two more extensions, namely variable target volumes and cell-type transitions.

1.4 The Cellular Slime Mould

As stated earlier, we use the cellular slime mould *Dictyostelium discoideum* as a paradigm system for wide-ranging coordination during the multicellular stage of an organism. Much research has been done on *Dictyostelium*. In this section we describe both the experimental and theoretical background.

1.4.1 The life cycle

The slime moulds belong to the kingdom of Protista. Although the phylogenetic position of the slime moulds has been a source of confusion, several analyses suggest a divergence before the plant, animal and fungal clade, but late in the evolution of the Protista (Kessin, 1997).

The primary habitat of *Dictyostelium* is forest soil. Under normal conditions the cellular slime mould consists of unicellular amoeboid cells that move around and feed on bacteria. They themselves are predominantly preyed upon by nematodes (Kessin *et al.*, 1996). When food becomes scarce, the amoebae enter a stage of aggregation. This leads to the formation of a multicellular organism that eventually forms spores, which are dispersed and able to survive during harsh conditions. During the multicellular development all amoebae are still self-sufficient. When completely disorganised and offered fresh bacteria, the amoebae promptly return to the vegetative stage and consume the available bacteria; when disorganised in the absence of bacteria, the same multicellular development promptly arises again (Raper, 1940).

Aggregation is the first stage of this fascinating process of morphogenesis. Initially the amoebae begin to communicate by emitting cyclic adenosine monophosphate (cAMP) signals, which are transmitted from amoeba to amoeba in the form of waves of excitation: Amoebae respond to stimulation by cAMP with an increase in cellular cAMP synthesis and subsequent secretion. The cAMP receptors, however, become desensitised, which terminates the cell response. Afterwards, the cAMP is degraded by phosphodiesterase, and returns to its resting level. The cAMP receptors become sensitive again, and the amoeba can again be stimulated. Diffusion of cAMP through the medium causes the signal to be relayed in space; the relayed signal takes the form of the observed macroscopic cAMP waves (Höfer *et al.*, 1995b). Thus, the cAMP waves in *Dictyostelium* are a particular instance of wave patterns in excitable media (Tyson & Murray, 1989).

The spatial pattern of these waves is usually rather complicated. It consists of many rotating spiral waves, or of target waves that are generated by high-frequency pacemakers at their centre. The patterns already show a high amount of self-organisation, whereby more or less equal amounts of amoebae aggregate to one centre, a property which is only weakly dependent on cell density. Different strains show different 'preferences' for either spirals or target waves during development, although strain behaviour is essentially interchangeable, for example, by adjustment of humidity (Kellerman & McNally, 1999).

The amoebae respond mechanically to the chemical signal via chemotaxis and start moving in the direction of the cAMP gradient. After propagation of 20-30 waves of cAMP, the amoebae collect in coalescing aggregation streams containing about 10^4 to 10^6 cells; then they collect in a compact aggregate, which is called the mound. Thereupon they begin to separate into two major cell types, prestalk and prespore cells. The prestalk cells sort out to the top of the mound and form a tip[2]. As soon as the tip is formed, the mound starts to elongate and forms a long thin structure, which is called the first finger. This structure usually tips over and forms a slug, which starts to migrate towards the soil surface. The prestalk cells occupy the anterior 30%, while the prespore cells occupy the posterior part; the whole slug is surrounded by a slime sheath. The slug senses the environment for cues such as light incidence, temperature and pH gradients and air streams, in order to orientate itself towards the surface. When the slug comes into a suitable environment for fruiting body formation, the tip reaches up, and the prespore cells crawl in underneath: the so-called culminant is formed, which initially is more or less hemispherical. Now the prestalk cells start to form the stalk, which elongates downwards through the cell mass to anchor itself to the base, while the

[2]During this stage, as well as during the later stages, increasingly more (sub) cell types can be discriminated, such as, for example, the anterior-like cells.

prespore cells move upwards. These peculiar cell movements have been referred to as the “reverse fountain”. In this way, the fruiting body is eventually formed, with a spore-filled globule at the top of a thin tapering stalk. At the base the so-called basal disc is formed, which gives the organism its scientific name; the spore head is surrounded by an upper and lower cup. Finally, to close the life cycle, the spores are dispersed and germinate again as unicellular amoebae.

There is yet another morphogenetic pathway, namely sexual development, which is accompanied by cannibalism. This occurs in the dark, usually under wet conditions. Mating begins with the appearance of tiny amoebae that move about much more rapidly than their larger vegetative counterparts. Shortly after their appearance, these gametes fuse in pairs to form binucleates, or sometimes even multinucleates. Within each binucleate the nuclei swell, migrate together and fuse. As this occurs, the cytoplasm increases in volume, so that once the nucleus forms, the cells are extremely large and are referred to as zygote giant cells. These giant cells secrete cAMP to attract the non-zygotic amoebae to their surfaces. Upon arrival these amoebae are ingested in a kind of cannibalistic phagocytosis. Chemotaxis occurs more rapidly than phagocytosis and therefore a zygote giant cell becomes surrounded by hundreds of cells. Once the zygote has ingested all of them it secretes a cyst wall before entering a period of dormancy. At germination meiosis occurs, and subsequent mitoses result in the production of many amoebae that emerge from the cyst (O’Day, 2000).

Some mechanisms, such as the cAMP signalling, are used in both pathways. It is often considered strange that the stalk cells give up their self-sufficiency during fruiting body formation. The mechanism of cannibalistic sexual development, however, puts this event in a different light. The sexual pathway is believed to have evolved before the fruiting body (Kessin, 1997), although this is still highly speculative. Although the sexual pathway has many interesting features, during the rest of this thesis it will nevertheless be completely ignored (as is normally the case when *Dictyostelium* is used as a model organism).

1.4.2 Key elements of morphogenesis

A number of key elements can be observed as the slime mould develops into a fruiting body. Here we describe the ones we think are most essential, and which we use in the full model. We discuss both the experimental observations and indicate how we have implemented them.

Motility

> Motility is a complex process that depends on the coordination of many cellular functions, including the conversion of information from the environment into a series of coordinated responses that culminate in directed cell movement. Motility is one of the most important processes in *Dictyostelium* morphogenesis. Motion is essential during aggregation, the mound stage, slug motion and formation of the fruiting body, and is involved in all kinds of processes, such as cell sorting. But obviously it is also needed during the unicellular state, for grazing bacteria and evading nematodes.

Motility is implemented by using the Glazier & Graner-model, and stems from membrane deformations, which are governed by something akin to energy minimisations and which take cell adhesion, chemotaxis and volume conservation into account.

Adhesion

Adhesion is essential for normal development in many respects (Fontana, 1995). Three forms of cell adhesion determine the life cycle: adhesion of bacteria to the surface of the growing amoebae, as the prerequisite for phagocytosis; cell-substratum adhesion, necessary for both locomotion of the amoebae and migration of the slug; and cell-cell adhesion, essential for transition from the unicellular to the multicellular stage, since multicellular organisms cannot exist unless they are able to adhere to each other (Bozzaro & Ponte, 1995). Differential cell adhesion plays a role in many processes during all stages of the development, such as cohesion, cell sorting, and contact-mediated regulation of gene expression. Nowadays, many different cell adhesion molecules have been identified and purified.

The Glazier & Graner-model that we use has been developed to describe differential cell adhesion. Differential adhesion is implemented in the model by varying the surface contact energies J_{τ_1,τ_2}.

cAMP signalling

The cAMP dynamics in *Dictyostelium* can be regarded as a very interesting realization of excitable media. During all stages, the motion of amoebae is orchestrated by waves of cAMP, which are formed by a combination of a pulsatile cAMP excretion and a cAMP-mediated cAMP response. This is accompanied by a chemotactic response towards cAMP. The field of aggregating amoebae is an unusual instance of pattern formation in excitable media, because cAMP is not only the substrate that forms the waves of excitation, generated by separate amoebae which receive and transmit the cAMP signal, but it is also an attractant for chemotactic motion of the amoebae. So, after excitation, the amoebae enter a phase of motion, during which the distance between the amoebae alters. Therefore, the next wave of cAMP will propagate through an excitable medium that differs slightly from the previous wave. Thus, in this system the wave of excitation changes the excitable medium itself. The velocity of motion of amoebae is low compared to the velocity of the wave of cAMP, and if we are interested in the short-time behaviour of this system, we can neglect the motion of the amoebae. However, if we want to model the process of aggregation itself, then the motion of the amoebae and its effect on the waves of excitation must be taken into account. The same holds for the later stages of the morphogenesis, since the slug also behaves like a moving 3D excitable system: slug motion has been shown to be organised by a scroll wave in the tip which breaks up into plane waves (Siegert & Weijer, 1991, 1992). Although both spiral waves and target waves are observed during the aggregation, it is still not certain whether the slug motion may also be organised by target waves that move backwards from the tip. On the one hand, Kellerman & McNally (1999) observed that strains which show target patterns during aggregation often skip the whole slug stage and culminate instantaneously. When conditions are altered so that such a strain also shows spiral waves, the chances of slug migration also increase, which indicates that a scroll wave is important for the slug stage, at least for its initiation. On the other hand, Bonner (1998) managed to develop an experimental method for producing migrating 2D (one-cell-thick) slugs which share most basic properties with normal 3D slugs. Obviously, these slugs do not have a scroll wave. In chapters 3 and 4 we model migrating 2D slugs organised by target waves. The cAMP waves, combined with chemotaxis, are again essential during the culmination stage, where they organise the upward motion and, at the same time, force in a roundabout way the downward elongation of the stalk (see chapters 5 and 6).

In our model we use a mathematical caricature of the cAMP dynamics, namely the FHN system with piecewise linear 'Pushchino' kinetics (Panfilov & Pertsov, 1984). The chemotaxis is implemented by taking the local cAMP gradient and by using this value in the energy function that drives the membrane-rearrangements in the Glazier & Graner-module.

Ammonia

A number of other signalling molecules besides cAMP also play a role during development. One of these key molecules is ammonia (NH_3). The developmental roles of NH_3 have been frequently underestimated: NH_3 regulates the onset of aggregation, controls the timing of differentiation, functions as a morphogen for cell proportioning, determines whether or not the slug stage will be skipped completely, is connected to thermotaxis, phototaxis and acidotaxis during slug migration, regulates the timing of switching from migration to culmination, determines fruiting body orientation, and is linked with the final sporulation. For an overview, see Cotter *et al.* (1992). *Dictyostelium* is certainly not the only organism which uses NH_3 as a long-distance communication signal. For example, NH_3 also mediates communication between yeast colonies (Palková *et al.*, 1997).

In our model we use a PDE to describe the production and turnover of NH_3, which depend on factors like the local light intensity[3] and the presence of charcoal in the medium. NH_3 alters the excitability of the cells. This is implemented by modifying the parameter value that defines the excitability in the excitable medium module.

Cell differentiation

The amoebae differentiate into two major cell types, as well as many other (sub) cell types. The cell cycle phase at the onset of starvation imposes a relative preference for a specific cell fate. However, when prestalk cells

[3]To describe light refraction we developed a separate CA module, which uses a ray-tracing technique; see chapter 4.

or prespore cells are separated, they take on almost normal cell proportions within a few hours. The most important morphogens that control cell differentiation and transitions between cell types are: cAMP, required for both prestalk and prespore differentiation; differentiation-inducing factor (DIF), which induces prestalk and inhibits prespore differentiation; and NH_3, which antagonises DIF (Williams, 1988; Schaap *et al.*, 1996; Kay, 1997).

We do not implement cell differentiation in a detailed way in our model: it is assumed that cells never change their major cell type. The only cell-type transitions we use are to describe the maturation of prestalk cells, which changes cell adhesion, as well as properties connected with excitability. For this process we simply assume local cell induction by a non-specified process.

Extracellular matrices

From late aggregation onwards the multicellular mass is covered in a thin extracellular matrix, which contains mainly protein and cellulose (Smith & Williams, 1979). This is called the slime sheath. During slug migration, slime is continuously synthesised, and a trail of slime is left behind. It is unclear whether all cells in the slug contribute to the production; most of the slime may in fact be secreted by the outer layer of cells (Wilkins & Williams, 1995). Different cell types may also produce different amounts and elements of the slime sheath. The slime sheath plays an important role in slug formation, maintenance of the morphology and migration.

The extracellular matrix which surrounds the stalk, the so-called stalk tube, is quite different. This matrix is produced by the stalk cells, and is of a different composition, which makes it much stiffer. Its prime role is to strengthen the stalk that supports the spore head. In chapter 6 we show that it may also play a role in the downward elongation of the stalk.

The extracellular matrices are implemented as very large cells in the Glazier & Graner-module. The differences in stiffness are described by differences in the dissipation costs involved in changing their shape.

1.4.3 Model history

In the early seventies, *Dictyostelium discoideum* attracted the attention of theoreticians, and since then the organism has become a paradigm for theories of pattern formation during development. Three aspects make *Dictyostelium* very suitable for this task: the relative simplicity of the patterns; an almost invariant development over a huge range of total cell numbers; and a remarkable capacity to restore proportions, patterns and morphogenesis when disturbed and fragmented (Nanjundiah, 1997).

Various aspects of the development have been studied mathematically, in roughly the same order as the morphogenesis itself. Already in the forties, Bonner (1947, 1949) showed that both the aggregation and the later stages are organised by a signalling molecule which functions as a chemoattractant; he called the molecule acrasin, but it later turned out to be cAMP (Barkley, 1969). Very early in the seventies authors of several theoretical studies tried to explain the initiation of the aggregation in terms of breakdown of stability (Keller & Segel, 1970; Cohen & Robertson, 1971a,b; Nanjundiah, 1973). These studies showed that production and decay of a chemoattractant can lead to unstable modes, which could possibly be interpreted as aggregation and streaming. In 1973, however, Durston was the first to recognise that *Dictyostelium* aggregation fields behave as an excitable medium. He focused mainly on how the macro-scale phenomena could be understood in terms of an excitable medium. Alcantara & Monk (1974) were the first to elucidate the possible biological mechanisms by which the system behaves as an excitable medium.

The mechanism of cAMP signalling has been modelled in detail by Martiel & Goldbeter (1987). This model is based on experimental studies and describes the interaction between cAMP and its membrane receptor (this mechanism was first introduced by Segel *et al.*, 1986). The model takes into account both the desensitisation of the cAMP receptor by reversible phosporylation and the activation of adenylate cyclase that follows binding of extracellular cAMP to the unmodified receptors. By assuming that all the reversible binding steps in the kinetic model are rapid, these authors have shown that the model reduces to three coupled nonlinear ordinary differential equations: the fraction of a receptor in the active state, the intracellular cAMP concentration and the extracellular cAMP concentration. All the parameters in the reduced model are composites of many processes. The numerical solution of the model agrees in quantitative detail with experimental observations of the period, amplitude and form of the cAMP oscillations, as well as with the experimental observations of the adaptation to constant cAMP stimuli and the absolute and relative refractory period.

Their study, however, did not take the spatial geometry into account. To establish the effective diffusion coefficient (D_{eff}) of cAMP during aggregation, which was ignored in the above-mentioned study, Foerster *et al.* (1990) measured the velocity-curvature relation which they used to calculate D_{eff}. To obtain both the detailed time- and space-characteristics of the cAMP signal, Dallon & Othmer (1998) modelled the precise cAMP dynamics of two nearby cells. See also the work by Othmer & Schaap (1998), who, in an attempt to elucidate the detailed dynamics, carry the modelling to an extreme.

The first attempts to model the spatial patterns of the aggregation stage were made by Parnas & Segel (1977, 1978). They modelled aggregation using a one-dimensional (1D) grid, and showed that periodic cAMP signalling combined with chemotaxis leads to very efficient aggregation. MacKay (1978) used a 2D grid. His model used discrete cells that could be in different states and a number of transition rules that describe the cell-to-cell signalling. The model showed propagating waves of cell movement and aggregation in coalescing streams.

The model developed by Martiel & Goldbeter (1987), reduced to two variables, was implemented for the first time in a spatial context by Tyson & Murray (1989) and by Tyson *et al.* (1989), in order to study waves of excitation in a uniform 2D field of signal-relaying but immobile cells. To obtain propagation these authors added a diffusion operator to the equation that describes the extracellular cAMP. They showed that this model describes in quantitative detail experimental observations of rotating spiral waves of cAMP in fields of amoebae distributed over an agar surface. More recently, different mechanisms have been proposed to explain the formation of spiral waves during early aggregation (Pálsson & Cox, 1996; Levine *et al.*, 1996; Lauzeral *et al.*, 1997).

Using the Martiel & Goldbeter-model, Levine & Reynolds (1991) calculated that the stream formation could be due to an instability of the combined signalling-chemotaxis system. At the end of 1994 and the beginning of 1995, two studies appeared which, for the first time, really considered the interplay between the actual cell aggregation process and the cAMP dynamics. Vasiev *et al.* (1994) used an FHN-type model for the cAMP dynamics and a continuity equation for the amoebae motion, whereas Höfer *et al.* (1995a,b) derived a PDE model with intracellular and extracellular cAMP, as well as cell density. Both models were able to reproduce the cellular pattern formation during aggregation. These two studies, however, offered different explanations for the streaming instability. According to Höfer *et al.* (1995a,b) stream formation is due to a chemotaxis-driven instability[4]. Vasiev *et al.* (1994) on the other hand showed that stream formation can be due to a density-dependent wave speed, i.e. cAMP waves travel faster in regions with higher cell density. van Oss *et al.* (1996) elaborated this idea by combining the Martiel & Goldbeter-model for cAMP signalling with a discrete cell description. They showed that in the Martiel & Goldbeter-model, stream formation due to the dependence of wave speed on cell density occurs only when the turnover rate of intracellular cAMP is high.

The regulation of cell type proportions was modelled by Schaap *et al.* (1996). They showed that differential production and turnover of cAMP, DIF and NH_3, and their effects on cell differentiation, produce more or less correct proportions of the different cell types. The subsequent cell sorting was modelled by Sekimura & Kobuchi (1986) in a CA which incorporated both differential chemotaxis and differential cell adhesion. They found, in contrast to the differential adhesion hypothesis (Steinberg, 1963), that differential adhesion should operate in such a way that prestalk and prespore cells intermingle: in their model, small clumps of cells only slow down the sorting, which is driven completely by the chemotaxis. However, this can be regarded as a model artefact, since, as was indicated in section 1.3, CA models are not able to give a good description of cell sorting caused by differential adhesion. Umeda (1989) constructed a mixed-fluid model, and showed that cell sorting could be due to differential chemotaxis towards cAMP only. Glazier & Graner (1993) developed the two-scale CA model described in section 1.3, and showed that cell sorting patterns, as observed in submerged agglomerates of *Dictyostelium* (Takeuchi *et al.*, 1988), could be explained adequately by differential intercellular adhesion only (see also Graner & Glazier, 1992; Graner, 1993; Graner & Sawada, 1993). Cell-adhesion-driven cell sorting versus chemotaxis-driven cell sorting is still a source of debate (see Clow *et al.*, 2000, and the discussion in section 7.3.2 on page 114). The Glazier & Graner-

[4]Curiously, using an analytic caricature of their model, they showed that their condition for streaming is almost identical to the criterion for the chemotaxis-driven instability that Keller & Segel proposed back in 1970.

model formalism was used by Savill & Hogeweg (1997) to describe aggregation and mound formation (as well as the crawling slug). They made two important extensions to the model: (i) they added chemotaxis to the model by adding another layer with cAMP dynamics and using the local, subcellular cAMP gradient in the energy function; and (ii) they extended the model to 3D, so that it became possible for the first time to follow directly the transition from the aggregation stage to the mound stage. They showed that not only chemotaxis and wave propagation, but also cell adhesion play an important role in stream formation. They also showed that streams can be functional, because streams move faster than individual cells.

Further 3D work on the mound stage was done by Bretschneider *et al.* (1997). They combined discrete cells with the Martiel & Goldbeter-model and showed formation and elongation of the mound, as well as cell sorting by differential chemotaxis. Levine *et al.* (1997) and Jiang *et al.* (1998) have also studied the mound stage, albeit in less sophisticated models. Finally, Dormann *et al.* (1998) combined an FHN-model for the cAMP dynamics with a Navier-Strokes equation for the cell motion. They showed that cell sorting provides feedback to the wave geometry. This eventually leads to the formation of a twisted scroll wave, which later dominates the dynamics during the slug stage.

The first model for the mechanism underlying slug motion was constructed by Odell & Bonner (1986). They proposed that the forward motion may be achieved by a fountain-like circulation of cells. In the mixed fluid model of Umeda (1989), a continuous chemotactic motion forwards was assumed, leading to a number of very peculiar slug shapes. Both models, however, contradict experimental observations (Siegert & Weijer, 1991, 1992). On the basis of these experiments, Steinbock *et al.* (1993) showed that in a tube-shaped excitable medium with decreasing excitability (which is a caricature for a slug), a twisted scroll wave in the highly excitable prestalk zone breaks up into plane waves in the less-excitable prespore zone. Bretschneider *et al.* (1995) showed the same conversion of scroll waves into planar wavefronts in the more realistic Martiel & Goldbeter-model. Bretschneider *et al.* (1999) have added to this model the explicit motion of the cells, represented as spheres, while taking both cell-type specific chemotaxis and adhesion into account. The model created stable scroll waves that were able to generate coordinated slug migration. On the other hand, the above mentioned model developed by Savill & Hogeweg (1997) showed that target waves, which originate in the tip and move through the slug, can also drive a multicellular slug, when these are combined with chemotaxis and adhesion.

In contrast to the other stages, the culmination stage has not yet been modelled in terms of biological processes, although the shape changes of the culminant during the culmination have been modelled (Zeeman, 1977; Rubinow *et al.*, 1981).

In part II of this thesis we study the interactions of the slug with the environment and we describe how the cellular slime mould morphogenesis culminates in the formation of a fruiting body.

1.5 This Thesis

In **part I** of this thesis we study the general problem of complex pattern formation in a homogeneous excitable medium. In **part II** we couple the pattern formation mechanism to a CA module which describes the cell dynamics, in order to develop a comprehensive model of *Dictyostelium discoideum* morphogenesis. We use this as a paradigm to study multicellular coordination and development. The particular chapters are organised as follows:

In **chapter 2** we study the phenomenon of spiral breakup. Nowadays it is generally accepted that heart-fibrillations and sudden cardiac death are caused by the occurrence and breakup of spiral waves. This has triggered a whole range of research on the origin of spiral waves and the mechanisms behind spiral breakup (Panfilov & Holden, 1997). The formation of spirals and their breakup not only play a role in heart diseases, but they are also important in *Dictyostelium* development, and in chemical systems, such as the BZ-reaction.

In earlier models, the mechanism which breaks up spirals was connected to the meandering of the spiral tip (Bär & Eiswirth, 1993) or related to spatiotemporal instabilities of the wave train, which even occur in a 1D case (Panfilov & Hogeweg, 1993; Karma, 1993, 1994). It turned out that there is a simple criterion for this instability, which can be formulated in terms of the restitution curve. Both mechanisms lead to breakup close to the core. The new mechanism for breakup elucidated here specifically explains patterns observed in the BZ-reaction (Markus *et al.*, 1994; Markus & Stavridis, 1994a,b), but is expected to reflect a much more general principle. We show that due to a high diffusion rate of the inhibitory variable the wavefront can become laterally unstable. Due to this high diffusion rate, the wave velocity is restrained by the high level of inhibitor ahead of the wavefront. However, the influx of the inhibitor into the region ahead of the wavefront is smaller in the case of a convex wave than in the case of a straight wave. As a result, the convex wave can propagate faster. Therefore, microscopic variations in the wavefront will be enlarged, which can potentially lead to spiral breakup.

We show that we can zoom in on an interesting parameter region by using a genetic algorithm. The parameter region in which we find spiral breakup is at the edge between wave-like phenomena and (quasi) stable patterns. This is because high enough diffusion rates of an inhibitor generally lead to Turing-like patterns. Along this edge a number of other interesting patterns can be found, such as, for example, oscillatory behaviour that is driven solely by diffusion.

In **part II** we present a model for *Dictyostelium* development, and show that the morphogenesis can unfold as a result of the interplay between excitable media and differential adhesion, and the feedback between levels of organisation.

In **chapters 3 and 4** we look at the slug stage. The model for excitable media from the previous chapter is combined with a stochastic two-scale CA which describes cell rearrangements caused by differential adhesion. We link these modules to each other by adding chemotaxis to the CA, using the local cAMP gradient (see also Savill & Hogeweg, 1997).

Chapter 3 falls into two sections. The first part describes the slug motion.

The model slugs maintain their shape and crawl, with a velocity depending on slug size, as is found in experiments. We also show that the interaction between differential adhesion and chemotaxis, which is the same for all cells (in contrast to the claims made in earlier work), can explain fast and complete cell sorting.

In the second part we look at the thermotactic behaviour of the slug. We show that thermotaxis can be generated in our model by means of the collective behaviour of the amoebae, whereas individual amoebae can neither sense a temperature gradient, nor show temperature-dependent differentiation in motion velocity. Instead, differences in temperature alter the excitability of the cells, and thereby the shape of the cAMP wave. Chemotaxis towards cAMP then causes the slug to turn towards the temperature gradient. It is very striking that the mechanism still functions at extremely low signal-to-noise ratios. This is possible because the cAMP waves behave like spatiotemporal signal integrators.

In **chapter 4** we focus on another property of the slug that directs it to the soil surface, namely phototaxis. We add an extra CA module, in which we use a ray-tracing model to describe light refraction, and a PDE which describes NH_3 dynamics. We also include the effect that NH_3 has on the cAMP dynamics. Light rays are refracted and focused on the side of the slug that is opposite to the light source. Light increases NH_3 production, which decreases excitability. As reported in the previous chapter, this changes the shape of the cAMP waves, and the slug turns towards the light source. However, when the sensitivity to NH_3 is too high, the final direction of motion is at a certain angle with respect to the light source. This can explain the behaviour of mutants that also show so-called bi-directional phototaxis. When the light intensity is lower, or when NH_3 is absorbed by 'charcoal', the bi-directionality decreases or disappears, as is found in experiments. Our mechanism can explain not only phototaxis, but also orientation in a pH gradient (acidotaxis) and towards an air current (rheotaxis). These two types of orientation are due to an interference with the NH_3 balance: along a pH gradient the $NH_3/NH_4{}^+$ ratio changes, and an air current carries NH_3 away.

In the final two chapters we study the final stage of *Dictyostelium*, namely the culmination that leads to the formation of the fruiting body. The movement during the culmination has been likened to a "reverse fountain", because prestalk cells in the upper part form a stalk which moves downwards and anchors itself to the substratum, while prespore cells in the lower part move upwards to form the spore head.

In **chapter 5** we extend the model further with extracellular matrices, i.e. the slime sheath and stalk tube, and we introduce differences in stiffness. We also include cell differentiation generated by some kind of induction process. We show that the whole process of culmination can unfold by the interaction of cAMP signalling, differential adhesion, cell differentiation and production of extracellular matrices. Periodic upward movements towards the cAMP waves induce pressure waves, which squeeze the stalk downwards through the cell mass. The mechanism creates an elongated stalk; downward motion stops automatically when the base is reached and upward motion stops once the stalk formation has finished; and finally the spore head becomes rounded. Moreover, the mechanism is also self-correcting; for example, any deviations in the downward elongation of the stalk are quickly restored. A high number of experimental observations are in agreement with the mechanism we propose. The mechanism can, for example, explain the well-known phenomenon of two culminants orienting away from each other.

In **chapter 6** we look in greater detail at the mechanisms behind the culmination. More specifically, we look at the detailed requirements for the different subprocesses and study how they interact with each other. We show that it is not sufficient for stalk elongation to have only a (stiff) tube or only pathfinder cells; both are needed, since it is only in interaction that an elongated stalk can be created and that the resistance caused by the upward moving cells can be efficiently reduced, which makes the fast downward elongation possible.

We also look at the essential requirements for the large number of surface tensions between all the cell types. This gives us an indication of the ranking one expects to find in experiments on binding strengths. We end this chapter by connecting side-effects observed in the model with experimental observations. It is possible that our model may be able to provide an explanation for the array of aberrant phenotypes that can be created nowadays by mutation generating experiments.

Thus, the chapters of part II together demonstrate that it is feasible to model morphogenesis in a sense that goes well beyond pattern formation. Such an approach can be used to study how a facultative multicellular organism can sense the environment, on many different scales, and exhibit a coordinated response.

We have identified a whole set of mechanisms by means of which *Dictyostelium* is able to coordinate morphogenesis. These mechanisms are reviewed in **chapter 7**. In the last chapter we also look in greater detail at the modelling approach we have used. And finally we will point to the gaps in our knowledge and give suggestions for further research.

Part I

Pattern Formation in Homogeneous Excitable Media

2

Spiral Breakup in Excitable Tissue due to Lateral Instability

Athanasius F. M. Marée and Alexander V. Panfilov
Theoretical Biology and Bioinformatics,
Utrecht University, Padualaan 8,
3584 CH Utrecht, The Netherlands.

Physical Review Letters **78** (1997) 1819–1822

Abstract

In a simple two-component model of excitable tissue a spiral wave is found to break up into a large number of small spirals. More specifically, we used a modified FitzHugh-Nagumo (FHN)-model. Spiral breakup is found to occur when the recovery variable diffuses at a high rate. The breakup is caused by lateral instability of the wavefront. We analysed this instability using quasi one-dimensional (1D) computations and found that it could be connected to a negative eikonal-curvature relation for the parameter values at which spiral breakup occurs.

2.1 Introduction

Recent studies have demonstrated that spiral waves in excitable media can be generated by a phenomenon called spiral breakup (Winfree, 1989; Panfilov & Holden, 1990; Gerhardt *et al.*, 1990; Courtemanche & Winfree, 1991; Ito & Glass, 1991; Panfilov & Hogeweg, 1993; Karma, 1993; Bär & Eiswirth, 1993). This phenomenon was discussed recently in connection with the mechanisms of cardiac fibrillation (Winfree, 1994; Panfilov & Hogeweg, 1995); spiral breakup has also been found in experiments with the Belousov-Zhabotinsky (BZ) reaction (Markus *et al.*, 1994; Markus & Stavridis, 1994a,b; Nagy-Ungvarai & Müller, 1994; Ouyang & Flesselles, 1996). The mechanism has been discussed in several papers (Ito & Glass, 1991; Panfilov & Hogeweg, 1993; Karma, 1993). It was found to occur in models that show spatiotemporal instabilities of wave trains in 1D excitable media. The mechanism of this 1D instability is believed to be associated with the restitution properties of excitable tissue (Courtemanche *et al.*, 1993; Karma, 1994).

However, experimental data of Markus *et al.* (1994) and Markus & Stavridis (1994b) suggest another possible cause of spiral breakup. In their experiments the wavefronts develop a curly shape before they break down into chaos. This curly shape is similar to the shape that is expected to occur when the wavefront is laterally unstable (Kuramoto, 1980). The mechanism of this instability is associated with a negative slope of the so-called eikonal-curvature relationship. In this paper we report on the spiral breakup occurring in a two-component FHN-model due to lateral instability.

The lateral instability of a wavefront is related to a change in the slope of the eikonal-curvature relationship. This relationship expresses the normal velocity V of a wave as a function of its curvature k. Convex and concave waves are defined by $k > 0$ and $k < 0$, respectively. It is possible to derive the following relationship for waves with a small curvature: $V = V_0 - Dk$, where V_0 is the velocity of a planar wave, and D a constant usually referred to as the effective diffusion coefficient (D_{eff}) (Keener, 1991). Wave instabilities occur if D_{eff} is negative (Kuramoto, 1980). Therefore we studied the dependence of the velocity of the front on its curvature in a modified FHN-model (Panfilov & Hogeweg, 1993) in which we incorporated diffusion for both the recovery and the activator variable. We computed the value of D_{eff} from this dependency, and by using a genetic algorithm we were able to find parameter settings for which $D_{\text{eff}} < 0$. To determine the eikonal relationship, and to calculate D_{eff}, we used fast quasi-1D computations of the eikonal equation with constant curvature of the wave (Keener, 1991). In this equation, curvature and direction of motion are pre-defined. The diffusion term is given by:

$$\Delta = \frac{\partial^2}{\partial \xi^2} + k \frac{\partial}{\partial \xi}, \tag{2.1}$$

where k is the curvature and ξ the direction perpendicular to the wave.

2.2 The Model

We used the following model for an excitable medium, based on piecewise linear 'Pushchino kinetics':

$$\frac{\partial e}{\partial t} = \Delta e - f(e) - g, \tag{2.2a}$$

$$\frac{\partial g}{\partial t} = D_g \Delta g + \varepsilon(e,g)(ke - g), \tag{2.2b}$$

with $f(e) = C_1 e$ when $e < e_1$; $f(e) = -C_2 e + a$ when $e_1 \leq e \leq e_2$; $f(e) = C_3(e-1)$ when $e > e_2$, and $\varepsilon(e,g) = \varepsilon_1$ when $e < e_2$; $\varepsilon(e,g) = \varepsilon_2$ when $e > e_2$, and $\varepsilon(e,g) = \varepsilon_3$ when $e < e_1$ and $g < g_1$. To make the function $f(e)$ continuous, $e_1 = a/(C_1 + C_2)$ and $e_2 = (a + C_3)/(C_2 + C_3)$. Using genetic algorithms, we found the following basic parameter values at which we studied spiral breakup: $C_1 = 43.3$, $C_2 = 6.5$, $C_3 = 18.3$, $a = 0.64$, $k = 9.1$, $g_1 = 1.95$, $\varepsilon_1^{-1} = 49.4$, $\varepsilon_2^{-1} = 4.4$, and $\varepsilon_3^{-1} = 2.8$. The shape of the function $f(e)$ specifies the fast processes. The dynamics of the recovery variable g in the model are determined by the function $\varepsilon(e,g)$. In $\varepsilon(e,g)$ the parameter ε_1^{-1} specifies the recovery time constant for relatively large values of g and intermediate values of e. This region corresponds approximately to the wavefront, waveback and to the absolute refractory period. Similarly, ε_2^{-1} and ε_3^{-1} specify the recovery time constant for large values of e, and for small values of e and g, respectively. These regions correspond approximately to the excited period, and to the relative refractory period, respectively. The dynamics of g at the wavefront and the waveback are slow, but during the excited and the relative refractory period the dynamics are faster. The only difference between this model and the previous model (Panfilov & Hogeweg, 1993) is that this model incorporates diffusion of both the activator and the recovery variable.

For numerical computations we used the explicit Euler method with Neumann boundary conditions. To determine the velocity of waves with a fixed curvature, a wave was initiated in the linear grid, and its velocity was measured after it had become constant. This procedure was repeated for different curvatures. To initiate the first spiral in a rectangular grid we used initial data corresponding to a broken wave, the break being located in the middle of the excitable tissue.

2.3 Results

We found that spiral breakup occurred spontaneously in the excitable media at high values of D_g. Figure 2.1 shows the evolution of a spatial pattern in a medium with $D_g = 2.55$. The spatial pattern starts to form as soon as one spiral wave has developed. This spiral makes several rotations [Fig. 2.1(a)]. The spiral wave becomes perforated [Fig. 2.1(b)], then becomes more and more perforated, and breaks into several interacting spiral waves of different sizes [Fig. 2.1(c)]. Finally, when there is a high density of small spirals, the pattern becomes relatively

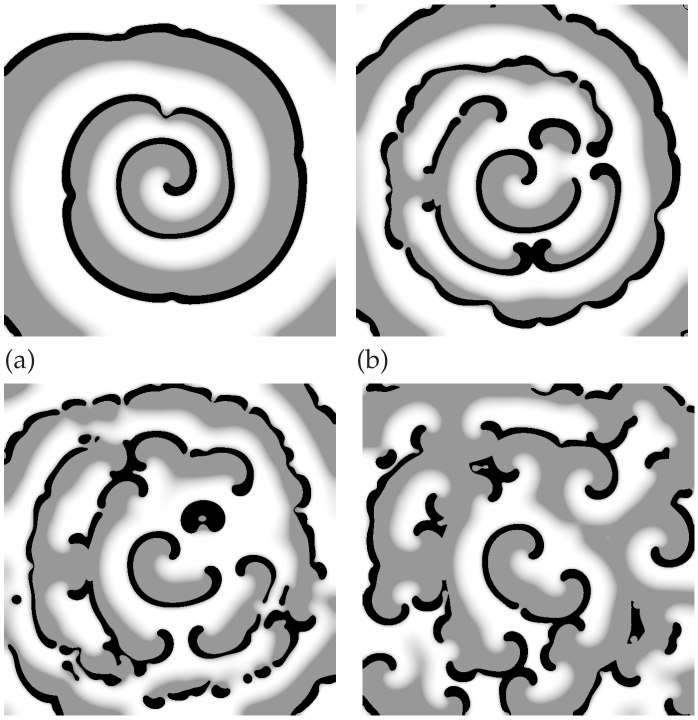

(a) (b) (c) (d)

Figure 2.1. The spiral breakup in model (2.2). The snapshots are at time (a) $t = 144$, (b) $t = 208$, (c) $t = 252$, and (d) $t = 608$. Numerical integration was done with space step $h_s = 0.15$, and time step $h_t = 0.0011$, on a grid of $1\,333 \times 1\,333$ elements. Black represents the excited state of the tissue ($e > 0.6$), dark grey shows the region where $g > 1.95$ (close to the absolute refractory state), and intermediate shading from grey to white shows different levels of g, $0.3 < g < 1.95$ (estimate of the relative refractory period). See also the colour plate on page 71.

stable [Fig. 2.1(d)]. These spirals are randomly distributed in space, but their centres remain in approximately fixed positions.

The process by which the spirals in our case were formed is shown in Fig. 2.2. The initial plane wavefront becomes unstable. In particular, part of the wavefront becomes retarded, the delay increases, and finally the wave breaks up and an excited spot is formed. This spot interacts with the following wave and creates two wave breaks, which develop into two spiral waves.

The breakup that occurred in our model was not due to discrete properties of our medium. We did computations for a wide variety of space steps ($0.05 \leq h_s \leq 0.85$). We studied the stability of spiral breakup at various spatial and time integration steps, and found that the patterns were similar for different degrees of calculation precision, but the value of the parameter D_g at which spiral breakup occurs increased as the calculation precision increased. We found that at $h_s < 0.2$


(a) (b) (c) (d) (e) (f)

Figure 2.2. Development of spiral breakup due to lateral instability. Enlargement of Fig. 2.1 region where first breakup occurred, measuring 172 × 352 elements. The snapshots are at time (a) $t = 140$, (b) $t = 144$, (c) $t = 148$, (d) $t = 152$, (e) $t = 156$, and (f) $t = 164$. Grey-scale coding is the same as in Fig. 2.1.

the shift saturated.

The mechanism of such breaks is due to the lateral instability of wavefronts. Figure 2.3 shows the relation between velocity V of a wave and its curvature k at the same parameter values at which we find breakup. We see that, for $k < 0.3$, velocity increases with increasing curvature, i.e. the wavefront here is unstable because of the lateral instability. For $k > 0.3$, velocity decreases with increasing curvature and wavefronts are stable again. The spiral cores are stable because they have the highest curvature.

The observation that, for small curvatures, velocity increases with curvature can be understood from a cross section through the wave. The insets of Fig. 2.3 show the values of e and g in such a cross section, for a straight and a convex wave, respectively. The velocity of a straight wave is restrained by g ahead of the wavefront. On the other hand, in the case of a convex wave the influx of g into the region before the wavefront is smaller, which leads to relatively low values of g and faster front propagation. This phenomenon is expected to be fairly general for excitable media with a high diffusion of the recovery variable (Kuramoto, 1980).

By applying regression analysis to the slope around $k = 0$ we calculated the D_{eff} [Fig. 2.4(a)]. At $D_g \approx 2.12$, $D_{\text{eff}} = 0$. Spiral breakup is found when $D_{\text{eff}} < -1.2$, i.e. at $2.5 < D_g < 2.6$. At higher values of D_g, propagationless patterns are found. We observed several types of propagationless patterns with static and oscillatory behaviour, comparable with and occurring in the same succession as the patterns described by Ohta *et al.* (1989).

We studied the dependence of the lateral instability and spiral breakup on the parameters of the excitable medium. We computed two values of D_g for different parameter settings. The first value (D_{g_1}) is the value of D_g at which $D_{\text{eff}} = 0$, and the second value (D_{g_2}) is the value of D_g at which propagationless patterns are found. The procedure was the following: We changed the value of one parameter and, by varying the value of D_g, we found the values D_{g_1} and D_{g_2}. The

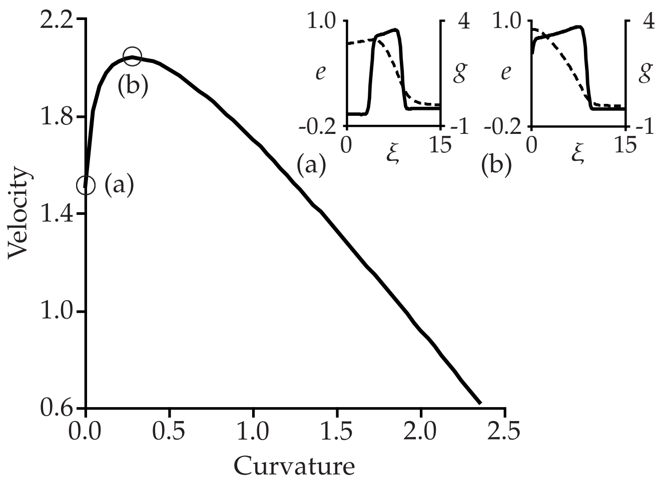

Figure 2.3. The relation between curvature and velocity of a wave. The insets show the values of e (solid lines) and g (dashed lines) in cross sections through the wave; (a) for a straight wave, and (b) for a convex wave with curvature $k = 0.28$. Computations were done on a linear grid of 1 000 elements. Numerical integration was the same as in Fig. 2.1.

results are shown in Fig. 2.4(b). For example, for 'basic values' of parameters and numerical precision as given in the figure caption, we get propagationless patterns at $D_g \geq 1.98$ and lateral instability ($D_{\text{eff}} < 0$) at $D_g \geq 1.68$ [large open circle in Fig. 2.4(b)]. We changed nine parameters, and found that all nine lines of $D_{g_1}(D_{g_2})$ are located in a small region. The differences in D_{g_1} are less than 10% for $D_{g_2} < 3$ and less than 20% for $D_{g_2} > 3$. Hence we can conclude that lateral instability is a general property of this model. We can also conclude that a good prediction of the occurrence of lateral instability can be made by using the value of D_{g_2}: For $D_{g_2} > 1.2$ we observed lateral instabilities.

Low values of D_{g_2}, at which there was no lateral instability, were found for media with low excitability. Low excitability can be caused by a high threshold (parameter a high), by a rapid increase of g during the excited period (parameter k high, or parameters ${\varepsilon_1}^{-1}$, ${\varepsilon_2}^{-1}$, or C_3 low), or by entering the refractory period at low values of g (parameter C_2 low). For example, for 'basic' parameter values and numerical precision as given in Fig. 2.4(b), $D_{g_2} = 1.98$, while $D_{g_2} = 1.2$ when a is changed to 0.98, or k to 17.3, or ${\varepsilon_1}^{-1}$ to 2.7, or ${\varepsilon_2}^{-1}$ to 1.9, or C_3 to 5.1, or C_2 to 5.1.

At higher values of D_{g_2}, the interval of values of D_g for which we have lateral instability increases. However, lateral instability does not necessary lead to spiral breakup for several reasons. First, a large refractory period prevents spiral breakup, even when the wavefront is laterally unstable [Fig. 2.5(a)]. This is found when ${\varepsilon_3}^{-1}$ is high or g_1 is low. In our case, if we increased ${\varepsilon_3}^{-1}$ to 10, or decreased g_1 to 0.9, spiral breakup disappeared. It explains why spiral breakup by lateral

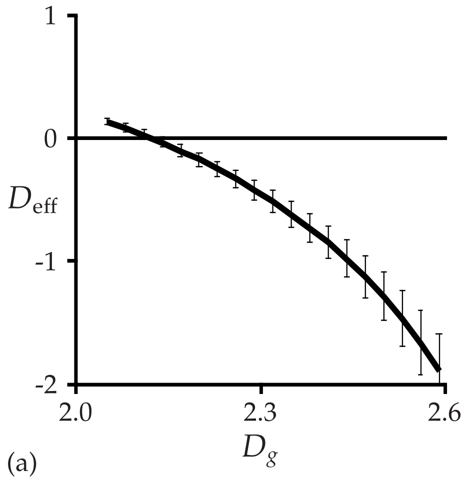

Figure 2.4. (a) D_{eff}, calculated with regression analysis for $k \approx 0$. For $2.15 < D_g < 2.6$, D_{eff} has a negative sign. For $D_g > 2.6$ only stationary patterns are found. Numerical integration was the same as in Fig. 2.3. (b) Lowest value of D_g at which propagationless patterns are found (D_{g_2}) against the value of D_g at which $D_{\text{eff}} = 0$ (D_{g_1}) for 4346 different parameter settings. Every time one parameter was changed, the other parameters were kept at the basic values. The large open circle shows position for basic values. Numerical integration was done with space step $h_s = 0.45$, and time step $h_t = 0.010$, on a linear grid of 444 elements.

instability is difficult to find in models with only one, slow, timeconstant for the recovery variable. Secondly, a large size of the excited region, i.e. where $e > 0.6$, prevents spiral breakup [Fig. 2.5(b)]. In these cases the instability is not strong enough to form new spirals. This is also the case partially because the large excited region is accompanied by a large refractory period. A large excited region is found when the threshold is low (parameter a low), when an increase of g during the excited period is slow (parameter k low, or parameters ${\varepsilon_2}^{-1}$ or C_3 high), when the system enters the refractory period at very high values of g (parameter C_2 high), or when there is a fast decrease of g behind the excited region (parameter ${\varepsilon_3}^{-1}$ low, or parameter g_1 high). For example, if we increased ${\varepsilon_2}^{-1}$ to 7.1, C_3 to 90.0, or C_2 to 7.9, or decreased a to 0.34, k to 6.5, or ${\varepsilon_3}^{-1}$ to 2.0, breakup disappeared. Thirdly, if ${\varepsilon_1}^{-1}$ or C_1 are high, the refractory period is large, but spiral breakup is found to occur in the core of the spiral. This eventually leads to a chaotic pattern of appearing and disappearing spirals [Fig. 2.5(c)]. The mechanism is a mixture of the spatiotemporal instabilities, as described earlier (Ito & Glass, 1991; Panfilov & Hogeweg, 1993; Karma, 1993), and the lateral instability, as described in this paper. We found this behaviour when we increased C_1 to 250, or ${\varepsilon_1}^{-1}$ to 100. Fourthly, when C_1 is decreased to 0.7, the spatially uniform system (2.2) passes a point of fold bifurcation for limit cycles. This causes the sys-

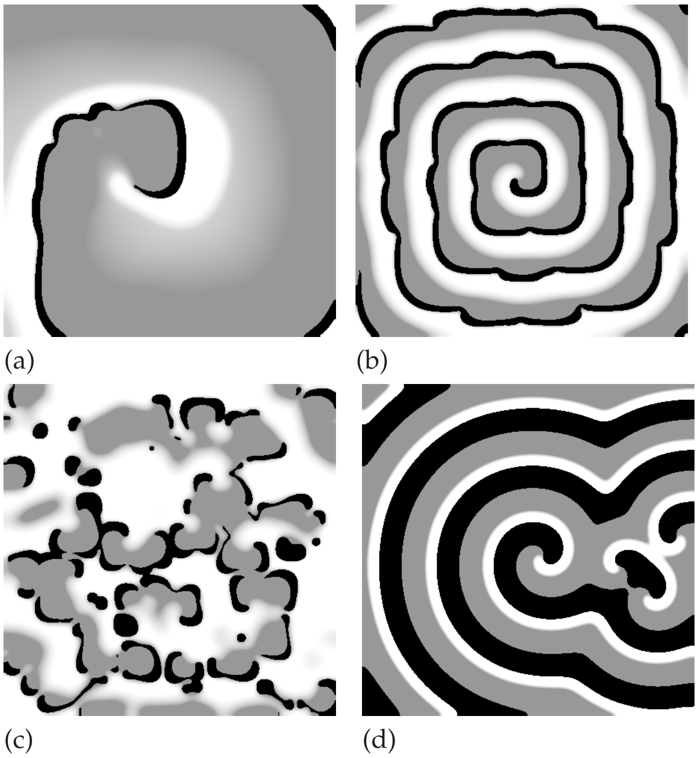

Figure 2.5. (a) Spiral breakup prevented by large refractory period; $g_1 = 0.9$, $D_g = 1.93$, and $D_{\text{eff}} = -1.5$. (b) Spiral breakup prevented by a large size of the excited region; ${\varepsilon_3}^{-1} = 2.0$, $D_g = 2.08$, and $D_{\text{eff}} = -1.4$. (c) Chaotic pattern of appearing and disappearing spirals; ${\varepsilon_1}^{-1} = 1\,000.0$, $D_g = 2.45$, and $D_{\text{eff}} = -4.4$. (d) Stable spirals found in autocycling regime; $C_1 = 1.8$, $D_g = 2.6$, and $D_{\text{eff}} = -7.5$. Numerical integration was the same as in Fig. 2.4(b), on a grid of 444×444 elements. Grey-scale coding is the same as in Fig. 2.1.

tem to autocycle after an initial stimulation. However, even before the bifurcation point ($C_1 < 2.3$), autocycling can be found in the spatial model. Such behaviour is recently also described by Tsyganov *et al.* (1996). The autocycling pushes aside all irregularities as caused by the lateral instability [Fig. 2.5(d), $C_1 = 1.8$]. Even considering the above points, we still find breakup by lateral instability in a fairly large region of the parameter space.

2.4 Discussion

The wave patterns obtained in our computations are similar to those obtained in the experiments performed by Markus *et al.* (1994) and Markus & Stavridis (1994a,b). The mechanisms of the instabilities are also similar. In the light-sensitive BZ reaction the slope of the eikonal-curvature dependence was found to be both positive and humped (Markus & Stavridis, 1994a), just as in our computations. However, it is not clear which mechanisms generate the positive slope in the BZ reaction. In our model the positive slope occurs because of the large diffusion coefficient of the inhibitor. In the light-sensitive BZ reaction the diffusions of chemical species are of the same order of magnitude. However, in the case of the BZ reaction, an increase in the concentration inhibitor Br^- is determined by its diffusion coefficient multiplied by the rate constant of its auto-catalysis. It is known that light enhances the production of Br^-, and it may be this enhanced increase in the Br^- concentration which leads to the curly wavefronts and spiral breakups (Markus & Stavridis, 1994a).

The mechanism of instability that causes the spiral breakup described in this paper is fundamentally different from the 1D instability which is responsible for the earlier observations of spiral breakup (Ito & Glass, 1991; Panfilov & Hogeweg, 1993; Karma, 1993). First, it is a pure two-dimensional mechanism, and it has no counterpart in 1D systems. Secondly, not only wave trains, but also solitary waves show this instability.

Although lateral instabilities of wavefronts have not been described earlier in models for excitable media, they have been found in bistable systems (Horváth *et al.*, 1993; Hagberg & Meron, 1994). Horváth *et al.* (1993) found an unstable wavefront but no spiral breakup. Hagberg & Meron (1994) showed that lateral instability made turbulence possible through Ising-Bloch front bifurcations. An analytical study of other types of spatial instabilities of wave trains was reported by Kessler & Levine (1990).

We expect the phenomenon of spiral breakup by lateral instability to be not uncommon in excitable media and that it is probably easy to find comparable behaviour in other models of excitable media with non-fixed time-scales for the recovery variable.

Acknowledgements

We are grateful to Prof. P. Hogeweg for valuable discussions and help in this research. We wish to thank S. M. McNab for linguistic advice.

Part II

Morphogenesis of *Dictyostelium discoideum*

3

Migration and Thermotaxis of *Dictyostelium discoideum* Slugs, a Model Study

Athanasius F. M. Marée, Alexander V. Panfilov and Paulien Hogeweg
Theoretical Biology and Bioinformatics,
Utrecht University, Padualaan 8,
3584 CH Utrecht, The Netherlands.

Journal of theoretical Biology **199** (1999) 297–309

Abstract

Dictyostelium discoideum slugs show a pronounced thermotaxis. We have modelled the motion of the *Dictyostelium* slug in the absence and in the presence of a thermal gradient. Our model is an extension of the hybrid cellular automata (CA)/partial differential equation (PDE) model, as formulated by Savill & Hogeweg (1997). The modelled slugs maintain their shape and crawl, with a velocity depending on slug size, as is found in experiments. Moreover, they show thermotactic behaviour: independent of the initial orientation, after some transient process the slugs start moving along the temperature gradient. The slug behaviour in our model is due to the collective behaviour of the amoebae. Individual amoebae can neither respond to a shallow temperature gradient, nor show differentiation in motion velocity. The behaviour is achieved by a modification of the cyclic AMP (cAMP) waves: differences in temperature alter the excitability of the cell, and thereby the shape of the cAMP wave. Chemotaxis towards cAMP causes the slug to turn. We show that the mechanism still functions at very low signal-to-noise ratios.

3.1 Introduction

The cellular slime mould *Dictyostelium discoideum* is a soil protozoan that feeds on bacteria. This model organism has been extensively studied, as the life cycle of the organism provides a unique opportunity to study the relation between signal transduction at the cellular level and morphogenesis and behaviour at the multicellular level. Upon starvation, individual amoebae aggregate and form migrating multicellular slugs. During aggregation the amoebae differentiate into prestalk and prespore cells. The prestalk cells group into the front part, while the rear part consists of prespore cells. Each slug culminates in a fruiting body consisting of a globule of spore cells on a slender stalk.

The aggregation is orchestrated by waves of cAMP, which are formed by a combination of a pulsatile cAMP excretion and a cAMP-mediated cAMP response; the amoebae show a chemotactic response towards cAMP. This combination of waves of excitation and chemotaxis persists during the slug stage.

Migrating slugs are orientated by temperature gradients. This thermotaxis shows a significant temperature adaptation, with positive thermotaxis at temperatures above the temperature during aggregation, and negative thermotaxis below this temperature (Whitaker & Poff, 1980). At night, the soil surface is cooler than the subsurface mulch, and hence the slug is directed by negative thermotaxis towards the surface. At daytime the reverse is true, but the slug still moves upwards, this time due to positive thermotaxis. As a result, the slug always tends to migrate towards the soil surface where it will fruit, thus ensuring good conditions for spore dispersal (Bonner *et al.*, 1985).

How a temperature gradient is converted into tactic behaviour is not yet fully understood, but several researchers have shown that ammonia (NH_3) plays an important role in this process, since temperature influences NH_3 production significantly, and thermotaxis diminishes when slugs are surrounded by NH_3 (Bonner *et al.*, 1989). Three roles of NH_3 have been proposed. First, thermotaxis may be due to negative chemotaxis away from NH_3. Several authors have reported such negative chemotaxis, and have shown that a slug can produce sufficient concentrations of NH_3 to account for such an orientation (Bonner *et al.*, 1986; Feit & Sollitto, 1987; Kosugi & Inouye, 1989; Yumura *et al.*, 1992).

A second role of NH_3 may be that it speeds up cell motion. Bonner *et al.* (1986) reported such an increase of cell motion due to NH_3. Based on this result, a model was constructed for thermotaxis (Bonner *et al.*, 1989). However, this report is still disputed. van Duijn & Inouye (1991) found that NH_3 only slightly, non-significantly, increased the chemotactic-locomotion speed. In fact, more detailed studies reported that average slug speed may be unaffected by NH_3 or temperature gradients (Smith *et al.*, 1982; Fisher, 1997). Furthermore, Davies *et al.* (1993) reported that NH_3 did not cause any change in the chemotaxis towards cAMP.

Thirdly, NH_3 may affect the cAMP signalling. Schindler & Sussman (1979) showed that NH_3 inhibits the cAMP-induced cAMP release. The underlying mechanism is that NH_3 blocks the intracellular cAMP accumulation, due to the inhibition of the transitory activation of adenylate cyclase in response to the binding of extracellular cAMP to cell surface receptors (Williams *et al.*, 1984; Davies *et al.*, 1993). Furthermore, Darcy & Fisher (1990) produced evidence that this inhibition of the cAMP signalling is important in slug behaviour.

We use only the latter role of NH_3 in our model. As a shortcut, we model the inhibition of the cAMP relay by NH_3 as a direct (negative) influence of temperature on the excitability.

There have been several models describing slug migration (Odell & Bonner, 1986; Williams *et al.*, 1986; Umeda, 1989; Bretschneider *et al.*, 1995; Savill & Hogeweg, 1997; Dormann *et al.*, 1998). However, until now no one has used a model for slug migration to describe thermotaxis. The purpose of this study, therefore, was to determine whether thermotaxis can be achieved using basic and accepted principles of *Dictyostelium* information processing at the cellular level. To study this topic, we used the model of Savill & Hogeweg (1997) because it handles pressure, deformation, and motion in a very elegant way, and enables us to investigate thermotaxis in the context of the complete development from single cells to fruiting bodies. The model of Savill & Hogeweg is three-dimensional (3D), but for our purposes we can use two-dimensional (2D) simulations. Besides, very recently Bonner (1998) presented a new method in which migrating 2D (one cell thick) slugs are produced at a glass-mineral oil interface. This creates the opportunity to compare our results directly with the experimental findings of Bonner.

In our model, thermotaxis is achieved by a modification of the cAMP waves, due to the differences in the excitability. These differences change the shape of the wave, and chemotaxis towards the wave leads to the tactic behaviour.

3.2 The Model

We have used the hybrid CA/PDE model of Savill & Hogeweg (1997), which is based on the CA model of Glazier & Graner (1993). In this model, a CA is used to represent individual amoebae, and a PDE to model the cAMP dynamics. An important feature of the model is that each amoeba is represented as a group of connected automata. As a consequence, amoebae can slide past one another and deform themselves and adjoining amoebae by means of small changes in their boundaries.

3.2.1 Description of the amoebae

The space where the slug crawls is a 2D lattice. Each lattice square represents an automaton as well as a grid point in the numerical PDE. Each amoeba has a unique identification number, σ, which is assigned to all automata which form the amoeba. $\sigma = 0$ represents the medium. Amoebae have also a label τ, which indicates whether their cell type is prespore, prestalk or autocycling prestalk ($\tau \in \{\mathrm{p, t, a}\}$).

Each automaton that is part of an amoeba's boundary, i.e. for which one of its eight neighbouring automata does not belong to the same amoeba, has dimensionless free energy bonds. The magnitude of these bonds depends on the cell types they connect. The energy bonds are given by $J_{\tau_1,\tau_2} > 0$, where τ_i are the types of the adjoining amoebae. The bond energy between an amoeba and the medium is given by $J_{\tau,M}$. The total free energy of an amoeba is given by:

$$H_\sigma = \sum \frac{J_{\text{cell,cell}}}{2} + \sum J_{\text{cell,medium}} + \lambda(v - V)^2, \tag{3.1}$$

where v is the volume of the cell, V the target volume, and λ the inelasticity. The final term ensures that the volume of a cell remains close to V.

In order to model an amoeba deforming its shape, we use the following rule: an automaton is chosen at random and the state of one of its neighbours is copied into it with a probability of occurring given by:

$$\Delta H < -0.8, \qquad \text{Prob} = 1, \tag{3.2a}$$

$$\Delta H \geq -0.8, \qquad \text{Prob} = e^{-\left(\frac{\Delta H + 0.8}{T}\right)}, \tag{3.2b}$$

where ΔH is the change in energy *if* the copying were to occur, and T the default motility of the amoebae. These equations model minimisation of the amoeba's free energy. We chose bond energies so that the amoebae adhere to each other, and also sort themselves into three fairly homogeneous groups, if it were possible. Autocycling cells adhere to each other more rigidly than prestalk cells do, and the latter adhere to each other more rigidly than prespore cells do.

3.2.2 cAMP dynamics

The cAMP signalling system is rather complex and can be described using detailed models, such as, e.g. Martiel & Goldbeter (1987) and Tang & Othmer (1994). However, the dynamics can be described reasonably well in a quantitative way by two variable simplified equations of the FitzHugh-Nagumo (FHN) type (see e.g. Grindrod, 1996). Such a description reproduces the overall characteristics of cAMP waves such as refractoriness, eikonal-curvature relation, etc. The main advantage of these models is their simplicity and therefore their capacity to connect the effects visible in these models with basic properties of the cAMP signalling in *Dictyostelium*.

Here we investigate the basic effects of heterogeneity in the excitability, but we are not concerned with the details of cAMP signalling. So for our present purposes, the FHN-models are preferred. In this paper, we use FHN-type equations with piecewise linear 'Pushchino kinetics' (Panfilov & Pertsov, 1984). This system allows for even greater control of the refractory periods and is much faster to compute than the classical system (Panfilov, 1991):

$$\left.\begin{aligned} \frac{\partial c}{\partial t} &= D_c \Delta c - f(c) - r, \\ \frac{\partial r}{\partial t} &= \varepsilon(c)(kc - r), \end{aligned}\right\} \text{ inside the amoebae} \tag{3.3}$$

$$\left.\begin{aligned} \frac{\partial c}{\partial t} &= D_c \Delta c - d_c(c - c_0), \end{aligned}\right\} \text{ outside the amoebae} \tag{3.4}$$

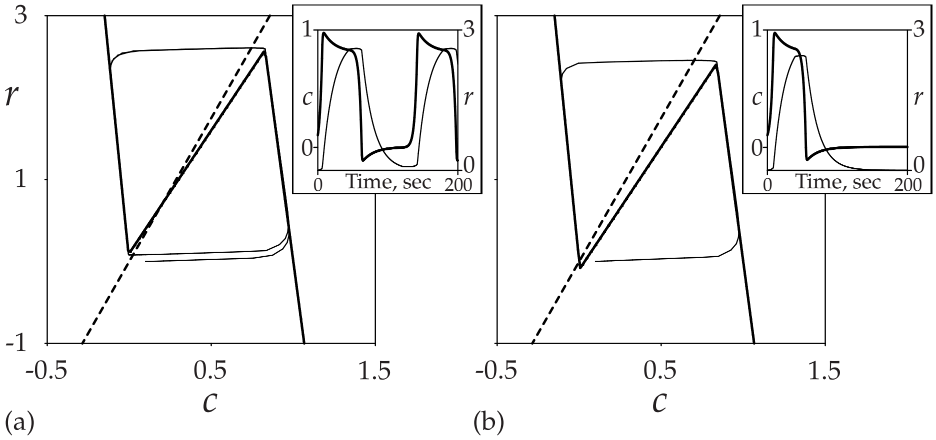

Figure 3.1. Phase plane of c and r for (a) $a_\tau = -0.1$; and (b) $a_\tau = 0.1$. The thick solid lines denote the $dc/dt = 0$ nullclines, the thick dashed lines denote the $dr/dt = 0$ nullclines. The thin lines depict trajectories starting from $c = 0.1$ and $r = 0$. The insets show the corresponding behaviour of c (thick lines) and r (thin lines) in time. Parameters: $C_1 = 20$, $C_2 = 3$, $C_3 = 15$, $\varepsilon_1 = 0.5$, $\varepsilon_2 = 0.0589$, $\varepsilon_3 = 0.5$, and $k = 3.5$.

with $f(c) = C_1 c$ when $c < c_1$; $f(c) = -C_2 c + a_\tau$ when $c_1 \leq c \leq c_2$; $f(c) = C_3(c - 1)$ when $c > c_2$ and $\varepsilon(c) = \varepsilon_1$ when $c < c_1$; $\varepsilon(c) = \varepsilon_2$ when $c_1 \leq c \leq c_2$ and $\varepsilon(c) = \varepsilon_3$ when $c > c_2$. To make the function $f(c)$ continuous, $c_1 = a_\tau/(C_1 + C_2)$ and $c_2 = (a_\tau + C_3)/(C_2 + C_3)$. c represents cAMP concentration, and r refractoriness of the cells. Outside the amoebae a small decay d_c of cAMP, caused by external phosphodiesterase, is implemented. The arbitrary zero level c_0 is chosen such that cAMP leakage into the medium does not decrease the period of autocycling.

Weijer *et al.* (1984) showed that the tip of the slug can be seen as a high-frequency pacemaker, whereas the body of the slug just conducts waves of cAMP. We can model this in the following way. For positive values of parameter a_τ, the model describes an excitable medium, while for negative values of a_τ, a stable limit cycle appears in phase space. Therefore, to describe the excitable amoebae, we have chosen $a_p = a_t = 0.1$, whereas to describe the autocycling amoebae in the tip, $a_a = -0.1$.

To illustrate these basic properties of the model, we plot in Fig. 3.1 the phase plane of c and r. Figure 3.1(a) shows the situation when $a_\tau = -0.1$. The nullclines intersect at an unstable equilibrium point, and the dynamics show a stable limit cycle. The inset shows the oscillatory behaviour in time. Figure 3.1(b) shows the phase plane when $a_\tau = 0.1$. Now the equilibrium point is stable, and the system relays a cAMP signal if the initial concentration of cAMP exceeds the threshold value.

We simplify the whole process of differential NH_3 production due to the temperature gradient, followed by differential inhibition of the cAMP-modulated cAMP response due to NH_3, by stating that the temperature gradient causes a spatial gradient in the excitability. We have chosen to model the differences in the excitability by changing the value of a_τ, since in this model a_τ represents the threshold for cAMP relay, which is directly related to the excitability. We superimpose on the values of a_τ a gradient along the y-axis, with a slope of a_{grad} per grid point, and with decreasing excitability from top to bottom. We normalise the gradient by taking the upmost automaton that is occupied by the slug as the reference point to calculate all a_τ values. We use a normalised gradient to assure that the behaviour is independent of the location of the slug in the field.

3.2.3 Chemotaxis

The natural way to incorporate chemotaxis in the model is to use the spatial gradient of the cAMP wavefront. We do this by modifying the change in energy ΔH in eqn (3.2), and hence the probability of the neighbour copying its state into the automaton, as a function of the difference in the cAMP concentrations in the two automata (Savill & Hogeweg, 1997):

$$\Delta H' = \Delta H - \mu(c_{\text{automaton}} - c_{\text{neighbour}}), \tag{3.5}$$

where $\Delta H'$ is the new change in energy. This equation implies that an amoeba is more likely to move to an area with a higher cAMP concentration and less likely to move to an area with a lower cAMP concentration. All amoebae obey this rule and μ is invariant over all amoebae. Since the amoebae only move chemotactically during a short period after arrival of the cAMP wave, rule (3.5) is only applied when c is above a threshold $c_{th} = 0.05$ and r below a threshold $r_{th} = 0.2$.

3.3 Slug Migration

In all simulations a slug is initiated with a tip consisting of autocycling prestalk cells, and a body consisting of 40% prestalk and 60% prespore cells.

Figure 3.2(a) shows slug motion in a simulation without thermotaxis. Repeatedly the chemotactic signal spreads from the autocycling cells in the tip towards the posterior part of the slug. The subsequent chemotactic motion pushes the tip forwards, and as a result the whole slug moves ahead. We see that the slug does not follow a straight line. Its trail shows alterations in direction, caused by small variations in the way the tip is pushed forwards.

3.3.1 Stability of the slug shape

As can be seen in Fig. 3.2, during the simulations, which take up 300 000 time steps (8 hours and 20 minutes), the shape of the slug is approximately fixed. This stable configuration results from two forces; one elongates the slug, and the other one rounds it. The surface tension forces the slug to round, since this is the optimal low-energy configuration, whereas the convex-shaped cAMP wave causes a motion of the amoebae towards the central axis, and therefore forces the slug to elongate.

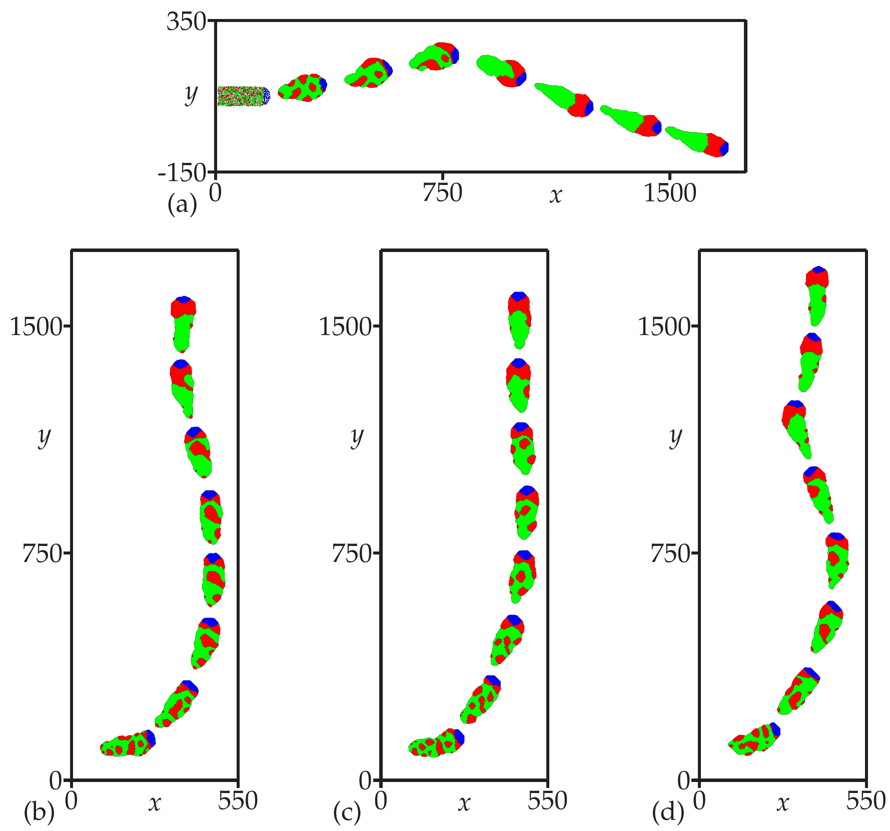

Figure 3.2. Time sequences from simulations of motion during the slug stage of *Dictyostelium*. (a) Motion without a temperature gradient. (b) Simulation of thermotaxis with a temperature gradient from top to bottom. (c) Simulation of thermotaxis with Gaussian noise on the a_τ parameter at every grid point, with a refreshment rate of 2 seconds (20 time steps). (d) A simulation of thermotaxis with Gaussian noise on the level of the amoebae. The first frame in (a) shows the initial distribution for all four simulations; the first frames in (b), (c) and (d) show the state after 30 minutes (18 000 time steps). Successive frames with intervals of 1 hour (36 000 time steps). The axes are in grid points. There are 430 amoebae. One time step (solution of the PDE) corresponds to about 0.1 seconds and one grid point to 5 μm. Cell types are $\tau \in \{\mathrm{a, t, p}\}$ where a is autocycling prestalk (blue), t is prestalk (red), and p is prespore (green). Bond energies are $J_{a,a} = 3$, $J_{t,t} = 5$, $J_{p,p} = 7$, $J_{a,M} = 7$, $J_{t,M} = 8$, $J_{p,M} = 9$, $J_{a,t} = 6$, $J_{t,p} = 8$, $J_{a,p} = 9$. $T = 2$, $V = 30$, $\lambda = 0.6$ and $\mu = 200$. The parameters used for the PDE equations are $D_c = 1$, $c_0 = -0.3$, $d_c = 0.05$, and $a_{\mathrm{grad}} = 6 \times 10^{-4}$. Other parameters are as described in the legend to Fig. 3.1. Gaussian noise with mean = 0 and standard deviation (S.D.) = 0.02. The PDE equations are solved by the explicit Euler method (with time step equal to 0.01 and space step equal to 0.37). See also the colour plate on page 72.

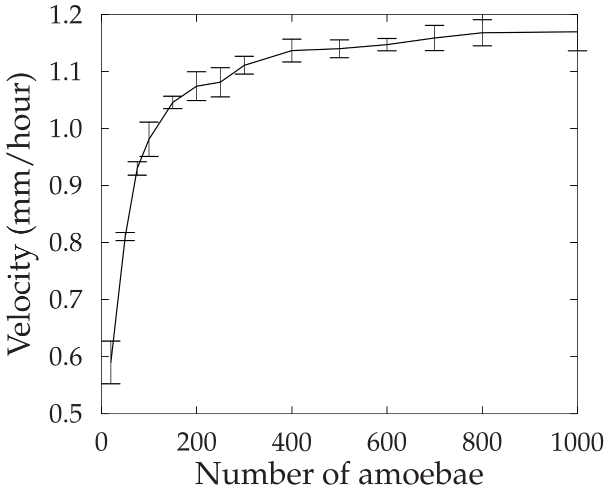

Figure 3.3. Plot of the velocity of the slug versus the number of amoebae during non-thermotactic motion. The means and standard error of mean (S.E.M.) (indicated by the bars) of five simulations per data point are presented. 1 mm/hour equals 0.0056 grid point per time step. All parameters are as described in the legend to Fig. 3.2(a).

Different surface tensions lead to different slug shapes. Hence we chose the values of $J_{\tau,M}$ so that the surface tension between the cell types and the medium, which is defined by Glazier & Graner (1993) as $J_{\tau,M} - \frac{1}{2}J_{\tau,\tau}$, is equal for all cell types.

The convex shape of the cAMP wave is caused by two factors: first, every new cAMP wave originates as a circular wave from a point source, which immediately leads to a convex wave shape. Secondly, the speed of the cAMP wave is lower at the slug boundary, because amoebae along the boundary of the slug are less excitable, due to loss of cAMP into the surrounding medium.

In our computations we have chosen an initial shape which is close to the final shape of the slug. By starting with another shape, which is thinner or thicker than the optimal shape, one adds extra transient behaviour, but the final configuration is the same.

3.3.2 Motion velocity

Figure 3.3 shows the relation between the slug mass and the motion velocity. To measure motion velocity, tracks of slugs were followed during $5\frac{1}{2}$ hours (200 000 time steps). We see that if a slug consists of 20 amoebae, velocity is only 50% of the maximum velocity, while larger slugs clearly move faster. This increase in motion velocity seems to saturate when the number of amoebae gets close to 1 000. Our results are consistent with the experimental data: it is known from experiments that the slug velocity increases with increase in the slug size (Bonner *et al.*, 1953;

Smith *et al.*, 1982), and Inouye & Takeuchi (1979) showed the saturation of velocity increase for large slugs.

The velocity increase we found is on the one hand due to the fact that more amoebae create more motive force to push the autocycling area forwards, since this region does not create a motive force by itself. On the other hand, to the fact that the motive force created by the slug does not solely depend on chemotaxis towards cAMP. Also the accompanying volume changes, and the binding strengths as well as the surface tension play an important role: First, due to the binding forces between the amoebae, amoebae start moving before the cAMP wave arrives, as they are pulled towards the chemotactically moving amoebae. Secondly, the surface tension creates a forward motion to fill up the dents in the slug shape just posterior of the cAMP wave. Thirdly, due to volume decrease during the chemotactic motion, as many cells push inwards, motion lasts after the cAMP wave has passed, to re-establish the old volume. Since all these depend on the slug size, the motion is faster when the slug is larger.

The saturation in volume increase with size, as described by Inouye & Takeuchi (1979), occurs in slugs with much larger number of amoebae than in our finding. This can be caused by the fact that we performed 2D simulations, and can be due to scaling reasons.

3.3.3 Cell sorting

It has been known for some time that cell sorting takes place mainly during the mound stage that precedes the slug stage. However, both dissociation experiments (Sternfeld & David, 1981) and transplantation experiments (MacWilliams, 1982) have shown that slugs are still fully capable of exhibiting cell sorting.

In our simulations we start from a random distribution of prestalk and prespore cells, and after 4 hours prestalk and prespore cells are completely sorted out. In our model, this cell sorting is solely due to differential adhesion, since there are no other differences between the cell types. When $J_{\tau,\tau}$ is smaller, amoebae with the same inelasticity λ deform less, since the final term in eqn (3.1), which ensures volume conservation, is relatively more important. As a consequence, the extra motive force of pulling the cells forwards is larger. In contrast, when $J_{\tau,\tau}$ is larger, the amoebae just deform and hence have a relatively slower motive speed. Thus, to obtain autocycling cells in the tip, followed by prestalk cells, and finally prespore cells, $J_{a,a} < J_{t,t} < J_{p,p}$. The binding energies between the cell types are less important for cell sorting. They are kept high enough to assure that the cell types do not mix, and are kept low enough to assure that amoebae of different cell types are still able to slide past one another, which is necessary for large-scale cell sorting.

In our simulations, if a clump of autocycling cells are positioned closely behind the tip, these cells become entrained to the cAMP signalling from the tip, and moreover, after some time, by the process of cell sorting as described above, the clump reunites with the autocycling cells in the tip (results not shown). Only if either the clump or the difference in the excitability with the surrounding cells is large enough, these cells themselves become a new source of cAMP signalling,

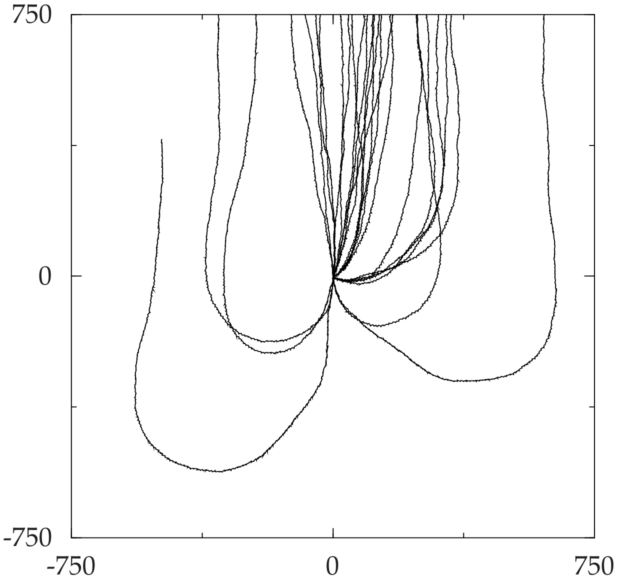

Figure 3.4. Change of the slug location in time, during 8 hours and 20 minutes (300 000 time steps). The location at $t = 0$ is set to (0,0), and the axes are in grid points. 25 simulations are presented, at an initial angle of 0, 45, 90, 135, or 180 degrees, and with five simulations per angle. $a_{\text{grad}} = 1.2 \times 10^{-3}$, all other parameters are as described in the legend to Fig. 3.2(b).

which, after some time, results in the break up of the slug into two small ones.

3.4 Thermotaxis

We were able to reproduce thermotaxis of the *Dictyostelium* slug. Figure 3.2(b) shows slug motion in a field with a temperature gradient directed from top to bottom. Initially the slug is orientated at an angle of 90 degrees to the direction of the gradient. Yet within 3 hours the slug orientates itself towards the gradient.

Figure 3.4 shows the tracks of *Dictyostelium* slugs from 25 different simulations, with initial angles of 0, 45, 90, 135, and 180 degrees to the temperature gradient. It can be seen that the final direction of motion does not depend on the initial angle. Even if the initial angle is 180 degrees, standard irregularities in the track cause small deviations in the angle that are large enough to elicit the subsequent turn, either to the left or to the right.

3.4.1 Mechanism of thermosensitivity

In our model, we assume a temperature dependence of the cAMP-induced cAMP release (presumably mediated by NH_3). We implement this as a change in the ex-

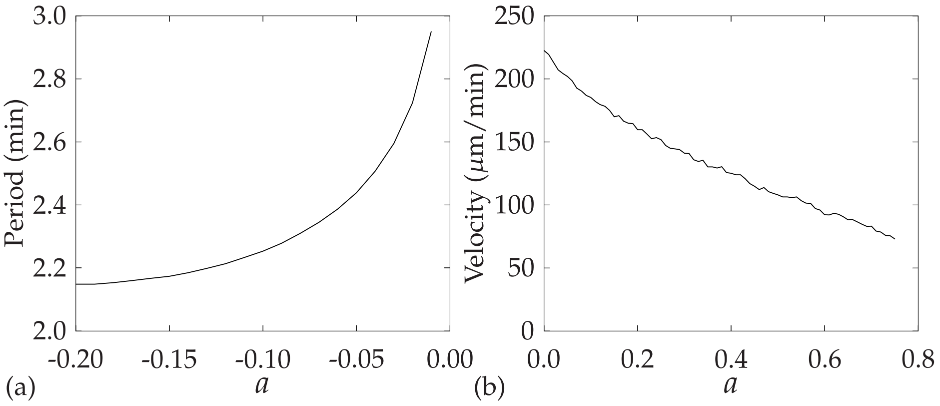

Figure 3.5. Plot of the autocycling period in the oscillatory regime (a), and the velocity of the cAMP wave in the excitable regime (b), versus parameter a. The period increases, while the velocity decreases with increasing a. 1 minute equals 600 time steps and 100 μm/minute equals 0.033 grid point per time step.

citability, i.e. by a modification of the value of the a_τ parameter. Hence, we change the cAMP threshold. An increased threshold changes both the period of autocycling and the velocity of the cAMP wave. Figure 3.5(a) shows the dependence of the period on a in the oscillatory regime, i.e. for negative values of a. Figure 3.5(b) shows the dependence of the velocity on a in the excitable regime, i.e. for positive values of a (note that in the oscillatory regime wave velocity depends on both period and relay). For reasonable values of a the period increases with increasing a, and over the whole range of values the velocity decreases. Both are important for the mechanism of thermotaxis as they influence both the source of the cAMP signal and the shape of the cAMP wave.

Figure 3.6 shows a close up of the cAMP wave. Figure 3.6(a) shows the cAMP wave during normal motion, while Fig. 3.6(b) shows the wave during thermotaxis. To emphasise the effect of the temperature gradient on the shape of the cAMP wave, we have chosen a rather high value of $a_{\text{grad}} = 2.5 \times 10^{-3}$. During thermotaxis, the source of the signal in the autocycling area shifts upwards, since in the upper direction a values are lower, and subsequently the autocycling period is shorter. Besides, as a result of the dependence of wave speed on a, the wave moves faster at the upper side compared to the lower side. As a consequence of both, the wavefront becomes slanted. However, the slant increases only up to a certain level, since it coincides with a curvature difference that limits the slant, due to the so-called curvature-effect.

Since the amoebae move perpendicular to the wavefront, a motive force is created that pushes the autocycling area upwards, and with it the source of the cAMP signal, thus initiating the turn towards the temperature gradient.

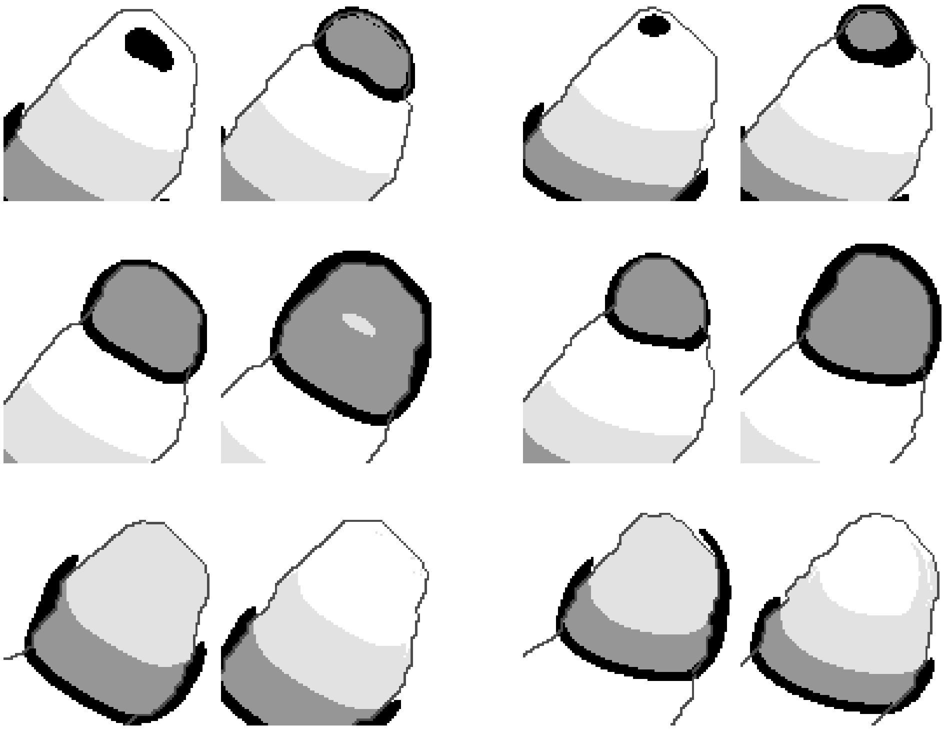

(a) (b)

Figure 3.6. Propagation of the cAMP wave: (a) during normal motion; and (b) during thermotaxis. During thermotaxis, the wave starts at a position shifted into the upper direction, and is slanted to the left. Successive frames after 15 seconds, 30 seconds, 1 minute, $1\frac{1}{2}$ minute, and 2 minutes (150, 300, 600, 900, and 1 200 time steps). Black shows the area where $c > c_{th}$ and $r < r_{th}$ (the wavefront); dark grey the area where $c > c_{th}$ and $r > r_{th}$ (the waveback); and light grey represents the area where $c < c_{th}$ and $r > r_{th}$ (the refractory period). $a_{\text{grad}} = 2.5 \times 10^{-3}$, all other parameters are as described in the legend to Fig. 3.2(a) and (b).

3.4.2 Thermosensitivity and the influence of stochastic noise

We studied thermosensitivity as a function of a_{grad}. Figure 3.7 shows the tracks of slugs from simulations with different gradient strengths. In all simulations, the initial angle is 90 degrees to the temperature gradient. In Fig. 3.7(a) and (b), we see that when the gradient is very steep, the slugs show a rapid turn towards the temperature gradient. After this turn, the track is very stable and perfectly aligned along the temperature gradient. In Fig. 3.7(c) and (d), we see that when the gradient becomes more shallow, turning of the model slug takes increasingly more time, and the final track becomes more and more unstable. In Fig. 3.7(e) the gradient is as small as $a_{\text{grad}} = 1.5 \times 10^{-4}$. Although the slugs do not move

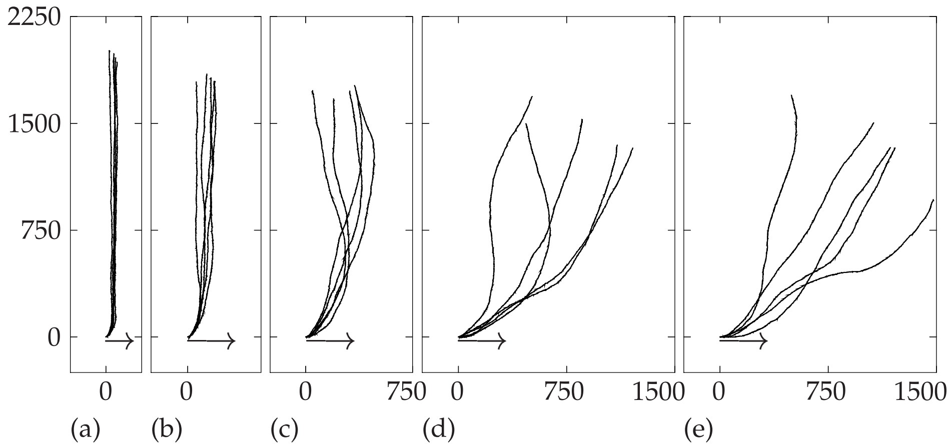

Figure 3.7. Change of the slug location in time, for different gradient strengths. The location at $t = 0$ is set to (0,0), axes are given in grid points, and the simulations lasted for 8 hours and 20 minutes (300 000 time steps). (a) $a_{\mathrm{grad}} = 2.5 \times 10^{-3}$; (b) $a_{\mathrm{grad}} = 1.2 \times 10^{-3}$; (c) $a_{\mathrm{grad}} = 6 \times 10^{-4}$; (d) $a_{\mathrm{grad}} = 3 \times 10^{-4}$; and (e) $a_{\mathrm{grad}} = 1.5 \times 10^{-4}$. All other parameters are as described in the legend to Fig. 3.2(b). For each gradient five simulations were done. In all simulations, the slug was initially positioned under an angle of 90 degrees with respect to the temperature gradient. The arrows indicate this initial orientation.

along the temperature gradient, they still move in the right direction. Note that we even found thermosensitivity for much smaller a_{grad}, i.e. $a_{\mathrm{grad}} = 6 \times 10^{-5}$.

However, in an environment with such shallow gradients, one expects to find a relatively high level of disturbance on the signal. Besides, there must exist some variation in the excitability between individual amoebae. Therefore, an important question is whether an addition of noise to the values of a_τ reduces or diminishes thermotaxis.

To test the sensitivity to disturbances, spatiotemporal Gaussian noise is added to the value of a_τ, with a refreshment rate of 2 seconds (20 time steps). We expect that in real slugs disturbances are high, relative to the shallow gradients at which a *Dictyostelium* slug still exhibits thermotaxis. Therefore we use a high noise term, with a normal distribution of mean=0, and S.D.=0.02, i.e. which is more than 30 times as large as a_{grad}. Figure 3.8 gives an impression of the signal to noise ratio for a certain moment in time. The ordinate denotes the location of the slug in the y-direction, the abscissa gives the corresponding increase of a_τ. The solid line shows the gradient in the absence of noise. The dots show the increase of a_τ for all individual automata in the presence of noise. Note that the gradient is very difficult to detect when noise is present. Figure 3.2(c) shows a simulation with this spatiotemporal noise. In spite of the high level of noise, both precision and turning velocity are not decreased. In fact, noise levels have to be increased more than ten times before thermotaxis diminishes.

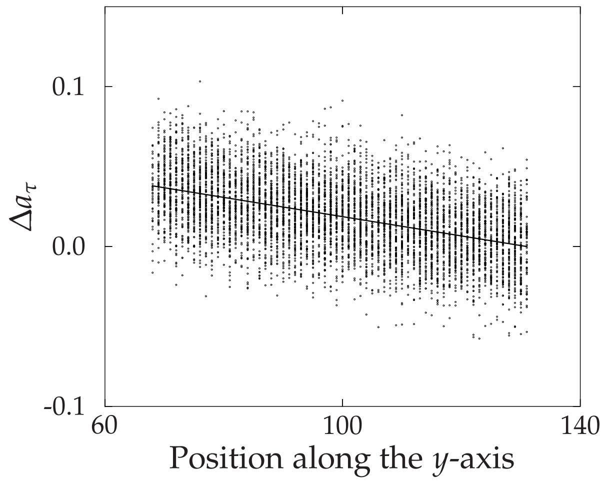

Figure 3.8. Plot of Δa_τ as a function of the y position at time $t = 0$ for the simulations in Fig. 3.2(b) and (c). The solid line shows the Δa_τ distribution in the absence of noise. The dots show the values of Δa_τ for all individual automata in the presence of noise.

Secondly, we create heterogeneity in the amoebae population. The same level of variation is used as in the previous simulation, but this time only one noise value is used for all grid points which are part of the same amoeba. This value is fixed during the whole simulation. Figure 3.2(d) shows such a simulation. Although the track is less stable compared to simulation 3.2(c), thermotaxis is still strong. Noise levels can be increased up to 60 times the gradient strength, but at higher values of the noise S.D., different sources of cAMP waves appear, which break the slug into an increasingly higher number of ever smaller slugs.

The mechanism behind this high resistance against noise is that the cAMP wave functions as a spatiotemporal integrator. Due to the curvature-effect, the cAMP wavefront is always a relatively smooth line. Differences in position are found only over longer distances. Consequently, the shape, as observed, results from the information integrated over longer time and larger distances. And since it is the chemotaxis towards this wave that gives rise to the thermotactic behaviour, global information integration becomes possible. The same process makes it possible to measure extremely small gradients, despite some internal noise generated by the model itself.

In the second experiment, with variation at the level of the individual amoebae, the variations are both temporally and spatially on a larger scale. Therefore, thermotaxis is more disturbed by this kind of noise.

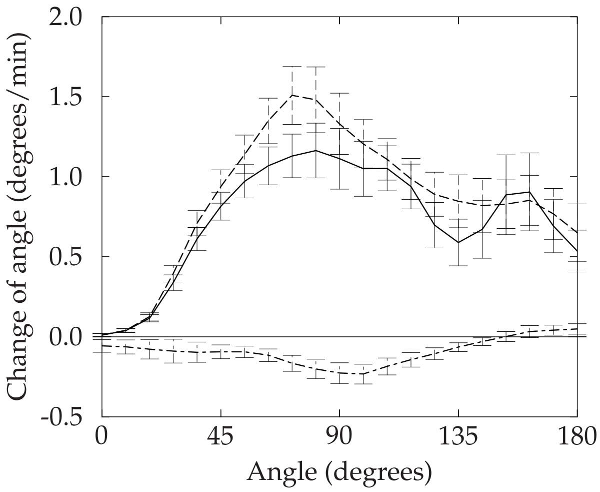

Figure 3.9. Change in the angle towards the thermal gradient versus the position the slug takes up relative to this gradient. The dashed line shows the change in the angle when only the autocycling cells in the tip of the slug are sensitive to temperature; the dashed-dotted line when only the non-autocycling cells in the body are sensitive; and the solid line when all cells are sensitive. $a_{\text{grad}} = 1.2 \times 10^{-3}$, all other parameters are as described in the legend to Fig. 3.2(b). The means and S.E.M. (indicated by the bars) of 10 simulations per line are presented. The means and S.E.M. were calculated at intervals of 9 degrees, using a Gaussian smoothing with an S.D. of again 9 degrees. The change of angle is calculated using a time difference of 2 minutes 30 seconds (1 500 time steps). Note that the direction of change of angle is towards the thermal gradient, i.e. the positive change means a decrease of the angle between the slug orientation and thermal gradient.

3.4.3 A partially thermosensitive slug

Several researchers have stated that the process of orientation is located in the slug tip (Smith *et al.*, 1982; Fisher, 1997). This could either indicate that there is an inherent difference between the different cell types, for example that only autocycling amoebae in the tip are thermosensitive, or that there is a functional difference between parts of the slug, i.e. all amoebae share the same thermosensitivity, but differ in behaviour solely due to their relative position inside the slug.

Figure 3.9 shows the velocity at which slugs turn towards the temperature gradient. The turning velocity is calculated using data from 10 simulations per line, taking into account the symmetry left and right of the direction of the gradient. The figure shows the differences in the turning velocity, whether or not the tip or the rest of the slug is thermosensitive.

If the slug tip is not thermosensitive, indeed no thermotaxis whatsoever can be observed. On the other hand, desensitising the rest of the slug has no negative effect on thermotaxis. For certain angles the turning velocity is even slightly higher. Still, both when the whole slug is thermosensitive and when only the tip is thermosensitive, slugs turn with approximately the same velocity and the same precision towards the temperature gradient.

3.5 Discussion

3.5.1 Slug motion and cell sorting

We have shown that our model can reproduce important features and processes which occur in the slug, such as slug motion, cell sorting, shape conservation and the dependence of slug velocity on its mass.

In the model we have developed, the motive force is obtained by a combination of chemotaxis towards cAMP and cell adhesion (see also Savill & Hogeweg, 1997). Instead, Williams *et al.* (1986) suggested that circumferential cells may squeeze and push forwards the inner cell mass, while Odell & Bonner (1986) suggested that this may be achieved by a fountain-like circulation of cells. However, fluorescence images indicated neither the circumferential movement of cells toward the inner cell mass nor active movement backwards (Yumura *et al.*, 1992).

Siegert & Weijer (1992) showed that 3D scroll waves organise the tip. Based on these results, Bretschneider *et al.* (1995) made a model to describe slug motion directed by scroll waves, which is essentially the same mechanism as we use. For reasons of simplicity, we did only simulations in 2D, and therefore, such waves were not possible in our simulations. However, behind the tip the scroll wave rapidly breaks up into planar waves, due to decreasing excitability (Dormann *et al.*, 1996). We state that in our model we focused on these planar waves. Obviously, 3D simulations will extensively enlarge the set of possible behaviours, but the recent experiments of Bonner (1998) show that all observations of 2D slugs are consistent with what one finds in normal 3D slugs.

In all our simulations, we used a tip consisting of oscillatory amoebae, while the rest of the slug only relayed the signal. However, the change in the excitability might be much more gradual, with many more cells being in the oscillatory regime (Siegert & Weijer, 1992; Dormann *et al.*, 1996). Therefore we performed a number of control experiments, in which all cells were oscillatory, although the tip cells were still the most excitable ones ($a_t = a_p = -0.05$). All other conditions were kept the same. This caused no qualitative differences in any model behaviour: the high-frequency oscillations in the tip still enforce the global cAMP dynamics.

In order to obtain a stable shape of the slug, in our model, it is necessary to have a convex wave shape, which is caused by the reduced relay at the slug boundaries. In real slugs this can be a consequence of the fact that migrating slugs are covered with slime sheath, a viscous extracellular matrix secreted by its cells. We have not explicitly modelled the slime sheath, but we interpret the diffusive loss of cAMP as being due to diffusion into this sheath. However, if we use Neumann boundary conditions, which means that there is no flux of cAMP through the boundary and hence no reduced relay, all other behaviour, such as slug motion, cell sorting and thermotaxis, are still preserved. That is, only the shape becomes inconsistent.

During the slug stage, cell redifferentiation still occurs, but it is likely to be a marginal and slow process (Schaap *et al.*, 1996), and was left out of the model. Instead we focused on cell sorting. In our simulations, we used 40% prestalk cells, while a more realistic value is around 25%. Reducing the percentage of prestalk cells in our computations to 25% does not significantly change the results of our paper: complete cell sorting is still observed, although on a slightly longer time-scale. Hence, to present both thermotactic behaviour and cell sorting in the same time sequence, we increased the number of prestalk cells used. Cell sorting with a small amount of prestalk cells is slow due to the formation of very small clumps of prestalk cells. This is mainly a side-effect of our 2D approach, since in 3D larger clumps are immediately formed, as a result of the higher amount of neighbouring amoebae (Savill & Hogeweg, 1997).

Umeda (1989) proposed a model for cell sorting, based on differential motive forces, and Bretschneider *et al.* (1997) also used differential chemotaxis to model sorting. However, Sternfeld (1979) found evidence that the cell sorting depends on differential cellular adhesion, and recently, Ginger *et al.* (1998) have found a cell surface protein which is important for both cell adhesion and cell sorting.

Sternfeld & David (1981) found that during the process of cell sorting, cAMP is also very important. In our model, the cell sorting takes place during the cell motions that accompany the cAMP waves. We find very slow and incomplete cell sorting when we do not include the chemotactic motion towards cAMP. This is in agreement with the above finding, as well as with the results of Tasaka & Takeuchi (1981), which show that cell sorting is facilitated by the movement of the amoebae.

MacWilliams (1982) and Meinhardt (1983) found that injecting prestalk cells into the rear part of a slug leads either to a movement of these cells towards the tip, or to the induction of a new tip, followed by the separation of a second slug. This is also in agreement with our results as described in section 3.3.3.

Bonner (1998) found that the amoebae in the tip of 2D slugs move around in a chaotic fashion, while the posterior cells move straight on. In our model, we find the same behaviour: in the tip all amoebae try to move towards the source of the cAMP signal, thereby creating chaotic and swirling motion. Behind the tip the closed cAMP wave leads to straight motion.

In our model, motion is far more continuous, compared to the pulsatile cAMP signal, due to the pushing and pulling at large distances from the wavefront. The small 2D slugs that Bonner (1998) has described, do also not exhibit sharp pulsatile motion.

3.5.2 Thermotaxis

We have shown that thermotaxis of *Dictyostelium* slugs can be explained solely by means of a temperature dependence of the cAMP-induced cAMP release and the consequences thereof for the excitability. It changes the shape of the cAMP wave, and chemotaxis towards the wave leads to the tactic behaviour: independent of the initial orientation, the slug turns towards and, afterwards, moves along the temperature gradient. The slug has a very high sensitivity, since even in the presence of extreme noise in the system (the signal-to-noise ratio can be as small as 1/300), it receives the temperature signal.

The slug behaviour in our model is due to the collective behaviour of the amoebae, as the temperature gradient is too shallow to be measured by individual amoebae. Instead, the information is first encoded as differences in the excitability.

The aim of this study was to describe the basic processes which can give rise to thermotactic behaviour. We have not modelled the translation of differences in temperature into differences in excitability. We assume that this process involves chemicals such as NH_3, and maybe several other chemicals, such as Slug Turning Factor (STF) (Fisher, 1997). In our paper, we have used a linear gradient which we normalised within the slug. In our view, such normalisation is a good approximation of slug behaviour at a short time-scale. However, at longer time-scales, the relation between temperature and excitability is clearly more complicated, since both positive and negative thermotaxis are observed, as well as slow adaptations to the absolute temperature (Whitaker & Poff, 1980). For very shallow gradients, we do not need adaptive processes (in our implementation: normalisation of the gradient) in our model, for excitability can be coupled directly to the absolute temperature. However, to describe larger temperature differences an adaptive process is necessary. Instead of the normalisation used here, the model could be extended with an extra equation for a, depending on temperature, which describes the differences in the excitability at a fast time-scale, as well as a return to the basal level at a slow time-scale. With such an extension, one could model the negative thermotaxis as well as the adaptation and compare both with observed experimental behaviour.

There has been a fair amount of dispute whether NH_3 speeds up the amoebae. Therefore, we did not include an increase in velocity due to NH_3 in our model. We do not state that amoebae under no conditions will have such a stronger motive force, but we show that it is not a necessary condition for thermotaxis: if there are differences in NH_3, which change excitability only, thermotaxis can already be found.

Recently, Bonner (1998) has concluded that his idea of differences in the speed of motion to explain thermotaxis is not consistent with what one sees in 2D slugs. Instead, he observes that many different and changing cells are involved in pushing the tip into a different direction, which is exactly in agreement with our results.

In our model, it is mainly the tip that controls the orientation, which is in agreement with experimental findings. However, continuous cell sorting and differentiation during the slug motion, which is accompanied by ongoing changes in position, makes it unlikely that only the tip is thermosensitive, since it is observed that such a special property is not needed for thermotaxis.

A very high number of genes are in one way or another related to thermotaxis (Fisher, 1997). We did not aim to include in our model all that is known, but instead we focused on the question which types of behaviour can be understood from some basic principles of signal transduction in *Dictyostelium*. In this light, the function of all these genes might be interpreted as the tuning of the parameters to get the favoured behaviour.

This method of cell modelling lends itself excellently for describing the morphogenesis of *Dictyostelium discoideum*, since the different behaviours observed during the developmental process are entirely driven by the local movements and responses of individual amoebae. It was used earlier to describe the process of aggregation, mount formation and slug motion (Savill & Hogeweg, 1997), and is used here to describe a range of observed behaviours during the slug stage. By extending the model once again to 3D, the next stages of development, as well as other facets of *Dictyostelium* morphology, may be clarified.

Acknowledgements

We are grateful to Nick Savill for helpful discussions. A. F. M. Marée was supported by the Priority Program Nonlinear Systems of the Netherlands Organization for Scientific Research.

4

Phototaxis during the Slug Stage of *Dictyostelium discoideum*: a Model Study

Athanasius F. M. Marée, Alexander V. Panfilov and Paulien Hogeweg
Theoretical Biology and Bioinformatics,
Utrecht University, Padualaan 8,
3584 CH Utrecht, The Netherlands.

Proceedings of the Royal Society of London. Series B. Biological sciences **266** (1999)
1351–1360

Abstract

During the slug stage, the cellular slime mould *Dictyostelium discoideum* moves towards light sources. We have modelled this phototactic behaviour using a hybrid cellular automata (CA)/partial differential equation (PDE) model. In our model, individual amoebae are not able to measure the direction from which the light comes, and differences in light intensity do not lead to differentiation in motion velocity among the amoebae. Nevertheless, the whole slug orientates itself towards the light. This behaviour is mediated by a modification of the cyclic AMP (cAMP) waves. As an explanation for phototaxis we propose the following mechanism, which is basically characterised by four processes: (i) light is focused on the distal side of the slug as a result of the so-called 'lens-effect'; (ii) differences in luminous intensity cause differences in ammonia (NH_3) concentration; (iii) NH_3 alters the excitability of the cell, and thereby the shape of the cAMP wave; and (iv) chemotaxis towards cAMP causes the slug to turn. We show that this mechanism can account for a number of other behaviours that have been observed in experiments, such as bi-directional phototaxis and the cancellation of bi-directionality by a decrease in the light intensity or the addition of charcoal to the medium.

4.1 Introduction

Upon starvation, individual amoebae of the micro-organism *Dictyostelium discoideum* start to aggregate and form migrating multicellular slugs. During the slug stage prestalk cells group in the anterior part of the slug, whereas prespore cells end up in the posterior part. Each slug culminates in a fruiting body consisting of a globule of spore cells on a slender stalk. The motion of amoebae is orchestrated by waves of cAMP, which are formed by a combination of a pulsatile cAMP excretion and a cAMP-mediated cAMP response. This is accompanied by a chemotactic response towards cAMP.

Migrating slugs are orientated by light (phototaxis), temperature gradients (thermotaxis), pH differences (acidotaxis), and wind (rheotaxis). The orientation towards light (as well as towards the other cues) leads to migration towards the soil surface, which is beneficial for spore dispersal (Bonner *et al.*, 1985).

A slug starts to turn towards a light source after 10 minutes of irradiation by light coming from one side (Yumura *et al.*, 1992). Phototaxis and thermotaxis must use different pathways, because even light intensities too low to cause a local increase in temperature elicit a response. During phototaxis the slug functions as a lens that focuses light on the side opposite to the light source. This so-called 'lens-effect' was first postulated by Buder (1920) for *Phycomyces*, and was shown by Francis (1964) to be the mechanism in *Dictyostelium* (see also Poff *et al.*, 1986). Several researchers have confirmed this lens-effect by, for example, illuminating only half of the slug (Francis, 1964), placing the slug in mineral oil (Bonner & Whitfield, 1965), or introducing neutral red into the cells (Häder & Burkart, 1983). In all these cases it has been found that a slug orientates away from the light, because light is prevented from focusing on the distal side, but instead illuminates the proximal side more, due to absorption.

It is not yet fully understood how the light signal is transformed into tactic behaviour. Bonner *et al.* (1988) argued that NH_3 could play an important role in this process, because they found that, on the one hand, light causes slugs to produce NH_3, whereas on the other hand, the response to light diminishes when the slugs are completely surrounded by NH_3. Several authors have reported negative chemotaxis away from NH_3, and have shown that the amount of NH_3 produced by slugs is sufficient for such a motion (Bonner *et al.*, 1986; Feit & Sollitto, 1987; Kosugi & Inouye, 1989; Yumura *et al.*, 1992).

Francis (1964) suggested that light may speed up cell motion, and that this could be a sufficient explanation for phototaxis. This led to the hypothesis that light stimulates the local production of NH_3, which, in turn, stimulates the cells to move faster, forcing the slug to turn towards the light (Bonner *et al.*, 1986, 1988). However, there is still a dispute about whether NH_3 does indeed speed up cell motion, since more detailed studies reported that average slug speed may be unaffected by NH_3 or light, and not even a transient increase could be detected (Smith *et al.*, 1982; Fisher, 1997). Furthermore, Davies *et al.* (1993) did not find that NH_3 caused any change in chemotaxis towards cAMP.

During phototaxis the trails of slugs belonging to certain mutant strains can become unstable, bi-directional (Fisher & Williams, 1981), or even multidirectional (Fisher *et al.*, 1985). We specifically focus on the bi-directional mutants. At low light intensities their bi-directionality decreases, or even disappears (Poff *et al.*, 1986). Moreover, even at high light intensities the trail of such mutants can be made more stable and to deviate less from the direction of light if activated charcoal is added to the substrate (Fisher & Williams, 1981; Haser & Häder, 1992). There are some indications that this reaction is related to the absorption of NH_3 by the charcoal (Bonner *et al.*, 1986; Haser & Häder, 1992). In general, slugs orientate towards a piece of charcoal, but if the charcoal is first saturated with NH_3, it is no longer capable of attracting slugs (Bonner, 1993). This is yet another indication that the main effect of the charcoal is to absorb NH_3.

In this paper we model phototaxis in terms of an NH_3-mediated modification of the shape of cAMP waves only; no differences in chemotactic response were assumed. We show that this modification is sufficient to account not only for phototaxis, but also for a number of other behaviours which are observed in connection with phototaxis.

4.2 The Model

There have been several models describing slug migration (Odell & Bonner, 1986; Williams *et al.*, 1986; Umeda, 1989; Savill & Hogeweg, 1997; Bretschneider *et al.*, 1995, and chapter 3). However, these models were not used to describe phototaxis. In this study we have extended our model for thermotaxis (see chapter 3), a hybrid CA/PDE model, which was formulated by Savill & Hogeweg (1997) to describe the development from single cells to crawling slugs. In these hybrid models a CA is used to represent individual amoebae and light, and PDEs to model diffusible chemicals. The models are based on a special CA model-formalism, developed by Glazier & Graner (1993). The strength of this formalism is that amoebae are represented as a group of connected automata instead of point-like objects. Therefore amoebae can slide past one another and deform themselves and adjoining amoebae by means of small changes in their boundaries. Very recently, Jiang *et al.* (1998) have used the same formalism to describe tip formation during the mound stage of *Dictyostelium*.

In our previous study, on thermotaxis in *Dictyostelium* slugs, we showed that taxis can develop as a result of differences in the excitability of the amoebae. These differences in excitability cause the cAMP waves to change shape, which, via the chemotaxis towards cAMP, causes the slug to turn. We have made several extensions to our previous model: the CA has been extended with a description of irradiation and refraction, an extra PDE has been added to describe the NH_3 dynamics, and the cAMP-modulated cAMP response has become dependent on the NH_3 concentration. Since the relationship between NH_3 and cell speed is still under dispute, we have decided to omit from our model any difference in chemotaxis between cell types or due to NH_3.

We study phototaxis in two-dimensional (2D) slugs. This is not a limitation of our model, because Bonner (1998) has recently managed to develop an experimental method for producing migrating 2D (one cell thick) slugs which share most basic properties with normal three-dimensional (3D) slugs.

Each amoeba occupies about 30 automata in the CA, and has an associated label τ, which indicates whether the cell type is prespore, prestalk or oscillatory prestalk ($\tau \in \{\text{p, t, a}\}$). Each automaton that is part of an amoeba's boundary has a number of dimensionless free energy bonds. The magnitude of these bonds depends on the cell types they connect. The energy bonds are given by $J_{\tau_1,\tau_2} > 0$, where τ_i are the types of the two amoebae. The bond energy between an amoeba and the medium is given by $J_{\tau,M}$. The total free energy of an amoeba is given by:

$$H_\sigma = \sum \frac{J_{\text{cell,cell}}}{2} + \sum J_{\text{cell,medium}} + \lambda(v - V)^2, \tag{4.1}$$

where v is the volume of the cell, V the target volume, and λ the inelasticity. The final term ensures that the volume of a cell remains close to V. Minimisation of the free energy of the amoebae causes deformation of the boundaries. The probability that the boundary will be deformed is either 1 if $\Delta H < -0.8$, or $e^{-\left(\frac{\Delta H + 0.8}{T}\right)}$ if $\Delta H \geq -0.8$.

We choose bond energies so that the amoebae adhere to each other, but also so that, if given the possibility, they will sort themselves into three fairly homogeneous groups. Oscillatory cells adhere together more rigidly than prestalk cells, and the latter adhere together more rigidly than prespore cells. For further details, see chapter 3.

The luminous intensity l is calculated using the ray-tracing technique. For some basics on ray-tracing, see, for example, Stavroudis (1972). In our computations, for every position along the upper border of the CA a ray is initiated, with a downwards ray direction. Light that enters or leaves a slug is refracted. First, one finds the point where the ray intersects the slug surface. At that point the normal to the surface is calculated: after assigning the value 0 or 1 to automata outside or inside the slug and taking the eight-neighbourhood into account, we compute the local gradient. The direction of the gradient is used as the surface normal. Knowing the surface normal and the angle of incidence, which is the angle between the incident ray and the surface normal, the direction of the refracted ray is determined using Snell's law. We use a refractive index of 1.369, which is the value of the refractive index for *Dictyostelium*, as measured by Häder & Burkart (1983). Next, one finds the point of intersection of the refracted ray with the slug surface, and so on. To map the ray, which can move not only horizontally and vertically, but in any direction, onto the discrete CA, we use Bresenham's line algorithm (Bresenham, 1965). To obtain the luminous intensity values at each point, we add up the intensities of all individual rays passing through it. By default, the intensity of an individual ray is set to 1, which we refer to as the default light intensity. To change the intensity of the light source, we simply change the intensities of the incoming rays.

Three PDEs are used to describe the cAMP and NH_3 dynamics. The cAMP dynamics can be described reasonably well in a quantitative way by two variable simplified equations of the FitzHugh-Nagumo (FHN) type. For some basic background on FHN-type models we refer to Grindrod (1996). Such a description reproduces the overall characteristics of cAMP waves such as refractoriness and curvature relation. The main advantage of these models is their simplicity, and therefore their capacity to connect the effects visible in these models with basic properties of the cAMP signalling in *Dictyostelium*. FHN-type models are appropriate for a preliminary qualitative study of the behaviour, but, of course, are not adequate for a detailed quantitative study.

Here we investigate the basic effects of heterogeneity in excitability, but we are not concerned with the details of cAMP signalling. So for our present purposes, the FHN-models are preferred.

For this study we used the following equations, in which c represents cAMP concentration, and r refractoriness of the cells. The third PDE describes the NH_3 concentration:

$$\frac{\partial c}{\partial t} = D_c \Delta c - f(c, \tau, n) - r, \tag{4.2a}$$

$$\frac{\partial r}{\partial t} = \varepsilon(c)(kc - r), \tag{4.2b}$$

$$\frac{\partial n}{\partial t} = D_n \Delta n + g(l) - d_{n_{\text{in}}} n, \tag{4.2c}$$

with $f(c, \tau, n) = C_1 c$ when $c < c_1$; $f(c, \tau, n) = -C_2 c + a(\tau, n)$ when $c_1 \leq c \leq c_2$; $f(c, \tau, n) = C_3(c-1)$ when $c > c_2$, and $\varepsilon(c) = \varepsilon_1$ when $c < c_1$; $\varepsilon(c) = \varepsilon_2$ when $c_1 \leq c \leq c_2$, and $\varepsilon(c) = \varepsilon_3$ when $c > c_2$. To make the function $f(c, \tau, n)$ continuous, $c_1 = a(\tau, n)/(C_1 + C_2)$, and $c_2 = (a(\tau, n) + C_3)/(C_2 + C_3)$. If the luminous intensity is below the threshold $l_{th} = 3$, $g(l) = 0$, and if $l \geq l_{th}$, $g(l) = l$. The small decay $d_{n_{\text{in}}}$ is due to the assimilation of NH_3 into amino acids (Dunbar & Wheldrake, 1997). D_n is much larger than D_c, due to the relatively low diffusion coefficient of cAMP (Dworkin & Keller, 1977). Each automaton in the CA is associated with one grid point in the discretised numerical PDEs.

Weijer *et al.* (1984) showed that the tip of the slug can be seen as a high-frequency pacemaker, whereas the body of the slug behaves as an excitable medium. This can be modelled using parameter $a(\tau, n)$, which gives a stable limit cycle at negative values, and describes an excitable medium at positive values. Therefore, positive values are used to describe excitable amoebae, whereas negative values are used to describe the oscillatory amoebae in the tip.

Our description of NH_3 action is based on the following experimental data. Schindler & Sussman (1979) found that NH_3 inhibits the cAMP-induced cAMP release; Williams *et al.* (1984) established that this is because NH_3 blocks intracellular cAMP accumulation by inhibiting the transitory activation of adenylate cyclase in response to the binding of extracellular cAMP to cell surface receptors; and Darcy & Fisher (1990) produced evidence that this inhibition of the cAMP signalling is important in slug behaviour.

Since in the model $a(\tau, n)$ represents the threshold for the cAMP response, we use the parameter a to express the inhibiting effect of NH_3 on the cAMP-modulated cAMP response. We do this by specifying an NH_3-dependent increase of a. We assume that this increase saturates:

$$a(\tau, n) = a_{0_\tau} + \frac{bn}{1 + n/p}, \tag{4.3}$$

with $a_{0_p} = a_{0_t} = 0.1$ and $a_{0_a} = -0.1$.

Outside the amoebae we only implemented a small cAMP decay, d_c, caused by external phosphodiesterase, and when we modelled absorption of NH_3 by charcoal, we also implemented an NH_3 decay $d_{n_{\text{out}}}$:

$$\frac{\partial c}{\partial t} = D_c \Delta c - d_c(c - c_0), \tag{4.4a}$$

$$\frac{\partial n}{\partial t} = D_n \Delta n - d_{n_{\text{out}}} n, \tag{4.4b}$$

where c_0 is the minimal value of variable c. To create either an NH_3 gradient or a background NH_3 concentration, we used fixed values for the NH_3 concentration along the border of the whole CA. The dynamics inside and outside the slug were not modified.

Chemotaxis is incorporated in the model by using the spatial gradient of the cAMP wavefront (Savill & Hogeweg, 1997): $\Delta H' = \Delta H - \mu(c_{\text{automaton}} - c_{\text{neighbour}})$, where $\Delta H'$ is the new change in energy. This makes it more likely that an amoeba will move towards a location with higher cAMP concentration and less likely that it will move towards one with lower cAMP concentration. Chemotaxis is only taken into account when cAMP is above a threshold $c_{th} = 0.05$ and refractoriness below a threshold $r_{th} = 0.2$.

Although the process of cell sorting already starts during the mound formation, slugs are still fully capable of generating the prestalk-prespore pattern due to cell sorting (Sternfeld & David, 1981). The first cells to sort out are the prestalk A cells, which form the tip and are the source of the cAMP waves (Williams *et al.*, 1989; Siegert & Weijer, 1992). Therefore in all simulations a slug is initiated with a tip consisting of oscillatory prestalk cells. As a 'worst case scenario' with respect to the cell sorting, the remaining prestalk cells, together with the prespore cells, are distributed randomly in the body of the slug. Please note, however, that slugs which have completed cell sorting show the same phototactic behaviour as slugs which are still in the process of cell sorting.

4.3 Phototaxis

We were able to reproduce phototaxis in *Dictyostelium discoideum*. In Fig. 4.1 we demonstrate the phototactic behaviour of our model slugs in the form of a time-lapse image; Fig. 4.1(a) shows a simulation of phototaxis with light radiating from top to bottom. The inset shows the initial configuration. The oscillatory prestalk cells are coloured blue, the remaining prestalk cells red, and the prespore cells green[1]. Initially, the slug moves at an angle of 90 degrees relative to the light source, but after 2 hours 30 minutes the angle has decreased to 30 degrees. Within 7 hours the slug has turned completely towards the light. The differences in adhesion between the various cell types are important for the cell sorting (see chapter 3), but have little effect on the phototactic behaviour.

[1]We have not tried to add pseudo-realism by matching the colours to experimental data from staining experiments.

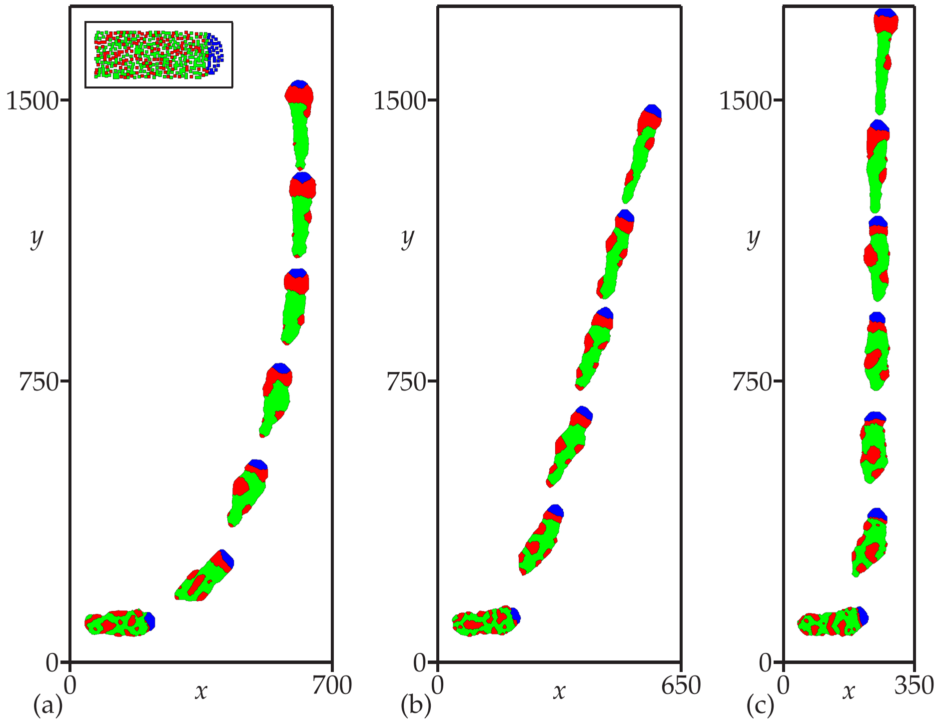

Figure 4.1. Time sequences from simulations of motion during the slug stage of *Dictyostelium*. (a) A simulation of phototaxis, with light radiating from top to bottom. (b) A simulation of a mutant with bi-directional phototaxis. (c) A simulation of the same mutant surrounded by NH_3-absorbing charcoal. The inset in (a) shows the initial distribution for all three simulations, two times enlarged, with a tip consisting of oscillatory prestalk cells and a body consisting of 40% prestalk and 60% prespore cells. The first frames show the state after 15 minutes (9 000 time steps). Successive frames with intervals of (a) and (c) 1 hour 15 minutes (45 000 time steps); and (b) 1 hour 30 minutes (54 000 time steps). There are 430 amoebae. One time step (solution of the PDEs) corresponds to about 0.1 s and one grid point to 5 μm. Cell types are $\tau \in \{a, t, p\}$ where a is oscillatory prestalk (blue), t is prestalk (red), and p is prespore (green). Bond energies are $J_{a,a} = 3$, $J_{t,t} = 5$, $J_{p,p} = 7$, $J_{a,M} = 7$, $J_{t,M} = 8$, $J_{p,M} = 9$, $J_{a,t} = 6$, $J_{t,p} = 8$, $J_{a,p} = 9$. $T = 2$, $V = 30$, $\lambda = 0.6$, and $\mu = 200$. The parameters used for the PDEs are $D_c = 1$, $C_1 = 20$, $C_2 = 3$, $C_3 = 15$, $\varepsilon_1 = 0.5$, $\varepsilon_2 = 0.0589$, $\varepsilon_3 = 0.5$, $k = 3.5$, $d_c = 0.05$, $c_0 = -0.3$, $D_n = 15$, $d_{n_{\text{in}}} = 0.01$, and $b = 0.1$. $p = 1$ in simulation (a), and $p = 4$ in simulations (b) and (c). In simulation (c), $d_{n_{\text{out}}} = 0.3$. The PDEs are solved by the explicit Euler method (with time step equal to 0.01 and space step equal to 0.37). The axes are given in grid points. See also the colour plate on page 73.

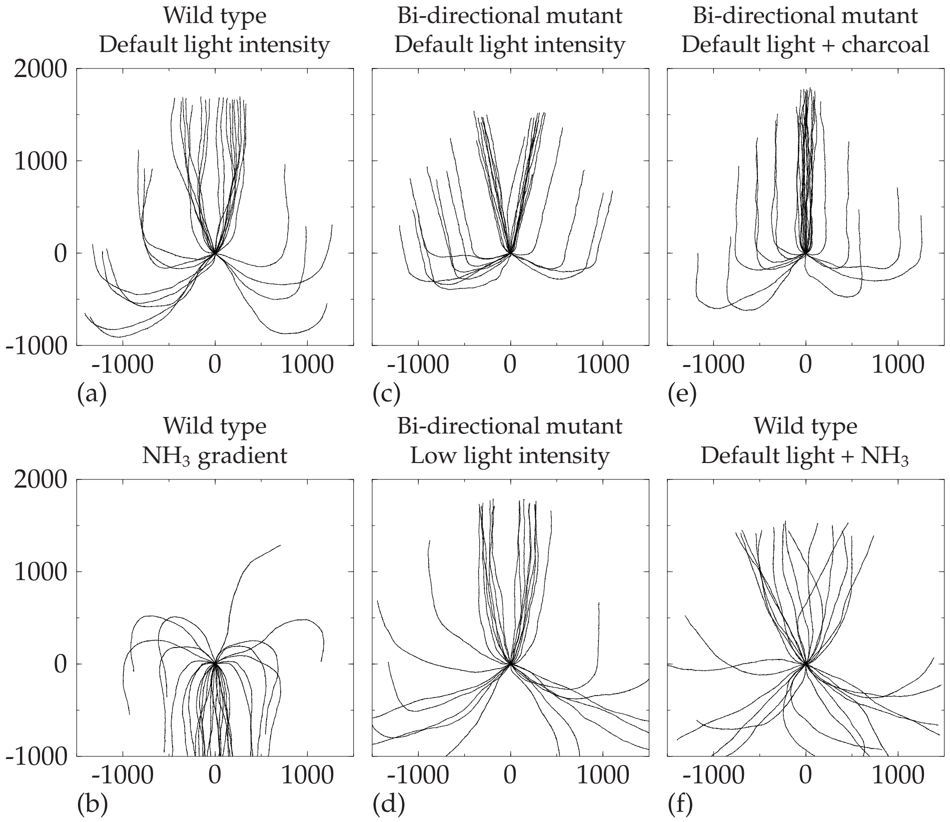

Figure 4.2. The change in the location of the slug in time, for different model experimental settings, as indicated above each figure. Light radiates from top to bottom; the source of the NH_3 gradient is also at the top. The location at $t = 0$ is set to (0,0), and the simulations lasted for 8 hours 20 minutes (300 000 time steps). The axes are given in grid points. For each plot 32 simulations were performed. Slugs were initially positioned with respect to the light source at intervals of 22.5 degrees, from 0 degrees onwards. Two simulations per angle were carried out. (b) NH_3 gradient of 0.02/grid point. (d) Mean light intensity of 0.8. To analyse the effect of mean light intensities below 1, we needed to use a continuous function for the NH_3 production: $g(l) = \frac{l^m}{(l_{th}-0.5)^m+l^m} l$, with $m = 12$. When a mean light intensity of 1 is used, simulations using the continuous function are qualitatively indiscernible from the simulations using the original split-function. (f) Background NH_3 concentration of 2.0. All other parameters are as described in the legend to Fig. 4.1.

In Fig. 4.2 the experiments are quantified, each plot showing the slug trails from 32 different simulations. All lines start at the same initial position (0,0), which is visible as a node where all lines originate. Every plot is based on 16

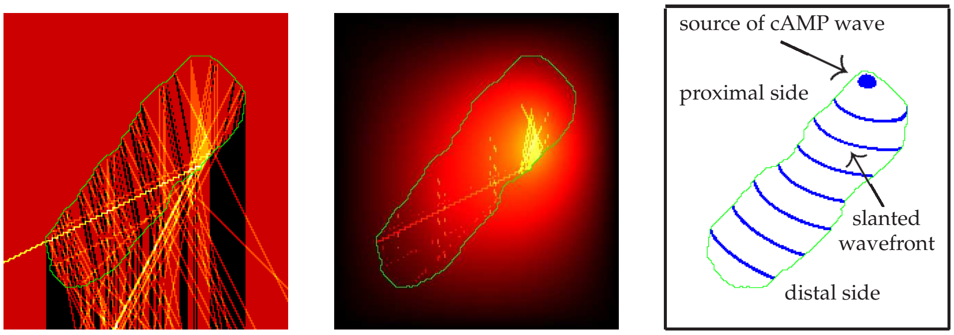

(a) (b) (c)

Figure 4.3. (a) Snapshot of the luminous intensity distribution during phototaxis. Light is focused on the distal side due to the lens-effect. (b) Snapshot of the distribution of NH_3. Lowest concentrations are found on the proximal side. Different levels of the luminous intensity and the corresponding NH_3 concentration are indicated by a colour ramp from dark red (low values) to bright yellow (high values). All parameters are as described in the legend to Fig. 4.1. (c) A schematic diagram that shows some of the basic properties of the cAMP wave during phototaxis. The blue lines show the wave shape at different locations in the slug. See also the colour plate on page 73.

different initial orientations, at intervals of 22.5 degrees.

Figure 4.2(a) shows normal phototaxis. The final orientation is independent of the initial angle, i.e. in the end the direction of motion is always towards the light. However, when the initial angle is larger than 90 degrees, turning of the model slug is initially slow.

The mechanism of phototaxis can be described as follows. As a result of the lens-effect, the light is focused on the distal side, as can be seen in Fig. 4.3(a), which shows the distribution of the luminous intensity. Figure 4.3(b) shows the corresponding NH_3 concentration. Note that although in a snapshot of the luminous intensity discrete effects are clearly visible, these do not affect the long-term behaviour, because the slugs' boundary is continuously changing its shape, therewith constantly changing the luminous intensity distribution. Because NH_3 inhibits cAMP it causes a longer oscillating period and a lower wave speed in the region of high NH_3 concentration (see chapter 3). Hence a region with the shortest oscillating period will be located on the proximal side, which will serve as the source of the cAMP waves [see Fig. 4.3(c)].

Hence the cAMP wave starts slanted, and remains slanted when it passes through the region where the light is focused, because in this region there are large differences in NH_3 concentration (and thus in wave speed) between the proximal and distal side. More posteriorly there are only small variations in the NH_3 concentration, and as a consequence the cAMP wave straightens out due to the curvature-effect [see Fig. 4.3(c)]. The slanted cAMP wave, combined with the chemotaxis towards cAMP, leads to the phototactic response: the amoebae move preferably perpendicular to the wavefront therewith pushing the oscillatory tip into the direction of the light source.

Our model also reproduces the experimentally observed negative taxis away from NH_3. Figure 4.2(b) shows the trails of 32 simulations in a field with the source of NH_3 located at the top, without any light. The negative chemotaxis is clearly visible. Note that individual amoebae in our model do not have any NH_3 taxis. The mechanism is simply that the NH_3 partly diffuses into the slug and causes an internal NH_3 gradient. This again gives rise to the differences in excitability which lead to the tactic behaviour.

Our model reproduces a deviation in the orientation towards light, similar to what is observed in the so-called bi-directional mutants. We found this behaviour when the decrease in excitability saturates at higher NH_3 concentrations. Figure 4.1(b) shows a simulation in which we increased the value of p (which gives the half-saturation concentration) four times. The slug still demonstrates pronounced phototaxis, but the final direction of motion is at an angle of 14 degrees. Figure 4.2(c) shows the trails of 32 different simulations. This figure clearly shows bi-directional phototaxis. Initially, turning can be slow, but the final deviation from the direction of the light path is independent of the initial angle. If initially the slug is positioned at an angle of zero degrees, random variations are amplified by up to 14 degrees.

In our model and in experiment, bi-directional phototaxis changes back into unidirectional phototaxis at low light intensities (Poff *et al.*, 1986). Figure 4.2(d) shows the trails of the 'bi-directional mutant' from the previous simulations when the light intensity is decreased from 1 to 0.8. Now turning takes much longer and the trails are less stable, because the signal is weaker. However, bi-directionality has indeed disappeared. At light intensities stronger than 0.8 bi-directionality can still be observed, though it is weaker; at weaker light intensities phototaxis becomes increasingly less pronounced.

From experiments it is known that charcoal reduces the deviation in slugs' orientation towards light. We found similar results in our model. Figure 4.1(c) shows such a simulation, in which the bi-directional mutant is surrounded by charcoal. We emulated the addition of charcoal by including the external absorption of NH_3 in eqn (4.4b). The slug moves straight to the light, and the bi-directional behaviour has disappeared. Figure 4.2(e) shows again that this result does not depend on the initial conditions. Even when the initial angle is 180 degrees, random deviations let the slug turn either to the right or the left.

The mechanism of bi-directional phototaxis can be explained as follows. In eqn (4.3), parameter p gives the NH_3 concentration at which the decrease in excitability is half-saturated, and thereby determines the range of NH_3 concentrations that affect the excitability. If this parameter is increased (and hence the range is enlarged), differences in excitability along the slug become larger. These differences are locally largest between the area on which the light is focused and the area on the other, more excitable proximal side. The source of the cAMP wave hardly changes position at all, because this location is determined mainly by the lowest NH_3 concentration. However, when the wave reaches the region on which the light is focused, the wave shape changes dramatically, as it moves much more slowly in the region of the light focus on the distal side of the slug than on the proximal side. As a result, the wave becomes much more slanted in this region than is found with normal phototaxis.

The model does not contain explicit forces. However, the adhesion between the amoebae and between the amoebae and the medium create a surface tension (Glazier & Graner, 1993), which preserves to a certain extent the shape of the slug. Therefore the chemotactic motion can create force on the slug itself, which has a torque, due to the slanted wavefront. Since the wave is only substantially slanted at a certain distance behind the tip, the oscillatory area is pushed away from the light by the momentum of this force. This is especially the case when the slug moves at a small angle to the direction of light: the light is focused on an area that is located at a larger distance behind the tip, which creates a longer lever. Hence, at small angles the bi-directional mutant moves away from the light. Note that the effect is caused by differences in motion direction and not by differences in motion speed. In fact, when following individual amoebae, we observe rather wriggling paths of motion. Only the gross activity shows the fixed bi-directional motion.

The absorption by charcoal decreases the NH_3 concentration. This has only a marginal effect on the position with the lowest concentration and thus on the source of the new cAMP wave, but reduces the slant of the cAMP wave and thereby the momentum of the force sufficiently to re-establish unidirectional phototaxis. The effect of decreasing the light intensity works via the same principle as the addition of charcoal, namely it creates lower NH_3 concentrations. The main difference between low light intensity and adding charcoal is that at low light intensities the signal becomes weaker, which causes slower turning and more unstable trails, whereas when charcoal is added the signal remains strong, and therefore, stability and turning velocity are still very high.

In our last simulations we considered the experimental observation that external NH_3 decreases phototaxis. Figure 4.2(f) shows the trails of our original unidirectional phototactic slug when surrounded by an NH_3 concentration of 2.0. Obviously, phototaxis diminishes, because the high concentration of NH_3 strongly interferes with the phototactic signalling system. However, very high concentrations are needed to suppress phototaxis completely, since it is driven by relative differences in NH_3 concentration, and not by absolute values.

Next, using the data from Fig. 4.2, we analysed the velocity at which slugs turn towards the light. Figure 4.4(a) shows the change of angle versus the angle by which the slug deviates from the light source. Figure 4.4(b) gives a more detailed graph of the change of angle between 0 degrees and 22.5 degrees. To obtain the figure, we took into account that this turning is, to the left and right, symmetric around the direction of the light path. For normal phototaxis, there is only one stable direction of motion, namely towards the light source. The bi-directional mutant turns much faster, since its sensitivity to NH_3 is much higher, but the phototactic force towards the light and the momentum of the force away from the light equilibrate at an angle of 14 degrees, which is clearly visible in Fig. 4.4(b). At low light intensity the turning velocity of the mutant is much lower again, but, as can be seen in Fig. 4.4(b), the final direction is towards the light source. When the

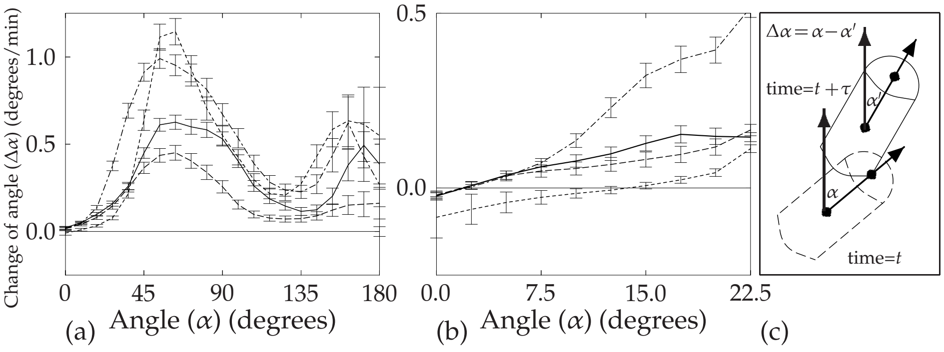

Figure 4.4. (a) Change of angle towards the light source ($\Delta\alpha$) versus the position the slug takes up relative to the direction of irradiation (α). (b) A more detailed graph of the change of angle between 0 degrees and 22.5 degrees. (c) Scheme to indicate method used to calculate the change of angle. The various types of lines show the change of angle made by the wild type (solid lines), the bi-directional mutant (dotted lines), the mutant at low light intensity (dashed lines), and the mutant surrounded by charcoal (dashed-dotted lines). The means and standard error of mean (S.E.M.) values (indicated by the bars) were calculated using the data of Fig. 4.2. The means and S.E.M. values were calculated at intervals of (a) 9 degrees; or (b) 2.5 degrees, using a Gaussian smoothing with an s.d. of again 9 degrees and 2.5 degrees, respectively. The angle α is calculated using the mean location of the oscillatory area relative to the mean location of the rest of the slug. The change of angle $\Delta\alpha$ is calculated using a time difference τ of 2 minutes 30 seconds (1 500 time steps).

mutant is surrounded by charcoal, its turning velocity is lowered only slightly, but motion towards the light is again the only stable solution.

When the initial angle is larger than 90 degrees, little light is focused on the distal side. However, some light is still focused on this side every time a cAMP wave passes through the slug, because chemotaxis towards cAMP causes the slugs' boundary to become temporarily lenticular. This light causes slow but steady turning. When the angle becomes less than 90 degrees, the tip acts as a lens all the time, so the slug turns much faster. We find that especially around 135 degrees turning occurs very slowly. This creates the optical impression that these angles also represent stable solutions [see, for example, Fig. 4.2(c)].

In all our simulations we used a tip consisting of oscillatory amoebae, while the rest of the slug only relayed the signal. However, the change in excitability might be much more gradual, with at least all prestalk cells in the oscillatory regime (Siegert & Weijer, 1992; Dormann *et al.*, 1996). Therefore we performed a number of control experiments, in which all prestalk cells were oscillatory, although the tip cells were still the most excitable ones ($a_{0_t} = -0.05$). All other conditions were kept the same. This caused no qualitative differences in any of the the model behaviours: the high-frequency oscillations in the tip enforced the global cAMP dynamics.

Another assumption we made is that both cAMP and NH_3 can freely diffuse in and out of the slug. For NH_3, a volatile gas, this assumption is very reasonable, but for cAMP it is less clear what would be the correct boundary conditions. Therefore we also tested if our results depend on a specific choice of the boundary conditions. We repeated our experiments using Neumann boundaries, i.e. as if the slugs' boundary is impermeable to cAMP. We found that it does not affect the phototactic behaviour. However, the shape of the slug is less well preserved.

4.4 Discussion

We have described a mechanism that can explain phototaxis in *Dictyostelium discoideum*, including its bi-directional mutants. Previously proposed mechanisms, such as phototaxis due to an increase in the speed of the amoebae in the illuminated region of the slug (Bonner *et al.*, 1988), or bi-directionality due to actively turning towards and away from the light to correct the deviation from the preferred direction of motion (Fisher, 1997), are shown to be superfluous: all the experimental data can be explained by our mechanism, which uses only light focusing, NH_3 production, modification of the cAMP wave, and chemotactic motion.

The relative contributions to the phototactic behaviour of (i) the shift in the source of the cAMP waves towards the light, and (ii) the wave shape deformation, are difficult to discriminate because these properties both emerge from the local rules and hence can never be completely separated. For example, the velocity by which the cAMP wave moves away from a certain position affects the oscillating period and therewith the source of the new cAMP wave. However, both processes contribute to the phototaxis because if the wave does not start slanted, side-effects as described for bi-directional mutants are found, whereas without differences in wave propagation the wavefront restores itself too quickly and little directed motion is created.

During the slug stage chemotactic motion towards cAMP is hard to observe. However, there are many indications that slug motion is still driven by cAMP waves (Dormann *et al.*, 1998). In our model we observe that amoeboid motion is not restricted to the actual location of the cAMP wave, but is spread out over large distances due to pushing and pulling. Especially when chemotaxis is relatively weak (e.g. μ=100), a global and continuous motion is observed, in which responses to individual cAMP waves can not be distinguished. This behaviour is very comparable with what is observed by Bonner (1998) in migrating 2D slugs. Note, however, that the behaviour is still driven by periodical cAMP waves.

In contrast to our previous model which used a linear gradient of excitability, to mimic thermotaxis, the gradient in this study is dynamic and highly nonlinear. This is due to the light focusing which changes all the time during slug motion, and also to the NH_3 dynamics. Nevertheless, the mechanism accounts for all aspects of phototactic behaviour.

According to our model, in the first instance light information is encoded using NH_3. In the previous study we assumed a similar mechanism for the thermal information. So we propose that thermotactic and phototactic information converge at a very low level, before or while converging with the NH_3 signalling. This is in agreement with Fisher (1997), who showed in a review of phototaxis research, that thermotactic mutants are seldom found with unaffected phototaxis or vice versa, and thus information integration must occur at a very early stage.

We stated earlier that individual amoebae are not able to measure the direction of irradiation. Instead, the whole slug encodes differences in luminous intensity as differences in NH_3 concentration. The NH_3 changes the local excitability and hence the shape of the cAMP wave. It is the chemotaxis towards the cAMP wave which in the end induces the turning of the slug.

Fisher (1991) objects to the idea that NH_3 is the substance important for phototaxis, because is his view the NH_3 gradient in the open air would be too low to be measured, being flattened by the very high diffusion coefficient. However, the local NH_3 gradient is not measured by the amoebae either, and in our model only global concentration differences are necessary. The only gradient measured is the cAMP gradient, which is very steep due to its pulsatile nature and therefore relatively easily measurable. Obviously, no chemical could ever have such a steep steady-state gradient.

Another effect NH_3 could have on the amoebae is increasing the locomotive speed; however, there is a fair amount of dispute on this subject because some studies indicate that it does (Bonner *et al.*, 1986; van Duijn & Inouye, 1991), and other studies indicate that it does not (Smith *et al.*, 1982; Fisher, 1997). Besides, other chemicals such as O_2 could also be able to speed up the motion (Bonner *et al.*, 1995). We did not include such modifications of the locomotive speed in our model, and show that locomotive differences (whether they occur or not) are not needed for phototaxis.

Neither did we include an explicit difference in chemotaxis between the cell types, although Siegert & Weijer (1992) have shown that prestalk cells move faster than prespore cells. Nevertheless, such a difference in motility emerges in our model, solely due to differential adhesion.

Fisher (1997) proposed that with phototaxis slugs always move at a certain angle to the direction of light, but that in the case of the wild type this angle would be just too small to be measurable. Instead, we find that bi-directional phototaxis occurs when NH_3 sensitivity is too high. We did not implement different mechanisms for positive and negative phototaxis, but we found that both emerged from our model as an effect of the turning mechanism, negative phototaxis being caused by the slanted wavefront at a certain distance behind the tip. Thus we predict that it will in fact be fruitless to search for the "direction-dependent sign reversal in slug behaviour" which makes "slugs that travel more directly towards the light correct their error with a turn away from the light" (Fisher, 1997).

Another observation that can be clarified by our model is that when slugs are formed at high cell density, bi-directional phototaxis becomes more extreme (Fisher & Williams, 1981). At high cell density NH_3 concentrations will become higher, and, as a result, the bi-directionality will be stronger.

Besides NH_3, there is another chemical, called Slug Turning Factor (STF), that plays a role in the process of phototaxis (Fisher, 1997). We did not include this substance in our model for reasons of simplicity, but the effect of STF may be similar to that of NH_3.

The multidirectional phototaxis found by Fisher *et al.* (1985) may have been caused by a very low mean turning velocity at certain angles [see, for example, Fig. 4.4(a)]. With such low turning rates, a circular histogram with multiple preferred directions will be found, as well as (when individual measurements are plotted) groups of data clustered close to a zero change of angle (as presented by Fisher *et al.*, 1985).

Other tactic behaviours of the slug can also be interpreted in terms of the same mechanism as that presented in this paper. First, Bonner *et al.* (1985) observed that migrating slugs tend to migrate towards the acid side of a pH gradient. This so-called acidotaxis, which is weak compared to phototaxis or thermotaxis, is most probably caused by a change in the NH_3/NH_4^+ ratio (Schindler & Sussman, 1979; Bonner *et al.*, 1985, 1986). A low pH value decreases this ratio; hence a pH gradient will coincide with an NH_3 gradient. If NH_3, and not NH_4^+, is the active substance able to decrease excitability, then acidotaxis becomes directly comparable with the negative chemotaxis away from NH_3 as described earlier. Secondly, Haser & Häder (1992) found rheotaxis: slugs orientate themselves in an air stream. This also fits into our model because the NH_3 concentration will be lower on the proximal side. The same reasoning also holds for the observed motion towards a piece of charcoal provided it is not saturated with NH_3. Finally, migrating slugs repel each other (Kosugi & Inouye, 1989), rising fruiting bodies orientate away from each other (Bonner & Dodd, 1962) and this orientation is affected by NH_3 (Feit & Sollitto, 1987). Once again, higher NH_3 concentrations between the slugs or fruiting bodies, produced by the slugs themselves, could account for this behaviour.

Although all behaviours can be explained by one basic mechanism, they all work together to ensure that the final fruiting takes place in a favourable environment: they let the slugs move towards the soil surface and fruit at regular spatial intervals.

4.5 Conclusions and Predictions

Our study shows that a whole set of previously described phototactic behaviours can be explained solely with differences in NH_3 concentration, which are caused by differences in luminous intensity, and which cause alterations of the excitability. The model predicts that no 3D properties are needed for phototactic behaviour. The behaviour of the simulated 2D slugs is strikingly similar to that of the experimental 2D slugs of Bonner (1998), and both resemble the behaviour of 3D slugs closely. We predict that phototaxis by wild type and mutants can also be observed in experimental 2D slugs. The motion of individual cells can be followed in the simulations and also in the above mentioned experiments. Our simulations make strong predictions about the directions of motion during phototaxis of individual amoebae of the wild type and mutants.

The specific form of the tip, as normally observed in migrating slugs, is neither found in our simulations, nor in the experiments of Bonner (1998). Indeed, Siegert & Weijer (1992) showed that the tip is organised by 3D scroll waves. Hence we predict that the specific form of the tip is a 3D property, which cannot occur in 2D slugs. However, we have demonstrated that this is not essential for the behaviour studied here. We therefore predict that the thin elongated tip is less of an organising centre than has been previously proposed.

Acknowledgements

We are grateful to André Noest for helpful discussions about the statistics. We wish to thank S. M. McNab for linguistic advice. A. F. M. Marée was supported by the Priority Program Nonlinear Systems of the Netherlands Organization for Scientific Research.

Colour Plates

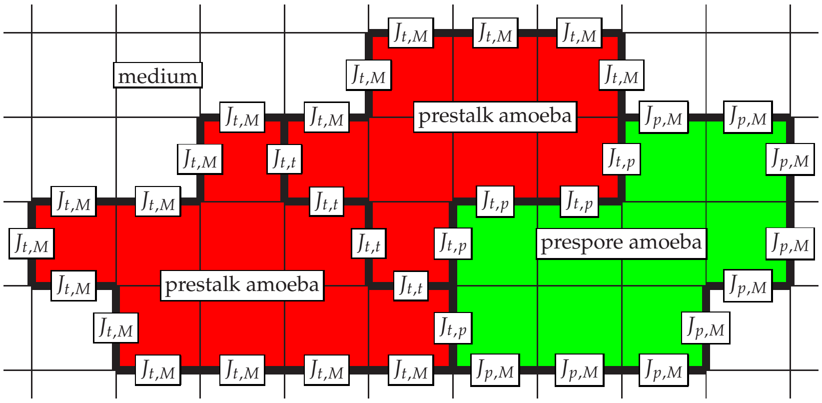

Figure 1.1 on page 7

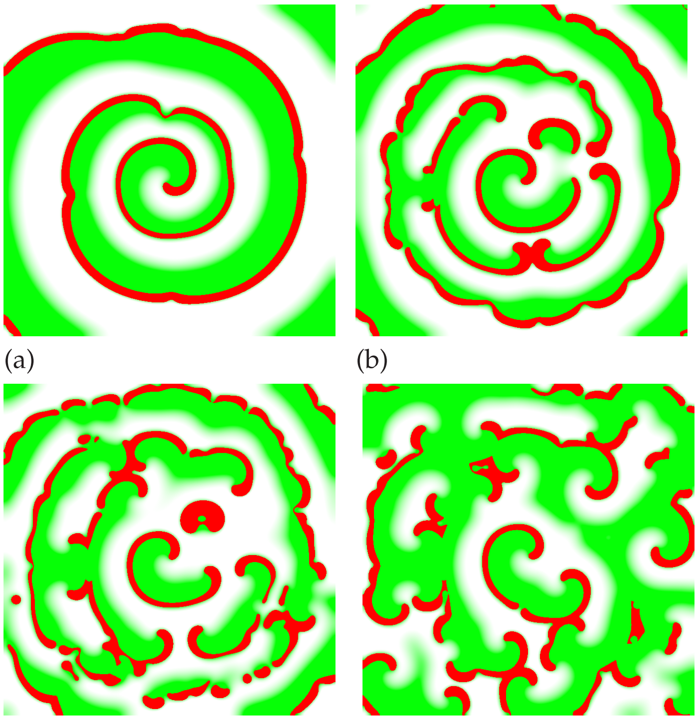

(a) (b)

(c) (d)

Figure 2.1 on page 26

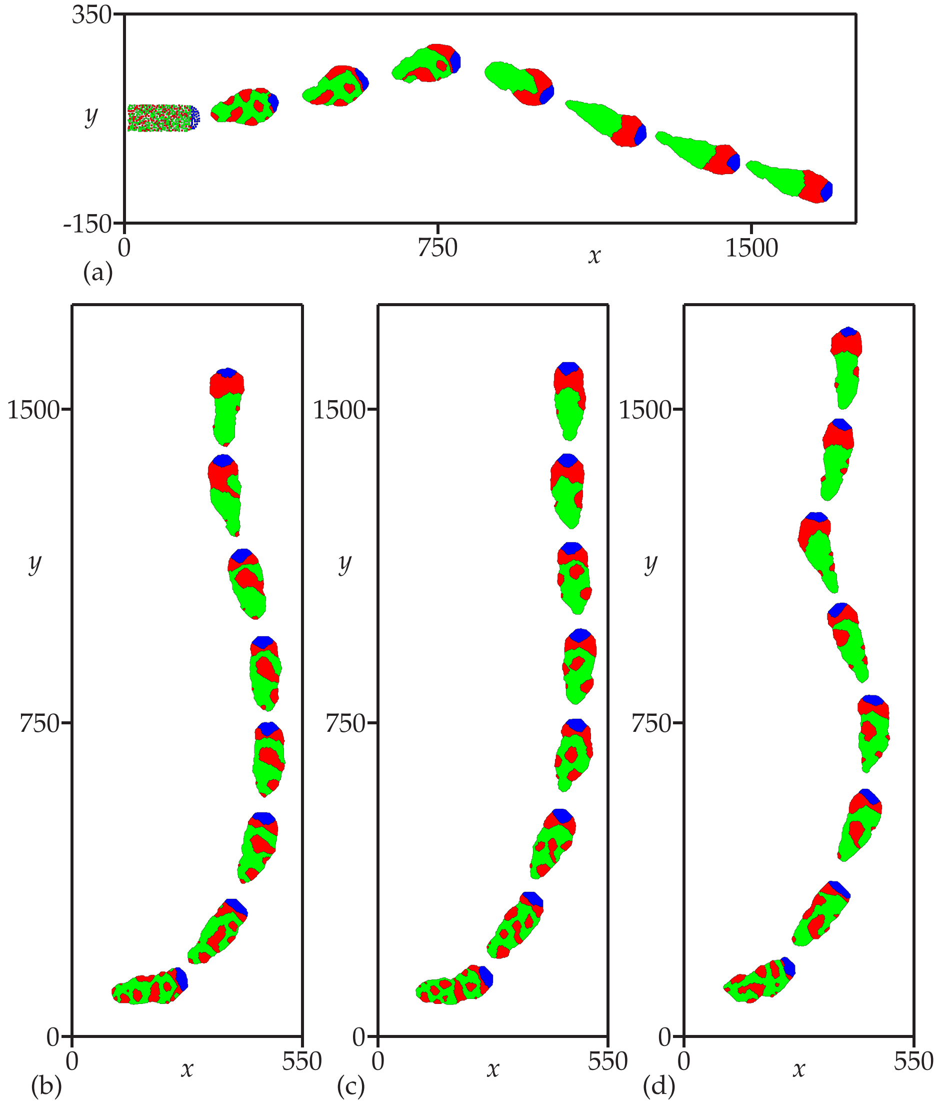

Figure 3.2 on page 41

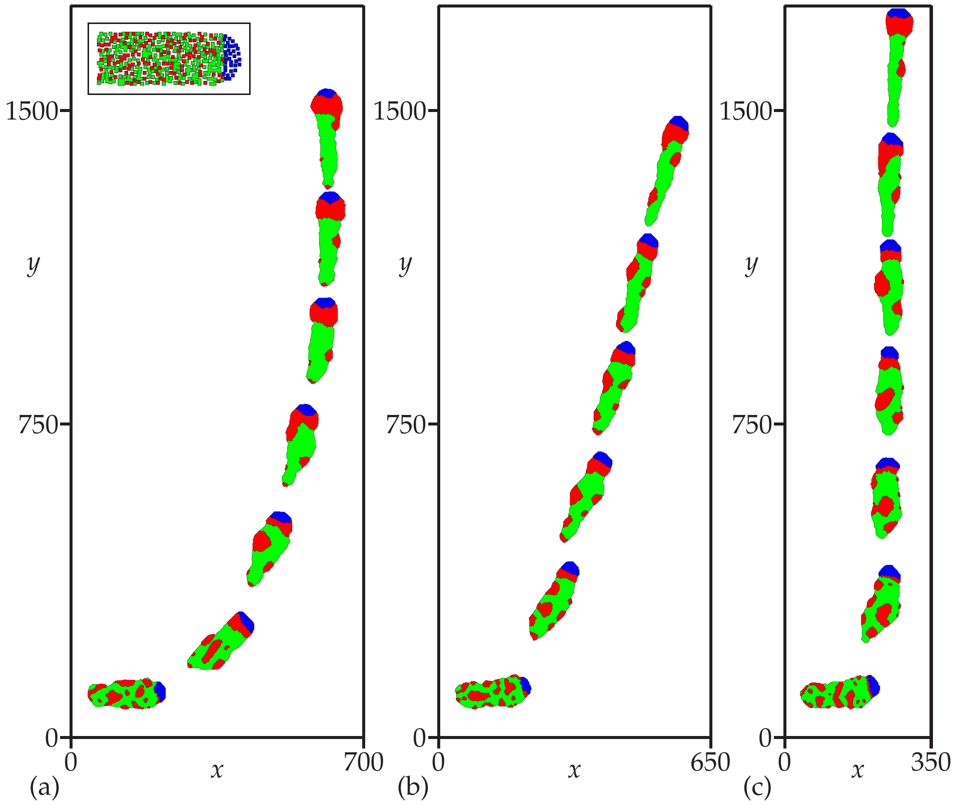

Figure 4.1 on page 61

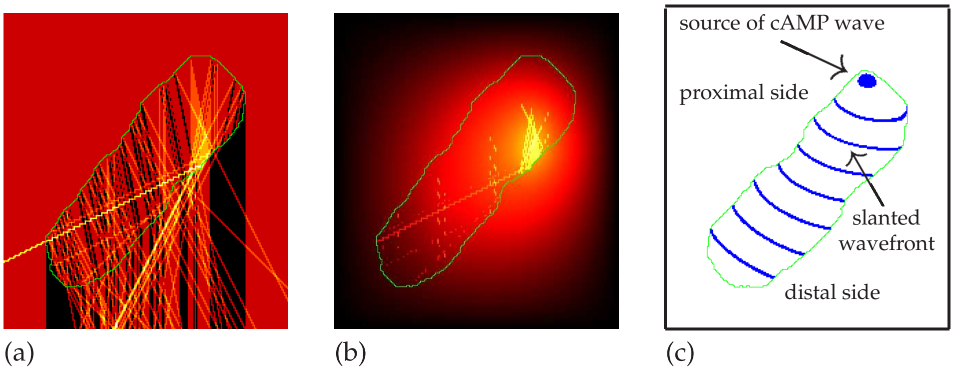

Figure 4.3 on page 63

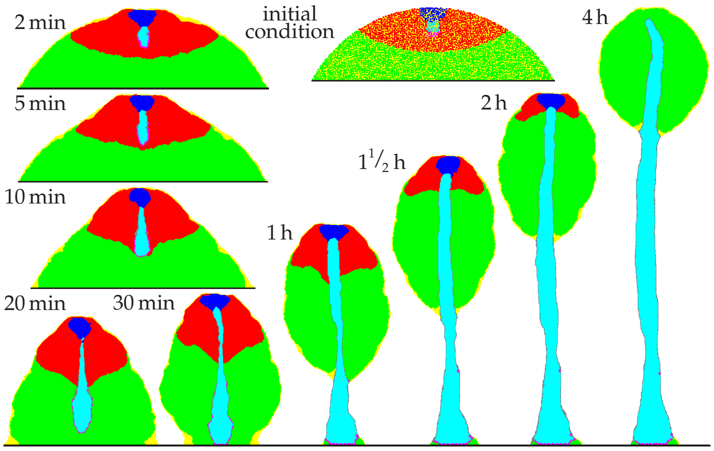

Figure 5.1 on page 81

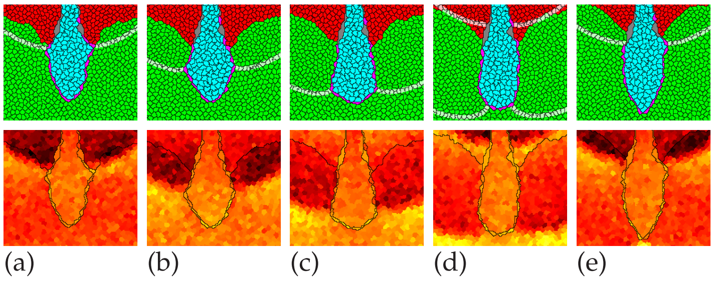

Figure 5.2 on page 82

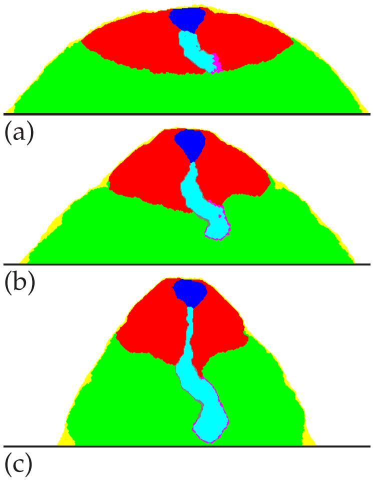

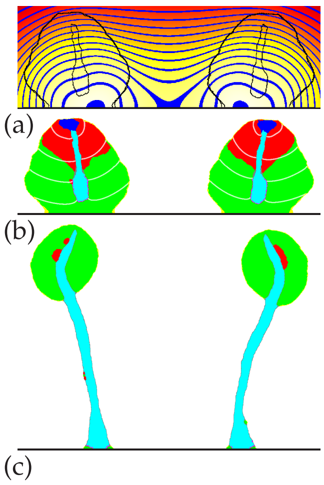

Figure 5.3 on page 83

Figure 5.4 on page 83

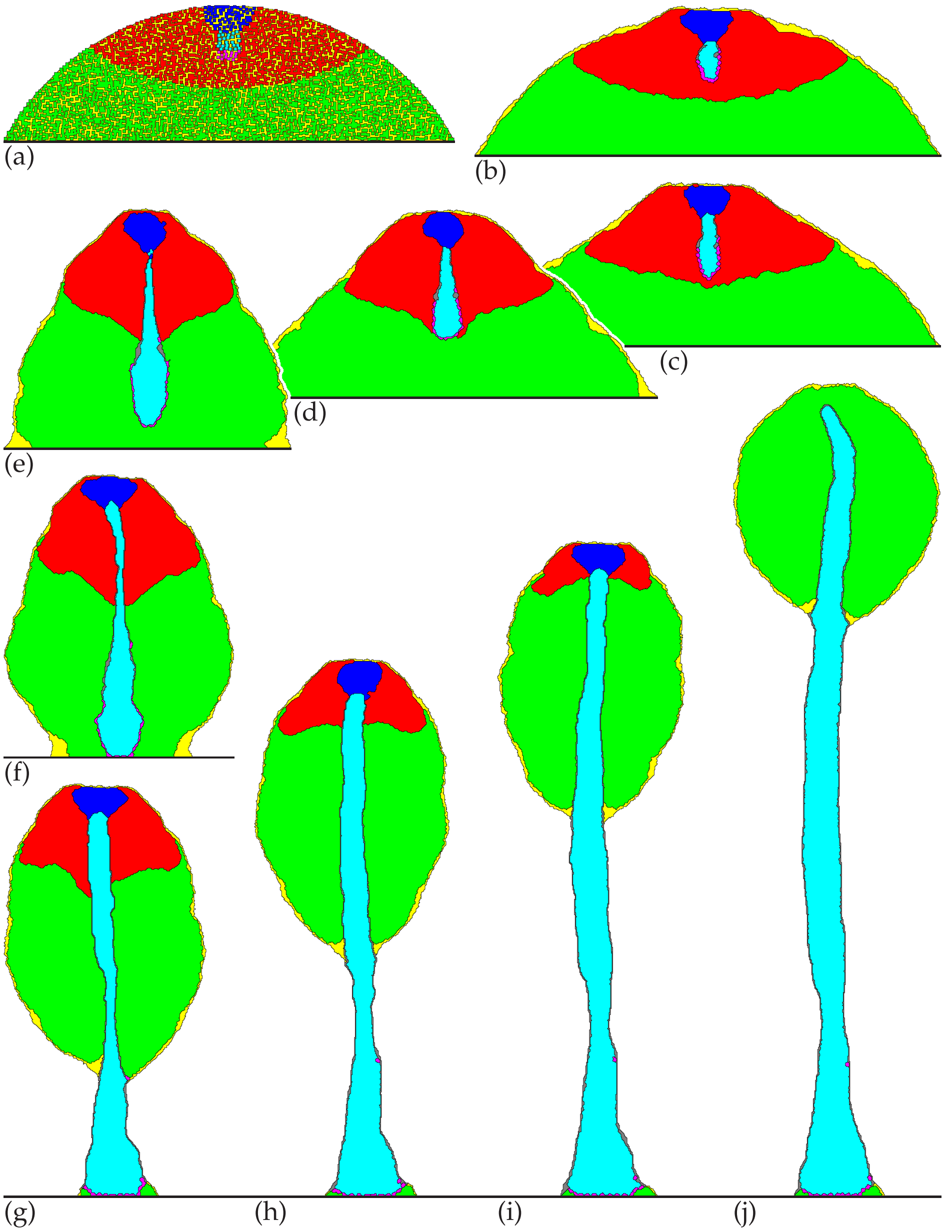

Figure 6.1 on page 95

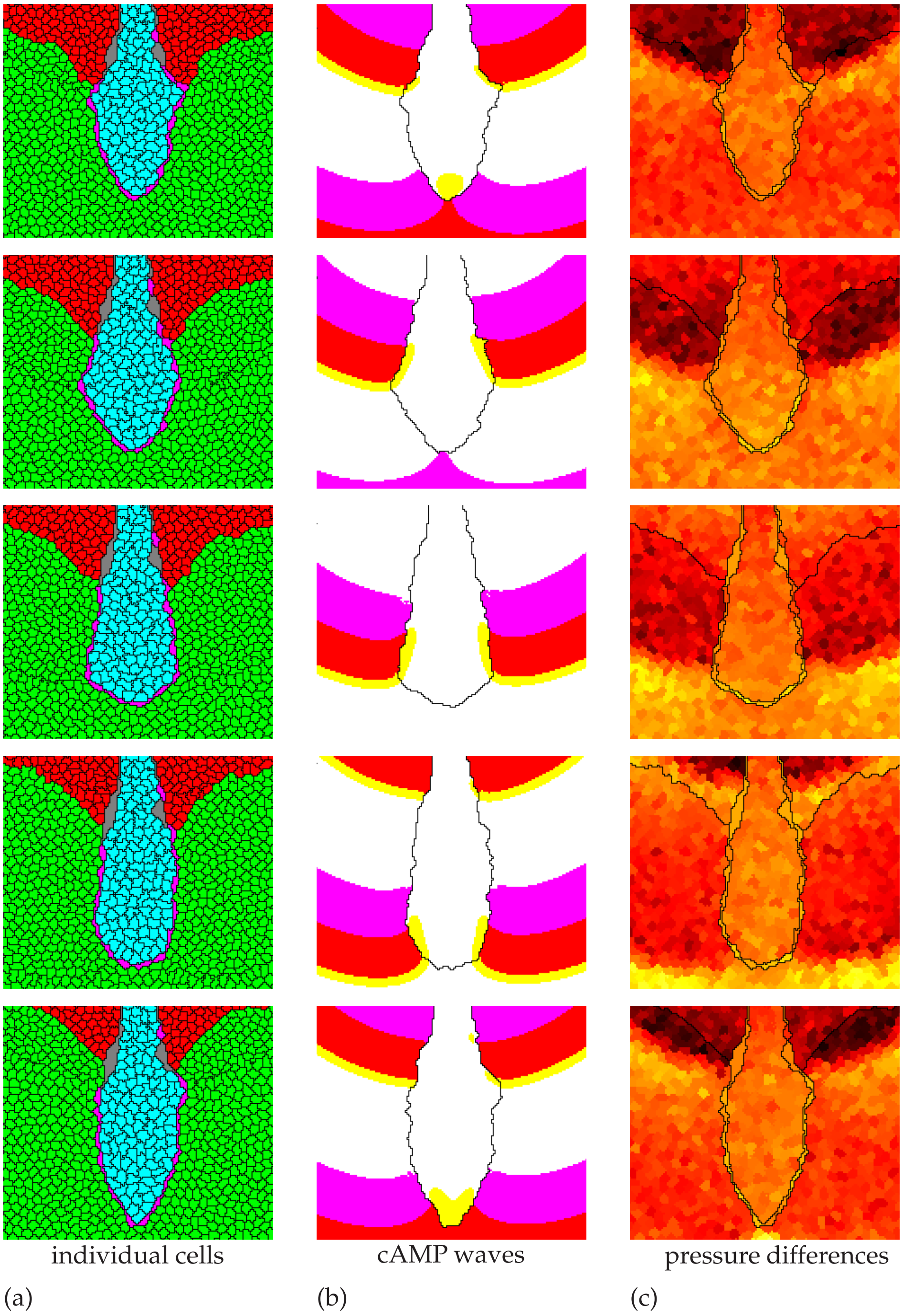

Figure 6.2 on page 97

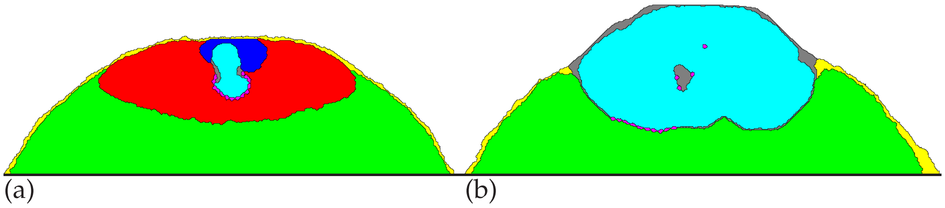

Figure 6.3 on page 98

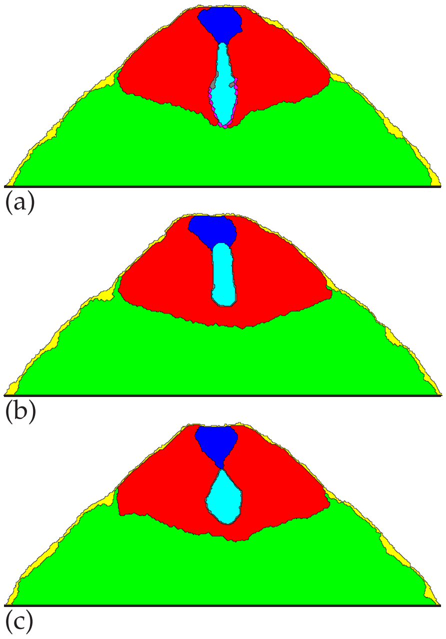

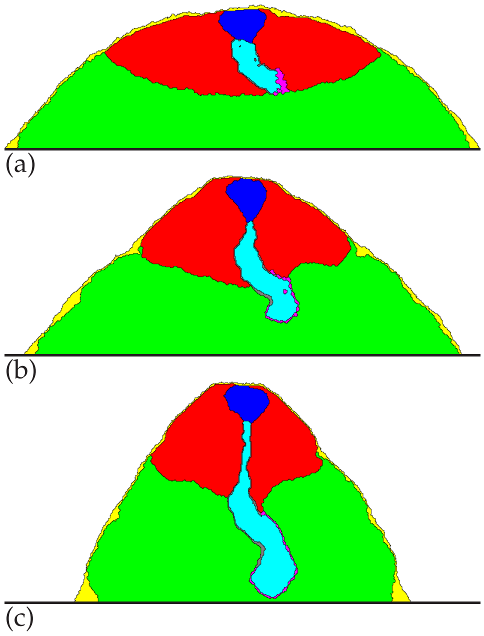

Figure 6.4 on page 99

Figure 6.5 on page 99

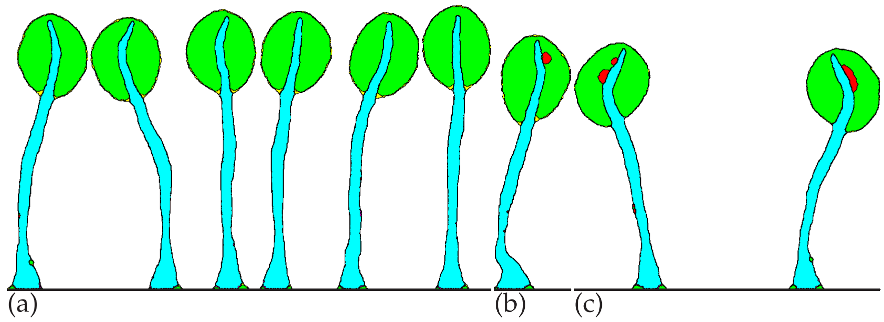

Figure 6.6 on page 101

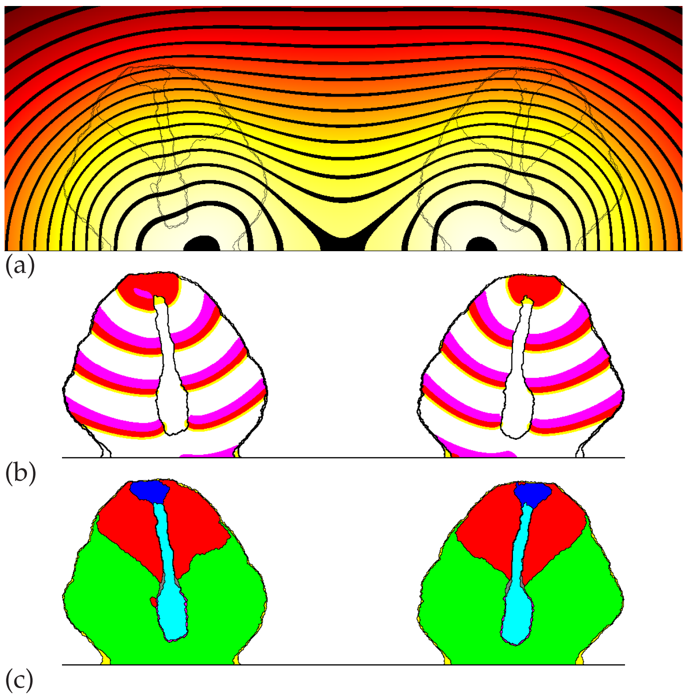

Figure 6.7 on page 102

5

How Slime Moulds Self-Organise into a Fruiting Body: the "Reverse Fountain" Explained

Athanasius F. M. Marée and Paulien Hogeweg
Theoretical Biology and Bioinformatics,
Utrecht University, Padualaan 8,
3584 CH Utrecht, The Netherlands.

Submitted

Abstract

Culmination of *Dictyostelium discoideum* morphogenesis involves complex cell movements which transform a mound of cells into a globule of spores on a slender stalk. The movement has been likened to a "reverse fountain", whereby prestalk cells in the upper part form a stalk that moves downwards and anchors itself to the substratum, while prespore cells in the lower part move upwards to form the spore head. So far, however, no satisfactory explanation has been produced for the downward elongation (Williams, 1997). Using a Monte-Carlo model, we now demonstrate that the processes that are essential during the earlier stages of the morphogenesis are in fact sufficient to produce the dynamics of the culmination stage. These processes are cyclic AMP (cAMP) signalling (Dormann *et al.*, 1998), differential adhesion (Bozzaro & Ponte, 1995), cell differentiation (Williams, 1997) and production of extracellular matrices (Wilkins & Williams, 1995). Our model clarifies the processes that underlie the observed cell movements. We show that periodic upward movements, due to chemotactic motion, are essential for successful culmination, because the pressure waves they induce squeeze the stalk downwards through the cell mass, a mechanism which has a number of self-organising and self-correcting properties and can explain many experimental observations.

5.1 Introduction

When individual amoebae of the cellular slime mould are starving, they aggregate to form a multicellular migrating slug, which moves towards a region suitable for culmination. We have modelled the process of culmination using a hybrid stochastic cellular automata (CA)/partial differential equation (PDE) model (Savill & Hogeweg, 1997, and chapters 3 and 4). Individual cells are modelled as a group of connected automata, i.e. the basic scale of the model is subcellular. Our model is an extension of the Glazier & Graner-model formalism (Glazier & Graner, 1993), in which cell displacements are driven by differential cell adhesions, combined with a sloppy volume conservation. We have added the following properties: cAMP signalling, chemotaxis, cell differentiation and rigidity.

5.2 The Model

Our model is based on the following experimental observations. Periodic cell movements occur during aggregation and slug migration (Dormann *et al.*, 1998), as well as during culmination (Durston *et al.*, 1976). Although the movement mechanisms are still under debate (Wang & Kuspa, 1997), there is increasing experimental evidence that the coordinated upward movement of the cells is organised by a combination of a pulsatile cAMP excretion and a cAMP-mediated cAMP response, accompanied by a chemotactic response towards the cAMP (Verkerke-van Wijk & Schaap, 1997). The cAMP waves originate in the prestalk A (PstA) region, which in both model and experiment is located in the uppermost part of the culminant. Then the cAMP signal is relayed by prestalk O (PstO) cells, which occupy the posterior part of the prestalk-zone, and by prespore cells, which occupy the lower part of the culminant (Williams *et al.*, 1993; Kitami, 1984).

During culmination a unidirectional conversion of cell types takes place: PstO cells differentiate into PstA cells, and PstA cells into stalk cells (Sternfeld, 1992). We assume that contact between the cell types is required for this process, since cell induction has not been detected even at a distance of a few cell diameters (Williams *et al.*, 1993). The newly created stalk cells produce a stiff extracellular matrix (Jermyn & Williams, 1991) and increase their volume by vacuolation (Watts & Treffry, 1976).

A special group of cells, which first appear during the slug stage (Jermyn & Williams, 1991), occupies the tip region of the downward elongating stalk (Sternfeld, 1992). Due to their position and the fact that the stalk elongates straight downwards, these cells are assumed to guide the elongation; they are therefore referred to as pathfinder cells (Jermyn & Williams, 1991). Although the symmetry in upward and downward motion is striking, neither stalk cells nor pathfinder cells respond to cAMP and no other clue as to the stimulus directing the downward movement has been found (Williams, 1997). Hence in our model, pathfinder cells simply differ from stalk cells in adhesion strengths. We start our simulations when stalk cell differentiation has just begun and a small number of pathfinder cells are positioned at the stalk tip.

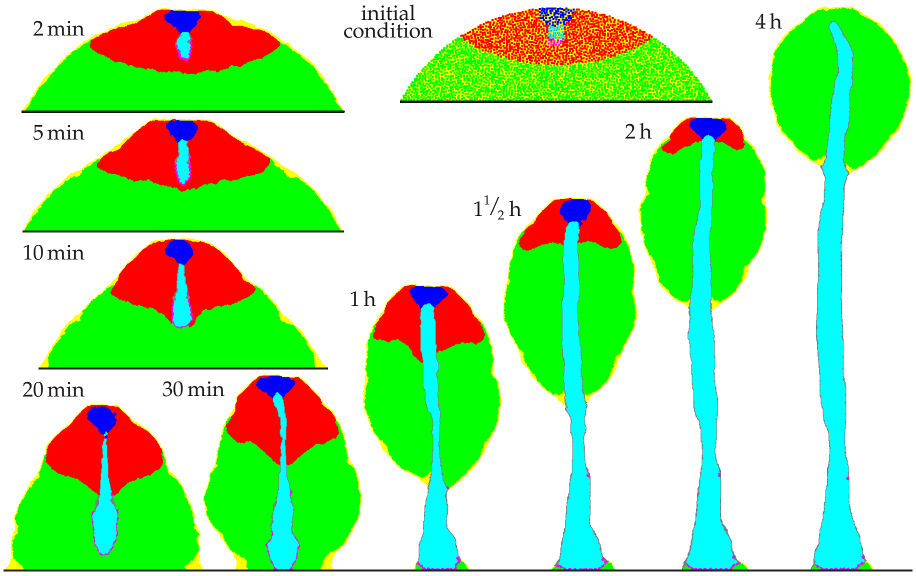

Figure 5.1. Time sequence of a simulation of the process of culmination. Cell types are $\tau \in$ {Psp (green), PstO (red), PstA (blue), St (cyan), Pf (magenta), Sl (yellow), Tu (grey)}. See also the colour plate on page 74.

In our model we have implemented only the above mentioned experimentally elucidated mechanisms. The CA is used to describe the individual cells, the PDEs are used to describe the cAMP dynamics. A more detailed description is given in the Methods section. Time and space are scaled so as to simulate realistic characteristics for the periodicity and signal propagation of the cAMP waves (Siegert & Weijer, 1989, 1992).

5.3 Results

We now describe and explain the process of culmination as it unfolds in the model and refer to experiments in which comparable behaviour has been observed. Figure 5.1 shows that on a time-scale consistent with experiments (Higuchi & Yamada, 1984) a mound of cells develops into a fruiting body. As a result of the strong adhesion between the stalk cells and the much weaker adhesion between stalk and PstO cells, the stiff matrix produced by the stalk cells is 'squeezed' outwards, where it accumulates at the boundary between the two cell types: very rapidly a stalk tube is formed (Williams *et al.*, 1993). The top of the tube forms a gate through which prestalk cells can enter (Watts & Treffry, 1976). The gate remains open as a result of the combined effect of ongoing induction, differential adhesion and stiffness of the matrix. Periodically cAMP waves, originating in the PstA region, move downwards through the cell mass. These waves, combined with the chemotactic response, lead to the upward cell motion (Chen *et al.*, 1995).

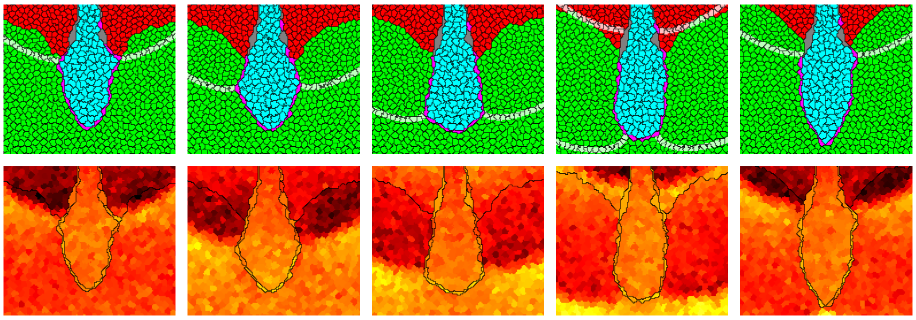

(a) (b) (c) (d) (e)

Figure 5.2. Detailed view of the stalk elongation during the simulation of Fig. 5.1. Top row shows all individual cells. Light bands indicate the regions of chemotactic motion towards cAMP. Bottom row shows the pressure differences, indicated by the mean cell volume of individual cells, averaged over five samples at intervals of 2 seconds. Volumes are indicated by a colour gradient from dark red (small volume) to bright yellow (large volume). (a) at 14 minutes 40 seconds, (b)–(e) with subsequent intervals of 40 seconds. See also the colour plate on page 74.

Due to the adhesion, the pathfinder cells immediately surround the stalk tip (Jermyn & Williams, 1991). Although neither the pathfinder cells nor the stalk cells are chemotactic, the tip elongates downwards at a greater speed than the chemotactic upward motion. The stalk tip reaches the base around 20 minutes after entering the prespore region, which is just as fast as observed in experiments (Sternfeld, 1992). The mechanism can be elucidated as follows (see Fig. 5.2): downward moving cAMP waves periodically trigger an upward directed chemotactic response. Because chemotactically moving cells push cells in front of them and pull cells that are behind them, pressure differences are created. Hence the cAMP waves are always accompanied by pressure waves, which are much broader. The pathfinder cells are pushed and pulled by these pressure waves, which results in a peristaltic motion of the stalk tip. The pathfinder cells, and along with them the stalk cells, are thereby squeezed downwards. Newly recruited stalk cells are transported through the tube by the combination of pushing at the tube gate, due to the surface tension between PstA and stalk cells, and pulling at the stalk tip, due to the peristaltic motion.

Although an elongated shape moving against a flow has a very strong tendency to bend sideways, the mechanism revealed by our model very efficiently restores any such deviation. Figure 5.3 shows that even if initially the stalk is bent 90 degrees, it extends downwards again after only 15 minutes. When the stalk tip is not precisely pointing downwards, the cAMP waves reach one side earlier. Hence, the moment this side is pushed, the other side is still pulled. This force efficiently transports the cells inwards, instead of downwards, and restores the original orientation. Peristalsis also explains the position of the pathfinder cells. When more than half of the pathfinder cells happen to be positioned along

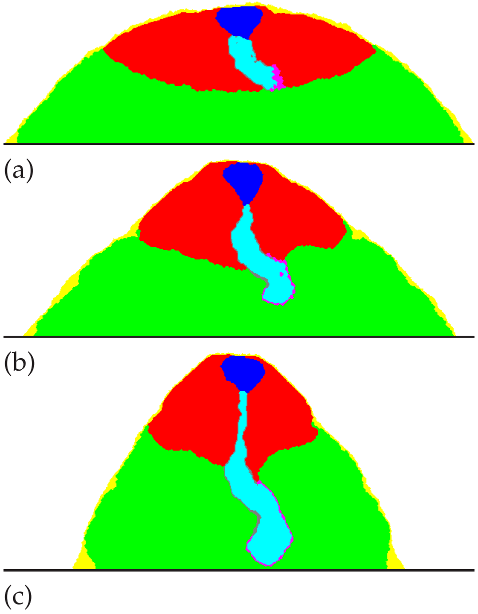

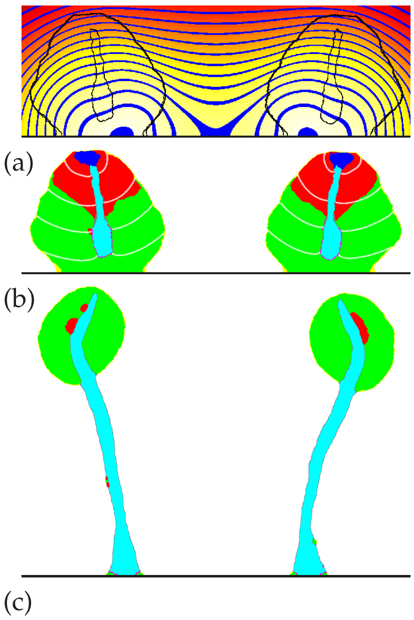

Figure 5.3. Restoration of the direction of stalk elongation. Initially, the stalk tip is bent 90 degrees. (a) 50 seconds; (b) 8 minutes 20 seconds; and (c) 16 minutes 40 seconds. See also the colour plate on page 74.

Figure 5.4. Snapshot, after 20 minutes, of two culminants orienting away from each other due to NH_3 production. (a) The NH_3 distribution, indicated by a colour gradient from dark red (low concentration) to bright yellow (high concentration), with blue bands of iso-concentration; (b) the culminants, with slanted stalks. Light bands indicate the cAMP waves; (c) final configuration after 4 hours. See also the colour plate on page 74.

one side of the stalk, the imbalance is quickly rectified. This is because downward motion on the more crowded side is more efficient and pushes the cells back to the other side. Hence the pathfinder cells always remain positioned along the tip of the stalk, yet another property that is not explicitly incorporated in the model.

The downward motion stops automatically when the stalk tip reaches the base, because the tip is no longer completely surrounded by cAMP waves. The upward motion of the prespore cells also stops in a self-organising way when the PstA cell type is depleted. The cAMP waves now also cease, because the PstA cells were the ones which periodically produced the cAMP signal. Therefore the upward motion halts at the moment the stalk formation is completed. After the chemotactic motion has stopped, the prespore cell mass becomes rounded, due to surface tension properties. The tube, however, is too stiff to change its general shape. Thus, in the model, a globule of spores on a slender stalk is the stable final configuration. The indirect mechanisms described here not only generate the normal culmination process, but they are also self-correcting and self-terminating. We therefore refute the claim in the literature that the stalk is pushed downwards as a result of the addition of stalk cells at the top (Jermyn & Williams, 1991; Thomason *et al.*, 1999). Our model rules out this possibility.

Many other experimental observations are in agreement with our model. For example, when the differentiation of PstA cells into stalk cells is blocked, and hence no stalk is formed, in both model and experiments the culminant still moves upwards, but ends up as an erratic hair-like structure (Harwood *et al.*, 1992). In the model this is due to upward motion by chemotaxis, which does not stop because the prestalk pool is never emptied. However, the results of this experiment cannot be reconciled with the classical view that the cells are pushed upwards by the stalk elongation (Jermyn & Williams, 1991; Thomason *et al.*, 1999). When the rate of chemotactic motion is reduced (Chen *et al.*, 1995) or when upward motion is prevented by an extreme centrifugal force (40-50 G) (Kitami, 1985), no normal stalk formation is observed. The simple explanation provided by the model is that periodic upward motion is necessary for the downward elongation. In experiments a constriction develops at the base of the prespore zone before the stalk reaches the substratum (Chen *et al.*, 1998). In the model this is due to the combination of cellular adhesion and upward motion.

Finally, culminants orientate away from ammonia (NH_3) (Bonner *et al.*, 1986), as well as away from each other, apparently because they themselves produce NH_3 (Feit & Sollitto, 1987). Figure 5.4 shows how this behaviour can be accounted for: the cells produce a small quantity of NH_3, which inhibits the cAMP-induced cAMP release (by inhibiting the activation of adenylate cyclase, Williams *et al.*, 1984); NH_3 accumulates between the two adjacent culminants, and because cAMP waves move more slowly at higher NH_3 concentrations, the waves become slanted. The stalks, which extend perpendicular to the cAMP waves, move towards each other instead of straight downwards, and the fruiting bodies end up orientated away from each other.

5.4 Discussion

We have previously used the same model-formalism, including the same processes of differential adhesion, cAMP signalling and chemotaxis, to explain the aggregation of single amoebae into a mound and a moving slug (Savill & Hogeweg, 1997), as well as to unravel the mechanisms behind thermotaxis and phototaxis, which direct a slug to a suitable site for culmination (see chapters 3 and 4). These model studies together with the results reported in this paper demonstrate that the entire process of morphogenesis, except for the initiation and termination of the slug stage, can unfold without any need to change the parameters of these processes. Nevertheless many genes are up and down regulated during slime mould development, and much more is likely to become known about the genes involved in the near future. Many of these genes are certainly connected with processes not directly related to the cell movements, e.g. the maturation of spore cells. Evaluating the role of those genes that are involved in cell movement in the light of our model should generate interesting insights into evolutionary refinements and genetic robustness and should reveal how gene expression governs macrolevel phenomena. For example, it should be possible to interpret the aberrant phenotypes created by restriction enzyme-mediated integration (REMI) (Smith, 2000). Note that our model is completely defined at the (sub)cellular level, whereas the mechanisms at work are on larger scales, ranging from individual cells to slugs, to culminants, and finally even between culminants. We have demonstrated the feasibility of such multi-scale modelling for explaining the mechanisms involved in *Dictyostelium discoideum* morphogenesis. Undoubtedly, a similar approach could be adopted to unravel the mechanisms underlying other types of developmental processes (Hogeweg, 2000a).

Appendix

5.5 Methods

We have modelled the culmination using two-dimensional simulations, which are considered to be transverse sections. We used the Glazier & Graner-model (Glazier & Graner, 1993), extended in the following way. Each cell has a unique identification number, σ, which is assigned to circa 30 automata in the stochastic CA. Each cell also has a type label τ, which indicates whether the cell type is prespore, PstO, PstA, stalk or pathfinder ($\tau \in$\{Psp, PstO, PstA, St, Pf\}). Each automaton that is part of a cell's boundary has a number of dimensionless free energy bonds, given by $J_{\tau_1,\tau_2} > 0$. The values of J_{τ_1,τ_2} are given in Table 5.1. The total free energy of a cell is given by:

$$H_\sigma = \sum \frac{J_{\text{type,type}}}{2} + \sum J_{\text{type,Air}} + \sum J_{\text{type,Soil}} + \lambda(v - V)^2, \qquad (5.1)$$

where v is the actual volume, V the target volume, and λ the inelasticity. Minimisation of the free energy causes boundary deformation. ΔH gives the change in free energy if a deformation were to occur. The probability that a boundary will indeed be deformed is either 1 if $\Delta H < -H_{\text{diss}}$, or $e^{-\left(\frac{\Delta H + H_{\text{diss}}}{T}\right)}$ if $\Delta H \geq -H_{\text{diss}}$. H_{diss} represents the dissipation costs involved in deforming a boundary; T represents the default motility of the cells.

To describe the slime sheath and the stalk tube ($\tau \in$\{Sl, Tu\}), two entities are defined which follow the same rules and can deform in the same way as all cells. The stiffness of the stalk tube is described by a high H_{diss}. The slime sheath has a fixed volume; the volume of the stalk tube increases whenever a new stalk cell appears.

The induction of PstA cells into stalk cells is implemented by searching at fixed time intervals ($\Delta t_{\text{induction}}$) PstA-stalk cell contacts. The chance of changing one PstA cell into a stalk cell is proportional to the amount of contact area. The differentiation of PstO cells into PstA cells is modelled in the same way. During the first 15 minutes after their appearance stalk cells increase their target volume by 33%. Initially, the open space between the cells is filled with slime mass; the

Table 5.1. Parameter settings used in the simulations. For each cell type the values of J_{τ_1,τ_2}, the initial number of cells, their target volume and the type of cAMP dynamics (cAMP relay, oscillatory or small decay) are shown.

	J_{τ_1,τ_2}									#cells	V	cAMP
	Air	Soil	Psp	PstO	PstA	St	Pf	Sl	Tu			
Psp	20	11	9							1960	30	relay
PstO	27	14	13	7						1011	30	relay
PstA	33	16	13	10	3					79	30	oscill.
St	43	20	25	24	16	3				25	30–40	decay
Pf	35	8	10	10	17	7	11			14	30	decay
Sl	5	7	8	15	21	21	7	–		1	3 000	decay
Tu	5	9	10	11	12	3	5	1	–	1	3×#St	–

slime then spreads out over the cell mass, forming the slime sheath within a few time steps.

To describe the cAMP dynamics we use a discretised PDE with the same grid size as the CA. The cAMP can diffuse freely through all cells and through the slime sheath, but not through the tube, which is considered to be impermeable to cAMP, or into the air or soil. Excitable cAMP dynamics can be described reasonably well in a quantitative way by two variable FitzHugh-Nagumo equations with piecewise linear 'Pushchino kinetics' (Panfilov & Pertsov, 1984). Here we have used the same equations and parameter settings as used previously (see chapter 3). Table 5.1 indicates which kinds of cAMP dynamics were used for the different cell types.

Provided their refractoriness is not too high, prespore and prestalk cells respond to the cAMP signal by making a chemotactic movement towards cAMP. Chemotaxis is incorporated by using the local cAMP spatial gradient: $\Delta H' = \Delta H - \mu(\text{cAMP}_{\text{automaton}} - \text{cAMP}_{\text{neighbour}})$. One Monte-Carlo step, during which every CA is randomly updated once, corresponds to 0.1 seconds and one grid point corresponds to 5 μm.

In the simulation of Fig. 5.4, all prestalk and prespore cells produce 1×10^{-3} NH_3/second, which can also diffuse into the air. The inhibiting effect of NH_3 (n) on the cAMP dynamics is incorporated by increasing the value of parameter $a_{\tau,n}$, which defines the excitability of the cell (see chapter 4): $a(\tau, n) = a_\tau + \frac{b_\tau n^s}{1+(n/p)^s}$.

Parameters used are $T = 6$, $\lambda = 1$, $\mu = 200$, $H_{\text{diss}} = 0.8$, $H_{\text{tubediss}} = 30$, and $\Delta t_{\text{induction}} = 8.5$ seconds. In Fig. 5.4, $a_{\text{PstA}} = -0.20$, $a_{\text{PstO}} = a_{\text{Psp}} = -0.025$, $b_{\text{PstA}} = 0.0375$, $b_{\text{PstO}} = b_{\text{Psp}} = 0.075$, $p = 2$, $s = 3$ and $D_n = 15$.

Acknowledgements

We would like to thank Dr. S. M. McNab for linguistic advice. A. F. M. Marée was supported by the Priority Program Nonlinear Systems of the Netherlands Organization for Scientific Research.

6

Modelling *Dictyostelium discoideum* Morphogenesis: the Culmination

Athanasius F. M. Marée and Paulien Hogeweg
Theoretical Biology and Bioinformatics,
Utrecht University, Padualaan 8,
3584 CH Utrecht, The Netherlands.

Submitted

Abstract

The culmination of the morphogenesis of the cellular slime mould *Dictyostelium discoideum* involves complex cell movements which transform a mound of cells into a globule of spores on a slender stalk. We show that cyclic AMP (cAMP) signalling and differential adhesion, combined with cell differentiation and slime production, are sufficient to produce the morphogenetic cell movements which lead to culmination.

We have simulated the process of culmination using a hybrid cellular automata (CA)/partial differential equation (PDE) model. In the model, individual cells are represented as a group of connected automata, i.e. the basic scale of the model is subcellular. With our model we have been able to reproduce the main features that occur during culmination, namely the straight downward elongation of the stalk, its anchoring to the substratum and the formation of the long thin stalk topped by the spore head.

We conclude that the cAMP signalling system is responsible for the elongation and anchoring of the stalk, but in a roundabout way: pressure waves that are induced by the chemotaxis towards cAMP squeeze the stalk through the cell mass. This mechanism forces the stalk to elongate precisely in the direction opposite to that of the chemotactically moving cells. The process turns out to be 'guided' by inactive 'pathfinder' or 'vanguard' cells, which form the tip of the stalk. We show that the entire development is enacted by means of the above mentioned building blocks. This means that no global gradients or different modes of chemotaxis are needed to complete the culmination.

6.1 Introduction

When their bacterial food source is depleted individual amoebae of the cellular slime mould *Dictyostelium discoideum* aggregate to form a multicellular migratory slug, which is surrounded by a slime sheath. The slug has phototactic and thermotactic properties, which direct it to a suitable site for culmination. When it finds a good location or when time is running out, migration halts and in about 4 hours a fruiting body is formed; the fruiting body has a stalk that supports a spore head elevated above the substratum to facilitate spore dispersal.

Our theoretical understanding of *Dictyostelium* morphogenesis is progressing in the same way as the morphogenesis itself. Initially, the focus was mainly on the aggregation (Nanjundiah, 1973; Parnas & Segel, 1977; Tyson & Murray, 1989) and stream formation (MacKay, 1978; Levine & Reynolds, 1991; Vasiev *et al.*, 1994; Höfer *et al.*, 1995b; van Oss *et al.*, 1996); more recently the mound formation and slug migration have been studied (Bretschneider *et al.*, 1995; Savill & Hogeweg, 1997; Jiang *et al.*, 1998; Dormann *et al.*, 1998; Bretschneider *et al.*, 1999, and chapters 3 and 4). So far, however, the culmination stage has received little attention.

In this paper we specifically analyse the complex cell movements that lead to the formation of the fruiting body. The processes that are incorporated in our model to describe the culmination are basically the same as those that dominate the earlier stages of the development, from aggregation onwards. These processes are cAMP signalling and cell adhesion between a small number of differentiating cell types. The dynamics observed during culmination involve stalk formation, cell movement and cell differentiation. Below we describe what is known about these processes as a result of experiments.

6.1.1 Stalk formation

Very early during morphogenesis the amoebae are differentiated into two main cell types, prestalk and prespore cells. At the start of culmination the prestalk cells occupy the upper 30% of the culminant, while the prespore cells occupy the lower part.

The movement during culmination has been likened to a "reverse fountain", whereby the prestalk cells in the upper part form a stalk that moves downwards to anchor itself to the base, while the prespore cells from the lower part move upwards to form the spore head. The stalk moves remarkably fast through the centre of the cell mass: Sternfeld (1992) found that the tip of the stalk reached the base only about 20 minutes after penetrating the prespore region. Higuchi & Yamada (1984) found that the movement took only 11 minutes. When the stalk tip becomes anchored to the substratum, it becomes slightly thickened (Higuchi & Yamada, 1984). No lateral motion of the stalk has been observed.

The stalk is surrounded by an extracellular matrix, called the stalk tube. Its composition differs from that of the surface slime sheath in that it is much more rigid (Jermyn & Williams, 1991; Grimson *et al.*, 1996). The tube mass is excreted by the newly recruited stalk cells: EcmB, a stalk cell-specific protein, forms part of the stalk tube (Williams *et al.*, 1993); and when the differentiation into stalk cells is blocked, tube mass production seems to cease (Amagai *et al.*, 1983). At the top of the stalk tube a funnel-shaped gate is formed, through which the prestalk cells enter the tube.

The tip of the stalk is surrounded by a cluster of cells. These cells are believed to guide the straight downward motion of the stalk. Hence they are called 'pathfinder' or 'vanguard' cells (Jermyn & Williams, 1991). The culminant also forms a basal disc, which gives the organism its scientific name, and an upper and lower cup, which surround the spore head.

Gravity plays a minor role in stalk formation. Counter-intuitively, stalk length becomes slightly shorter when gravity decreases, but there is no difference between positively or negatively directed gravity (Kawasaki *et al.*, 1990). Normally, the stalk becomes positioned perpendicular to the substratum, independent of the orientation of the substratum with respect to the gravitational field. However, ammonia (NH_3) influences the process of culmination: culminants orientate away from NH_3 (Bonner *et al.*, 1986), as well as away from each other, presumably also due to NH_3 production (Feit & Sollitto, 1987).

6.1.2 Cell differentiation

The prestalk cells can be divided into prestalk O (PstO) cells, prestalk A (PstA) cells and prestalk AB (PstAB) cells. The PstAB cells form the upper part of the stalk, the PstA cells occupy the top 10% of the culminant, and the PstO cells occupy the lower part of the prestalk-zone. During culmination a unidirectional conversion of cell types takes place: PstO cells differentiate into PstA cells, and PstA cells into PstAB cells (Williams *et al.*, 1989; Sternfeld, 1992). Whereas the transition of PstO into PstA cells takes place slowly and gradually, differentiation of PstA into PstAB is very rapid, and happens only when PstA cells enter the stalk tube: the cells do not express the PstAB-specific marker until they are just inside the entrance (Jermyn & Williams, 1991). The PstAB cells rapidly differentiate into mature stalk cells. During this process, the cells become vacuolated, which leads to a significant volume increase (Williams *et al.*, 1989; Sternfeld, 1992).

However, a special group of PstAB cells develop during the slug stage. During this stage they are located in the central core at the front. These PstAB cells, which are initially present in the tip of the migrating slug, later on form the tip of the downward moving stalk, i.e. they form the above-described cluster of pathfinder cells. The remainder of the stalk consists of PstAB cells that are recruited only later, during the culmination stage. Hence the pathfinder cells are sometimes also called 'early stalk cells'. Pathfinder cells look like immature stalk cells, with little cytoplasm and a large central vacuole, but apparently they do not produce tube mass (Jermyn & Williams, 1991; Sternfeld, 1992; Jermyn *et al.*, 1996).

6.1.3 Cell movements

During culmination complex cell movements are observed. The cAMP plays a central role in the regulation of cell motion in *Dictyostelium*. There seems to be increasing evidence that cAMP signalling continues after aggregation is complete and organises cell movement during both slug migration and fruiting body formation (Verkerke-van Wijk & Schaap, 1997). Such coordinated cell movement is organised by a combination of a pulsatile cAMP excretion and a cAMP-mediated cAMP response, accompanied by a chemotactic response towards the cAMP. Because of their high-frequency pulsatile cAMP excretion, PstA cells are considered to be the source of the cAMP waves (Kitami, 1984).

However, there is, as yet, no clue as to the stimulus that directs the downward movement of the stalk and pathfinder cells (Williams, 1997). Stalk cells neither excrete cAMP nor exhibit negative chemotaxis away from cAMP. The pathfinder cells do not seem to respond to cAMP either: during the slug stage they often disappear in the slime trail in the case of prolonged migration (Sternfeld, 1992). Nonetheless, the symmetry in upward and downward motion is striking (Williams, 1997). It seems unlikely that the pathfinder cells are able to transport the whole stalk downwards, and it also seems unrealistic to assume that the stalk cells themselves move, for they lose their motility very quickly after entering the stalk tube (Watts & Treffry, 1976). Therefore is generally assumed that the tip elongates due to the addition of stalk cells at the tube mouth (Jermyn & Williams, 1991; Thomason *et al.*, 1999).

Not only cAMP, but also cell-cell adhesion and cell-substratum adhesion play an important role in regulating cell movements. Besides, adhesion plays a role in many other processes during all stages of the development, such as cohesion, cell sorting (a process that has been recently challenged by Clow *et al.*, 2000), and contact-mediated regulation of gene expression. Hence in many respects adhesion is essential for normal development (Fontana, 1995; Bozzaro & Ponte, 1995).

In this study we show that the following elements are sufficient to produce all the dynamics observed during the culmination: cAMP signalling, differential adhesion, cell differentiation and extracellular matrices. We show how a stalk surrounded by a tube is formed, how its fast and straight downward motion through the cell mass takes place – without the need for any other chemical or another mode of chemotaxis –, and how eventually a globule of spores on a slender stalk develops.

6.2 The Model

In the last few years several models have been devised to describe the mound and slug stage (see, e.g. Dormann *et al.*, 1998; Jiang *et al.*, 1998; Bretschneider *et al.*, 1999, and chapters 3 and 4). However, the culmination stage has hardly been modelled at all. Although Zeeman (1977) and Rubinow *et al.* (1981) tried to catch the shape of the culminant in mathematical equations, no dynamical model based on biological processes has yet been formulated.

The model described in this paper incorporates cell differentiation by local induction processes, cell-cell and cell-substratum adhesion, cAMP signalling with chemotaxis towards cAMP, and tube mass production. We show how these local processes and their interactions are sufficient to produce the dynamics of the culmination stage.

All the building blocks mentioned above can be very elegantly combined to interact with each other by means of the two-scale CA model-formalism developed by Glazier & Graner (1993), extended with an extra layer for PDEs (Savill & Hogeweg, 1997). In this hybrid formalism, the CA model-formalism is used to represent individual cells. They are, however, represented as a group of connected automata; that is, the basic scale of the model is subcellular. The PDEs are used to describe the cAMP dynamics.

From simplicity we have modelled the culmination using two-dimensional (2D) simulations. The simulations are considered to be transverse sections. Hence we obtain side views of the culminant. In some cases a fruiting body is seen to develop out of flattened quasi-2D slugs (Miura & Siegert, 2000), which is an extra support for such an approach. As our initial configuration we take the starting point of the final culmination, when the culminant forms a more or less hemispherical shape (Higuchi & Yamada, 1984).

6.2.1 Adhesion

In the model-formalism, cell-cell and cell-substratum adhesions are implemented as follows. Each cell has a unique identification number, σ, which is assigned to the about 30 automata in the CA which form the cell. Each cell has also a type label τ, which indicates whether the cell type is prespore, PstO, PstA, stalk or pathfinder ($\tau \in$\{Psp, PstO, PstA, St, Pf\}), i.e. PstAB and stalk cells are lumped together in one cell type. Each automaton that is part of a cell's boundary has a number of dimensionless free-energy bonds. The magnitude of these bonds depends on the types they connect. The energy bonds are given by $J_{\tau_1,\tau_2} > 0$. The bond energy between a certain type and the air is given by $J_{\tau,A}$, and between a certain type and the substratum by $J_{\tau,S}$. The total free energy of a cell is given by:

$$H_\sigma = \sum \frac{J_{\text{type,type}}}{2} + \sum J_{\text{type,A}} + \sum J_{\text{type,S}} + \lambda(v - V)^2, \qquad (6.1)$$

where v is the actual volume, V the target volume, and λ the inelasticity. The final term ensures that the volume of a cell remains close to V. Minimisation of the free energy causes deformation of the boundaries: at every time step all CAs are chosen in a random sequence, and for each CA we calculate whether it will copy itself into a random neighbour. The probability of such a change in cell shape is determined by the change in free energy ΔH if the extension were to occur. The probability is either 1 if $\Delta H < -H_{\text{diss}}$, or $e^{-\left(\frac{\Delta H + H_{\text{diss}}}{T}\right)}$ if $\Delta H \geq -H_{\text{diss}}$. H_{diss} represents the dissipation costs involved in deforming a boundary, which are associated with every change in cell shape. T represents the default motility of the cells.

To describe the slime sheath and the stalk tube, two entities are defined which follow the same rules; these can deform in the same way as all cells but have a

Table 6.1. The values of the energy bonds J_{τ_1,τ_2} and surface tensions γ_{τ_1,τ_2}, the initial number of cells, their target volume, and the type of cAMP dynamics (cAMP relay, oscillatory or small decay) used in the simulations. The surface tensions were calculated using eqns (6.2a) and (6.2b).

τ			$J_{\tau,\mathrm{Psp}}$	$J_{\tau,\mathrm{PstO}}$	$J_{\tau,\mathrm{PstA}}$	$J_{\tau,\mathrm{St}}$	$J_{\tau,\mathrm{Pf}}$	$J_{\tau,\mathrm{Sl}}$	$J_{\tau,\mathrm{Tu}}$	$J_{\tau,\mathrm{A}}$	$J_{\tau,\mathrm{S}}$	#cells	V	cAMP
Psp	15.5	6.5	9	13	13	25	10	8	10	20	11	1960	30	relay
PstO	23.5	10.5	5.0	7	10	24	10	15	11	27	14	1011	30	relay
PstA	31.5	14.5	7.0	5.0	3	16	17	21	12	33	16	79	30	oscill.
St	41.5	18.5	19.0	19.0	13.0	3	7	21	3	43	20	25	30–40	decay
Pf	29.5	2.5	0.0	1.0	10.0	0.0	11	7	5	35	8	14	30	decay
Sl	5.0	7.0	3.5	11.5	19.5	19.5	1.5	–	1	5	7	1	3 000	decay
Tu	5.0	9.0	5.5	7.5	10.5	1.5	-0.5	1.0	–	5	9	1	3×#*St*	–
	$\gamma_{\tau,\mathrm{A}}$	$\gamma_{\tau,\mathrm{S}}$	$\gamma_{\tau,\mathrm{Psp}}$	$\gamma_{\tau,\mathrm{PstO}}$	$\gamma_{\tau,\mathrm{PstA}}$	$\gamma_{\tau,\mathrm{St}}$	$\gamma_{\tau,\mathrm{Pf}}$	$\gamma_{\tau,\mathrm{Sl}}$						

much larger target volume V, and hence model-wise can be regarded as being two very large cells. This means that the slime sheath and stalk tube have their own identification number σ and type label τ ($\tau \in$ {Sl, Tu}). The slime sheath has a fixed target volume. The target volume of the stalk tube however slowly increases due to tube mass production by stalk cells. This is modelled by adding a fixed volume every time a new stalk cell appears. To describe the very stiff nature of the stalk tube, which we consider to be equivalent to the high effort required to deform its shape, we have considerably increased the dissipation costs (H_{tubediss}). Instead of varying the inelasticity λ to model such differences in stiffness, we decided to vary H_{diss}. We did this for two reasons: first of all, H_{diss} is the parameter which describes best what we consider to be 'stiffness', and secondly, the conservation of cells constrains the permissible λ-values.

The values for cell adhesion are given in Table 6.1. The choice and sensitivity of these parameters are discussed in the Results section. It is also useful to define surface tensions in terms of the bond energies J_{τ_1,τ_2} (Glazier & Graner, 1993). Surface tensions between cell types, and surface tensions between a cell type and the air (and, likewise, between a cell type and the substratum) are defined as:

$$\gamma_{\tau_1,\tau_2} = J_{\tau_1,\tau_2} - \frac{J_{\tau_1,\tau_1} + J_{\tau_2,\tau_2}}{2}, \qquad \gamma_{\tau,\mathrm{A}} = J_{\tau,\mathrm{A}} - \frac{1}{2} J_{\tau,\tau}. \tag{6.2a,b}$$

The surface tensions are also given in Table 6.1.

6.2.2 Cell differentiation

During culmination there is a rapid increase in the number of cell types that are functionally different. We have not tried to describe every different cell type, but instead we have restricted our comments to the cell types that seem to play key roles in the extension of the stalk and the formation of the spore head. We did not have to take into account the basal disc and the upper and lower cup, or the transition of prespore cells into mature spore cells.

The process of cell differentiation as described in the Introduction is implemented in the following way: since PstA cells become stalk cells only when they enter the stalk tube, we assume an induction process for which cell-cell contact is necessary. This is implemented by searching PstA-stalk cell contacts at fixed time intervals ($\Delta t_{\text{induction}}$) and by changing one PstA cell into a stalk cell. For each PstA cell the chance that the latter will occur is proportional to the amount of contact area. In the meantime PstO cells change into PstA cells, which is modelled in the same way. Note that we have used fixed time intervals to avoid instabilities in the transitions between the cell types. A very broad range of time intervals can be used, which affects only the height and thickness of the stalk.

After a stalk cell has appeared, it produces tube mass; this is implemented by directly increasing the target volume V of the stalk tube. And due to vacuolation the cell also increases its own volume. To model this process we slowly increase the target volume of stalk cells during the initial period following their appearance, i.e. during the first 10 000 time steps ($\pm$15 minutes when one time step represents 0.1 seconds), by 33%.

6.2.3 cAMP signalling

The cAMP plays a central role in our model. To describe the cAMP dynamics a discretised PDE is used with the same grid size as the CA. The cAMP can freely diffuse through all cells and through the slime sheath, but not through the tube, which is considered to be impermeable to cAMP, or into the air or substratum.

The cAMP dynamics can be described reasonably well in a quantitative way by simplified two-variable equations of the FitzHugh-Nagumo (FHN) type (see chapter 3). Here we use FHN-type equations with piecewise linear 'Pushchino kinetics' (Panfilov & Pertsov, 1984):

$$\frac{\partial c}{\partial t} = D_c \Delta c - f(c) - r, \tag{6.3a}$$
$$\frac{\partial r}{\partial t} = \varepsilon(c)(kc - r), \tag{6.3b}$$

when cell type $\tau \in$\{Psp, PstO, PstA\}, and

$$\frac{\partial c}{\partial t} = D_c \Delta c - d_c(c - c_0), \tag{6.4}$$

when cell type $\tau \in$\{St, Pf, Sl\},

and with $f(c) = C_1 c$ when $c < c_1$; $f(c) = -C_2 c + a_\tau$ when $c_1 \leq c \leq c_2$; $f(c) = C_3(c-1)$ when $c > c_2$, and $\varepsilon(c) = \varepsilon_1$ when $c < c_1$; $\varepsilon(c) = \varepsilon_2$ when $c_1 \leq c \leq c_2$, and $\varepsilon(c) = \varepsilon_3$ when $c > c_2$. To make the function $f(c)$ continuous, $c_1 = a_\tau/(C_1 + C_2)$, and $c_2 = (a_\tau + C_3)/(C_2 + C_3)$. In these equations c represents the cAMP concentration, and r the refractoriness of the cells.

There seems to be evidence that PstA cells periodically produce the cAMP signal and PstO cells relay the signal (Kitami, 1984). This can be implemented in the model by giving the first cell type a negative value of a_τ, and the second cell type a positive value of a_τ (see chapter 3). The prespore cells also relay the cAMP signal (see Discussion).

The response to the cAMP signal is a chemotactic movement towards the cAMP. We incorporate the chemotactic response by using the local cAMP spatial gradient: $\Delta H' = \Delta H - \mu(c_{\mathrm{automaton}} - c_{\mathrm{neighbour}})$, where $\Delta H'$ is the new change in energy. This makes it more likely that an amoeba will move towards a location with a higher cAMP concentration and less likely that it will move towards one with a lower cAMP concentration. Chemotaxis is only taken into account when cAMP is above a threshold $c_{th} = 0.05$ and refractoriness below a threshold $r_{th} = 0.2$. The stalk cells and pathfinder cells do not produce or relay the signal (Sternfeld, 1992) and they are not chemotactic (Williams *et al.*, 1989), which means that they are not involved in the signalling or in the response.

6.2.4 Initial condition

The initial condition for our model is based on the following observations. When the slug halts its forward movement, the tip lifts up and the rear part crawls in underneath, and a more or less hemispherical shape is formed (Higuchi & Yamada, 1984). This is the moment that we have taken as our starting point. At this stage, the uppermost part consists of PstA cells, lower down are PstO cells, and at the bottom are the Psp cells (Williams *et al.*, 1989). The initial core of pathfinder cells developed earlier, during the slug stage (Jermyn & Williams, 1991). We start our simulations when the stalk cell differentiation has just begun, presumably initially induced by the pathfinder cells. The stalk tube, however, has not yet formed. The stalk primordium is slightly submerged. If stalk formation were to start completely at the top, one would expect an invagination, but this is not observed. Hence it seems that cells somewhat deeper down in the culminant are involved in the prestalk-stalk transition (Watts & Treffry, 1976). Because the stalk cells produce tube mass locally, they are initially surrounded by this mass.

The open space between the cells is filled with slime mass, a worst case scenario to describe the fact that slime mass seems to be produced by all cells (Wilkins & Williams, 1995). This part of the initial condition is obviously very unrealistic. However, within a few time steps the slime spreads out over the cell mass and the slime sheath is formed. Clearly, this process of 'squeezing out' the slime mass and of slime sheath formation normally happens much earlier during development.

6.3 The Culmination of *Dictyostelium discoideum*

We were able to reproduce the culmination of *Dictyostelium discoideum*. Figure 6.1 shows a number of snapshots of the process. We have scaled the time step and space step so as to simulate realistic values for the cAMP dynamics. To attain the (for the slug stage) characteristic periodicity of 2-3 minutes (Siegert & Weijer, 1992), one time step must correspond to 0.1 seconds. To obtain a signal propagation velocity around 200 μm/minute (Siegert & Weijer, 1989), one grid point must

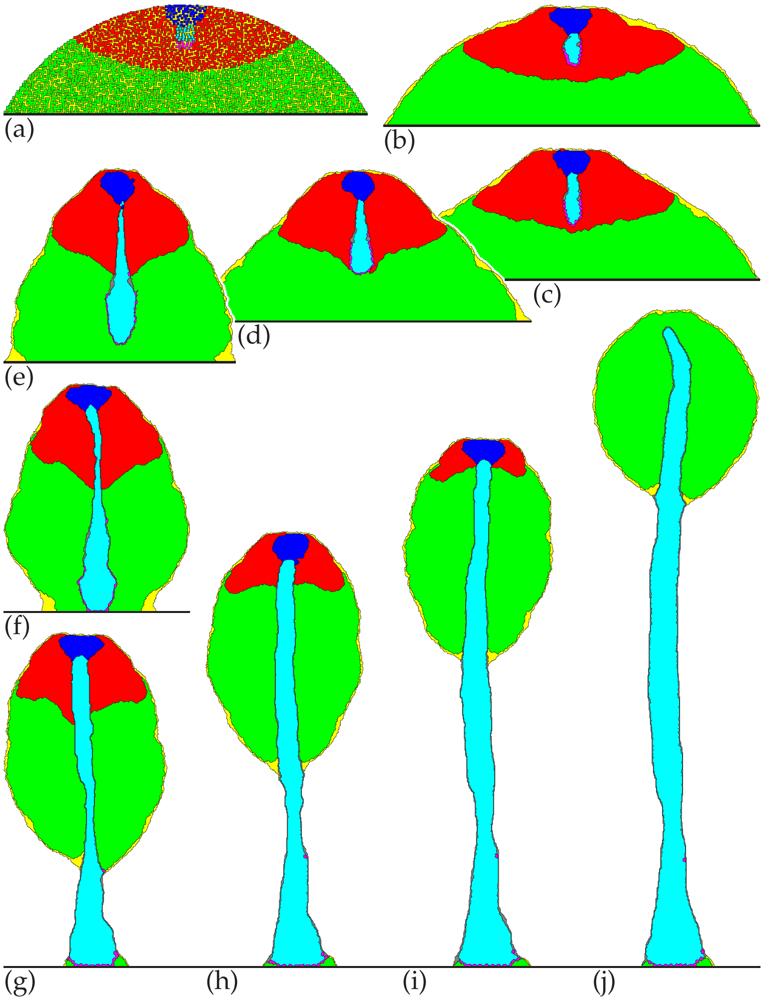

Figure 6.1. Time sequence of a simulation of the process of culmination. (a) Initial condition; (b) 2 minutes (1 200 time steps); (c) 5 minutes (3 000 time steps); (d) 10 minutes (6 000 time steps); (e) 20 minutes (12 000 time steps); (f) 30 minutes (18 000 time steps); (g) 1 hour (36 000 time steps); (h) 1 hour 30 minutes (54 000 time steps); (i) 2 hours (72 000 time steps); and (j) 4 hours (144 000 time steps). There are 3089 cells. One time step (solution of the PDEs) corresponds to about 0.1 seconds, and one grid point to 5 μm. Cell types are $\tau \in \{$Psp (green), PstO (red), PstA (blue), St (cyan), Pf (magenta), Sl (yellow), Tu (grey)$\}$. $T = 6$, $\lambda = 1$, $\mu = 200$, $H_{\text{diss}} = 0.8$, $H_{\text{tubediss}} = 30$, and $\Delta t_{\text{induction}} = 85$ (8.5 seconds). The other parameters are given in Table 6.1. The parameters used to describe the cAMP dynamics are $a_{\text{PstA}} = -0.1$, $a_{\text{PstO}} = a_{\text{Psp}} = 0.1$, $D_c = 1$, $C_1 = 20$, $C_2 = 3$, $C_3 = 15$, $\varepsilon_1 = 0.5$, $\varepsilon_2 = 0.0589$, $\varepsilon_3 = 0.5$, $k = 3.5$, $d_c = 0.05$, and $c_0 = -0.3$. The PDEs are solved by the explicit Euler method (with time step equal to 0.01 and space step equal to 0.37). See also the colour plate on page 75.

correspond to 5 μm. This scaling produces the correct timescale for culmination and a fruiting body of the correct size: a fruiting body about 6 mm high is formed, in about 4 hours.

Within a very short time-span, i.e. within 2 minutes, the tube mass produced by the stalk cells forms a tube round the stalk cells. The stalk tip, however, does not become surrounded by stalk tube; instead it is occupied by the pathfinder cells. The tube mouth is formed at the top of the stalk. Periodically cAMP waves, originating in the PstA region, move downwards through the cell mass. These waves combined with the chemotactic response towards the cAMP lead to upward cell motion. At the same time the stalk tip quickly moves downwards, apparently 'guided' by the pathfinder cells: the stalk elongation is directly perpendicular to the substratum, and the pathfinder cells continue to occupy the tip region. Within 20 minutes after passing through the prestalk/prespore interface the stalk arrives at the base. When the stalk reaches the substratum, the pathfinder cells anchor it and motion in the tip region halts. The culminant elongates upwards by continuous production of stalk cells combined with an upward motion of the spore mass. When the prestalk cell reservoir is empty, a spore head forms at the top of the stalk.

There are a number of processes which need to be looked at more closely: the formation of the tube, the fast downward elongation of the stalk, the fact that this elongation is perpendicular to the substratum, the anchoring of the stalk when it reaches the base, and the final configuration.

6.3.1 Tube formation

The stalk tube is formed very quickly. Due to strong cell adhesion between the stalk cells and weak adhesion between stalk and PstO cells, the tube mass is 'squeezed' outwards, where it accumulates at the boundary between the two cell types. The tube mouth remains open, i.e. the matrix does not extend over the top, due to the continuous formation of new stalk cells and the more moderate adhesion strength between stalk and PstA cells. It does not extend along the stalk tip either, because the pathfinder cells adhere strongly to both stalk cells and PstO cells. In addition, the stiffness of the tube slows down its extension, both along the stalk tip and the tube mouth.

6.3.2 Stalk elongation

The tip of the stalk elongates faster downwards than prestalk and prespore cells move upwards, although neither pathfinder cells nor stalk cells show a chemotactic response. Instead the pathfinder cells are pushed downwards by pressure waves that accompany the cAMP waves. Figure 6.2 'zooms in' on the process of downward motion. The figure shows the cAMP waves, the accompanying pressure waves, and the response of the pathfinder cells. Although chemotactic motion occurs only at the wavefront, directed motion is not confined to this region. Because cells push and pull each other, directed motion is observed over a very large area and takes place more or less all the time (see chapter 3). A cAMP

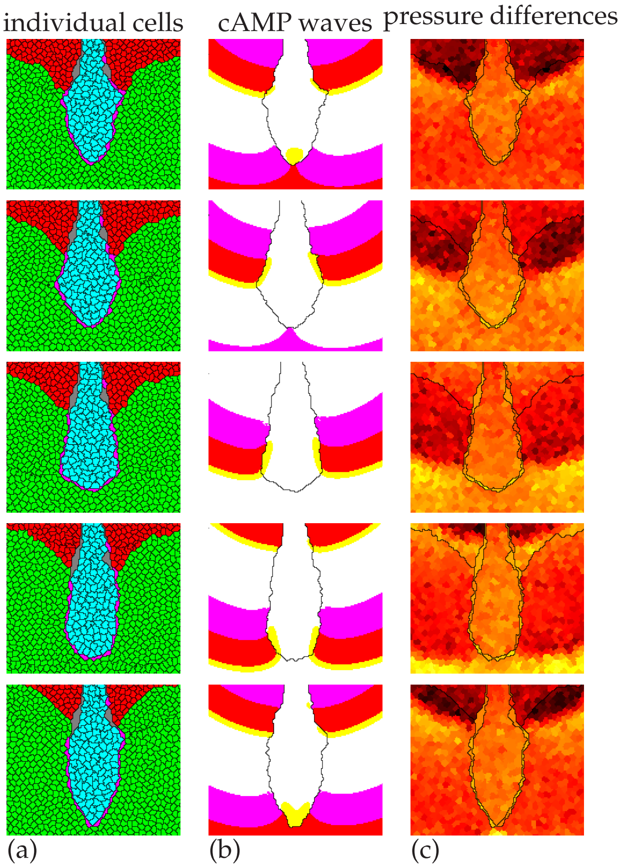

Figure 6.2. Detailed view of the stalk elongation during the simulation of Fig. 6.1. (a) All individual cells. Colour-coding is the same as in Fig. 6.1. (b) Propagation of the cAMP waves. Yellow shows the area where $c > c_{th}$ and $r < r_{th}$ (the wavefront); red the area where $c > c_{th}$ and $r > r_{th}$ (the waveback); and magenta represents the area where $c < c_{th}$ and $r > r_{th}$ (the refractory period). Cells only show chemotaxis in the yellow area. (c) Pressure differences, indicated by the mean cell volume of individual cells, averaged from five samples at intervals of 2 seconds. Volumes are indicated by a colour gradient from dark red (small volume) to bright yellow (large volume). Top frame at 14 minutes 40 seconds (8 800 time steps). Successive frames at intervals of 40 seconds (400 time steps). See also the colour plate on page 76.

wave is always preceded by a period of low pressure, because cells are already pulled away, and is followed by a period of high pressure, because chemotactically active cells push the cell mass. The low pressure pulls the pathfinder cells outwards and the high pressure pushes them inwards again. Because the cAMP wave moves downwards, the pattern of pulling and pushing the pathfinder cells also moves downwards. This means that the pressure waves create a peristaltic motion of the stalk tip, which is comparable to the motion of the intestine. The

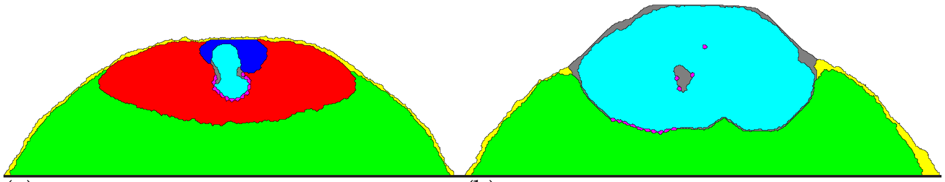

(a) (b)

Figure 6.3. The cAMP dynamics are needed for stalk elongation. Without cAMP signalling the stalk does not elongate downwards, but instead all stalk cells lump together in the upper part. Two snapshots are shown. (a) 8 minutes 20 seconds (5 000 time steps); and (b) 3 hours (108 000 time steps). The simulation is done without cAMP; all other parameters are as described in the legend to Fig. 6.1. See also the colour plate on page 77.

peristaltic motion efficiently squeezes both pathfinder and stalk cells downwards. A little further up the pathfinder cells that move downwards are replaced by tube mass. At the same time, but at the other end of the stalk, newly recruited stalk cells move into the tube. These cells are transported through the tube by the combination of pushing at the tube mouth, due to the surface tension between PstA and stalk cells, and pulling in the lower region, due to the peristaltic motion.

6.3.3 The role of cAMP and pathfinder cells in stalk elongation

The pressure waves are created by the chemotaxis towards cAMP. As a consequence, without periodic cAMP waves or chemotactic motion there will be no peristaltic motion and no displacement of the stalk. Figure 6.3 shows a simulation without cAMP dynamics. In this simulation, the culminant does not move upwards, and the stalk does not move downwards at all. Instead the cells just form one big cluster.

The pathfinder cells are also essential for stalk elongation. Figure 6.4(b) shows a simulation in which the pathfinder cells were omitted from the model. Now the stalk tip also becomes surrounded by the stalk tube. A kind of bag is formed due to the stiffness of the tube. The structure is filled with more and more stalk cells, but is not able to extend downwards or to keep its elongated shape. This is simply because the stiffness of the tube does not allow for any peristaltic motion. Figure 6.4(a) shows the culminant from the simulation of Fig. 6.1 at the same point of time. The stalk here does indeed extend much further.

But even if the tube were as flexible as all other entities, no normal stalk elongation would occur. Figure 6.4(c) shows that when we simulate a flexible tube, the stalk rapidly loses its connection to the PstA region. This is due to the fact that in this case the stalk can be squeezed downwards everywhere along the tube, with the efficiency that was previously found only in the region around the stalk tip. Moreover, Fig. 6.4(c) shows that under these circumstances the stalk completely loses its elongated form. Instead, very quickly the shape becomes more or less round. This is due to the resistance created by all the cells that move upwards, which make it look like a falling drop of water. In contrast, in Fig. 6.4(a) such an

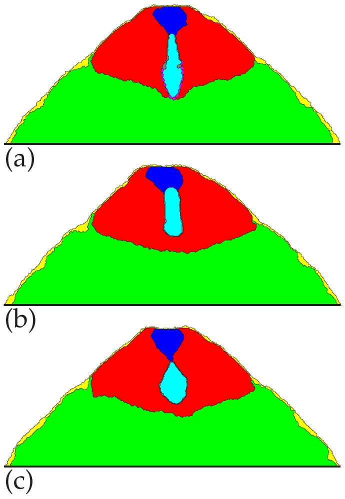

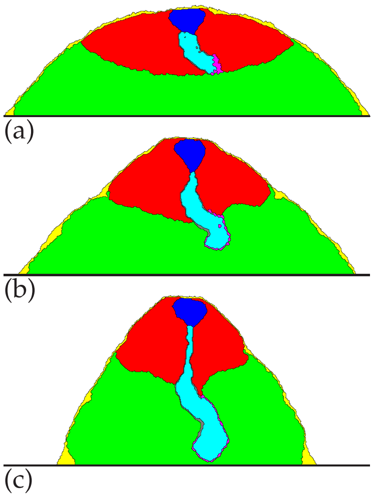

Figure 6.4. The pathfinder cells are needed for stalk elongation. Snapshots are shown of a simulation with, and two simulations without pathfinder cells. (a) Snapshot taken from the simulation of Fig. 6.1. (b) Without pathfinder cells, the stalk does not extend downwards, due to the stiffness of the stalk tube. (c) When the stalk tube is flexible (H_{tubediss} equals H_{diss}), the upper side of the stalk becomes detached, and the stalk tip flattens. All snapshots are taken at the same moment, i.e. after 8 minutes 20 seconds (5 000 time steps). All parameters [except H_{tubediss} in (c)] are as described in the legend to Fig. 6.1. See also the colour plate on page 77.

Figure 6.5. Correction of the direction of stalk elongation. In the initial configuration the stalk tip is bent 90 degrees. (a) 50 seconds (500 time steps); (b) 8 minutes 20 seconds (5 000 time steps); and (c) 16 minutes 40 seconds (10 000 time steps). The final fruiting body is shown in Fig. 6.6(b). All parameters are as described in the legend to Fig. 6.1. See also the colour plate on page 77.

effect cannot be observed. This is because with a stiff tube only the tip is easily pulled downwards; the rest of the stalk is much more resistant. Hence the stalk tip is pulled into a spiky shape. Such a shape efficiently reduces the resistance created by the upward moving cells and, in the long run, makes the whole stalk nicely elongated. The flat base of the 'stalk' without a stiff tube in Fig. 6.4(c) does indeed strongly reduce the downward elongation. In conclusion, both flexible pathfinder cells and a stiff tube are needed to make the fast descent of the stalk tip possible.

6.3.4 Correction of orientation

Pathfinder cells are necessary not only for the downward motion of the stalk and its elongated shape, they also ensure that the elongation is precisely in the opposite direction to the upward moving cells. This is really not trivial, since an elongated structure that moves against the flow always has a very strong tendency to bend sideways.

Figure 6.5 shows a simulation in which the stalk is initially bent 90 degrees. However, very rapidly the tip turns downwards again. Figure 6.6(b) shows the final configuration of this simulation, which does not differ much from the fruiting bodies of other simulations. The mechanism can be described as follows. Normally both sides of the stalk tip are pushed or pulled at the same time. Stalk cells are transported downwards, from the region where the stalk tip is pushed to the region where it is pulled. A different situation arises when the tip no longer points downwards, for example due to the combined effect of random fluctuations and the force exerted by the cells moving upwards. Now the cAMP waves no longer move perpendicular to the stalk, but arrive at one side sooner than at the other. Consequently, at the moment one side is pushed, the other side is still being pulled. This efficiently transports cells inwards, instead of downwards, and the original orientation is restored. Note that along the side which is pushed there is also a region which is pulled, and along the other side there is also a region that is pushed. These regions, however, are not located opposite to each other, and hence this does not lead to efficient cell transport.

Peristalsis also explains the position of the pathfinder cells. When more than half of the pathfinder cells happen to be positioned along one side of the stalk, the imbalance is quickly rectified. This is because downward motion on the more crowded side is more efficient and pushes the cells back to the other side. Hence the pathfinder cells always remain positioned along the tip of the stalk, yet another property which was not explicitly incorporated in the model.

In conclusion, the stalk tip always extends perpendicular to the cAMP waves, and any deviations are corrected. Since the tip of the culminant is the source of the cAMP waves, and is on top of the culminant, the stalk becomes positioned more or less perpendicular to the substratum.

6.3.5 Anchoring

Due to the mechanism described above the downward motion stops automatically: when the stalk tip reaches the base, it is no longer completely surrounded by cAMP waves, and therefore it does not move further downwards. The pathfinder cells which have not yet reached the base still have a tendency to move downwards but not sideways. Therefore, all pathfinder cells finally end up on the substratum, and the stalk tube surrounds the whole stalk. Obviously, in our model the pathfinder cells adhere quite strongly to the substratum, but this is not very important for the general behaviour.

6.3.6 Final configuration

New stalk is continuously added at the tube mouth until all prestalk cells are transformed into stalk cells. When the PstA cell type is exhausted, the cAMP waves also cease, because it is only the PstA cells that periodically produce the cAMP signal. Therefore, the moment the stalk formation is complete, the upward

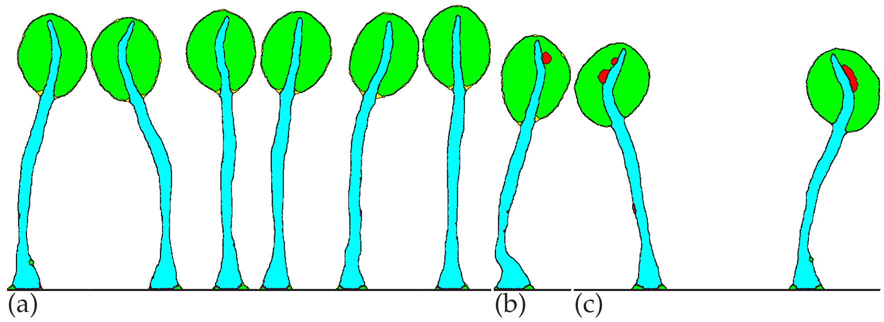

Figure 6.6. Variations in the final fruiting bodies that were formed by(a) six simulations with different random seeds; (b) the simulation of Fig. 6.5, in which the stalk tip was initially bent 90 degrees; and (c) the simulation of Fig. 6.7, in which two fruiting bodies orientate away from each other. The precise final configuration varies, but they all have the same general appearance. All parameters are as described in the legend to Fig. 6.1. See also the colour plate on page 78.

motion halts. After the chemotactic motion has stopped, the prespore cell mass becomes rounded, due to surface tension properties. The tube, however, is too stiff to change its general shape. Hence, in the model, a globule of spores on a slender stalk is a stable configuration.

The upward extension of the stalk is not specifically guided, and because of that some deviations in the direction of outgrowth can be observed. Figure 6.6(a) shows that due to random fluctuations during the culmination, the precise final configuration does indeed vary, but the fruiting body retains its general appearance. These two features are also observed *in vivo*.

Since in our model the process of culmination is so closely related to the cAMP dynamics, it it clear that any process that changes the cAMP waves will also change the final configuration of the culminant. In chapter 4 we showed that because NH_3 inhibits the cAMP-induced cAMP release (Williams *et al.*, 1984), NH_3 could play a key role in a number of tactic behaviours, especially phototaxis. Here we show that the default NH_3 production by the cells and its effect on the cAMP dynamics, combined with the sensitivity of the culmination process for such modulations, can account for the well-known phenomenon of culminants orientating away from each other (Feit & Sollitto, 1987). Figure 6.7 shows a simulation in which the cells produce a small amount of NH_3, which diffuses away into the air. The effect of NH_3 is implemented by increasing the threshold for the cAMP response, as described in chapter 4. NH_3 accumulates between the culminants, which decreases the excitability along the two sides that face each other. Because cAMP waves move more slowly at lower excitability, the waves become slanted (see chapter 3); and since the stalks extend perpendicular to the cAMP waves, they move towards each other instead of straight downwards. Therefore we end up with fruiting bodies that are orientated away from each other [see Fig. 6.6(c)].

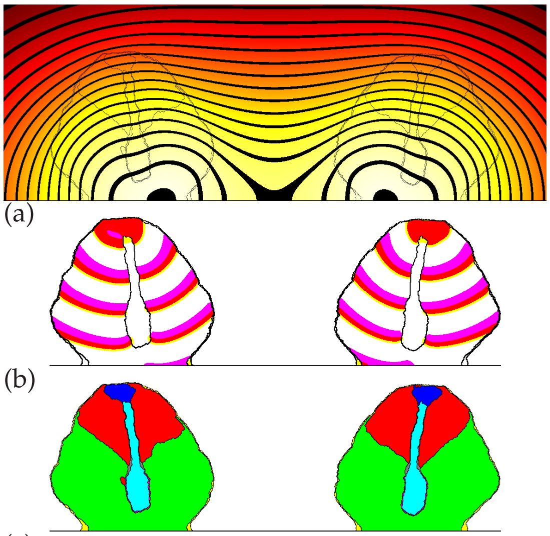

(a)

(b)

(c)

Figure 6.7. Two culminants orientating away from each other due to NH_3 production. (a) Shows the NH_3 distribution; (b) shows the cAMP waves; and (c) shows the culminants with slanted stalks. Time is 20 minutes (12 000 time steps). Colour-codings in (b) and (c) are the same as in Fig. 6.2. The NH_3 distribution is indicated by a colour gradient from dark red (low concentration) to bright yellow (high concentration). The black lines are curves of iso-concentration. All prestalk and prespore cells produce $1 \times 10^{-3} NH_3$/second. We have used a diffusion constant of 15. The inhibiting effect of the NH_3 (n) on the cAMP dynamics is implemented in the following way: $a(\tau, n) = a_\tau + \frac{b_\tau n^s}{1+(n/p)^s}$, with $a_{\mathrm{PstA}} = -0.20$, $a_{\mathrm{PstO}} = a_{\mathrm{Psp}} = -0.025$, $b_{\mathrm{PstA}} = 0.0375$, $b_{\mathrm{PstO}} = b_{\mathrm{Psp}} = 0.075$, $p = 2$, and $s = 3$. The NH_3 dynamics are solved by the implicit ADI method. All other parameters are as described in the legend to Fig. 6.1. See also the colour plate on page 78.

6.3.7 Cell adhesion

Adhesion plays an important role in the model behaviour. To reproduce all the dynamics of the culmination, the surface tensions γ, as defined in eqns (6.2a) and (6.2b), were adjusted in the following ways.

The γ's between the the PstA, PstO and Psp cells are such that they adhere to each other, but form fairly homogeneous groups. The γ between PstA and Psp is slightly higher so that all prestalk cells will remain together when the end of the culmination approaches.

By using 'normal' γ's between the slime mass and the various cell types *and* between the slime mass and the air, whereas the γ's between the various cell types and the air in fact are very high, a slime sheath is formed that completely surrounds the culminant. Similarly, because the γ's between the tube mass and the PstO and Psp cells are 'normal', whereas the γ's between the stalk cells and these cell types are very high, the stalk tube is formed. The γ between the stalk tube and the air is 'normal', and the γ between the stalk tube and the slime sheath is low (but not zero), so that the fruiting body will be surrounded by slime sheath and stalk tube, but both matrices will not intermingle.

Because of the differences in the γ's between the three main cell types and the slime sheath, the Psp cells have a tendency to engulf the PstO cells, which, in their turn, have a tendency to engulf the PstA cells (Takeuchi *et al.*, 1988). This helps as a compensation for the decreased upward motion close to the slime sheath. Upward motion is slower there due to some inward and outward motion, which smooths the pressure waves. These differences in γ also ensure that the spore head is eventually completely on top of the stalk.

The γ's between the pathfinder cells and the PstO and Psp cells are very low, so that they can move smoothly through the cell mass. Also the γ's between the pathfinder cells and the stalk cells and stalk tube are very low, so that the pathfinder cells can pull them downwards easily. The γ between the pathfinder cells and the Psp cells is lower than the γ between the pathfinder cells and the PstO cells, so that the pathfinder cells can move smoothly through the PstO-Psp interface. The same is done for the stalk tube.

The tension between the stalk cells and PstA cells is quite high, to ensure that stalk cells are pushed into the stalk tube, as a result of the surface tension. Because the γ between the pathfinder cells and the substratum is low, but between the stalk cells and the substratum is high, the pathfinder cells form the base of the stalk, and hence more or less determine the width of the inner part of the 'basal disc'.

6.4 Discussion

The "reverse fountain" is the woderful culmination of *Dictyostelium discoideum* morphogenesis. So far, however, no satisfactory explanation for this phenomenon has been given in the literature. Often it has simply been considered as a fact. For example, Jermyn & Williams (1991) state that the reverse fountain directs the PstA cells into the entrance of the stalk tube and that the tip extends downwards by the accretion of PstA cells at the entrance. In our model, a reverse fountain has not been defined; instead, it emerges from the local transition rules.

We have demonstrated the occurrence of the reverse fountain on the basis of (i) periodic waves of chemotaxis; (ii) flexible pathfinder cells; and (iii) a stiff tube.

6.4.1 Stalk formation

We have shown that periodic chemotactic motion towards cAMP waves creates periodic pressure modulations, which move downwards together with the cAMP waves. The flexible stalk tip, which is not chemotactic, is squeezed downwards by the peristaltic motion that is created by these 'pressure waves'. Because the pressure waves move in the same direction as the stalk, this process can occur much faster than normal chemotactic cell motion. The stalk tip pulls the stalk tube with it, although it resists movement due to its stiffness. New stalk cells are transported through the tube by the combined pushing at the apex and pulling at the base. Because the process of stalk elongation is so closely linked to the cAMP dynamics, the direction of the extending stalk can be maintained, and its displacement automatically halts when it reaches the base.

Hitherto, some authors have assumed that stalk elongation is due to the the fact that the stalk is pushed downwards through the culminant by the accretion of prestalk cells at the tube mouth (Jermyn & Williams, 1991; Thomason *et al.*, 1999). However, with our model we can show that the addition of new stalk cells at the apex cannoy be responsible for the fast and straight downward motion of the stalk, due to a number of mechanical problems. First of all, pushing the stalk downwards becomes increasingly more difficult during stalk formation, because the force is exerted only on a very small surface, whereas the frictional force, which is exerted over the whole surface of the stalk, increases linearly with stalk length. Secondly, because the whole cell mass moves upwards, and the force is exerted only at the apex, the stalk will have a strong tendency to move sideways. And thirdly, if the force exerted at the apex is strong enough to let the stalk reach the base (which in our model is only feasible by simulating extremely small culminants), then the tip will simply continue to extend, even after it reaches the substratum. But because the stalk cannot move further downwards, it flips to one side, and extends laterally. Strong adhesion to the substratum does not prevent this. In contrast, the above complications are not encountered with the mechanism that we propose.

An alternative mechanism might be that the stalk is pushed downwards by nearby cells, which, during the upward motion, push off against the stalk. A similar mechanism has been proposed for slug migration (Odell & Bonner, 1986). The model-formalism we use, however, ignores the fact that forces exerted to overcome friction and to accelerate lead to similar counterforces. Implicitly we assume that counterforces are simply passed on to neighbouring cells and extracellular matrix, and spread out without influencing the local motion. However, even if this assumption turns out to be incorrect and such forces are nevertheless able to influence stalk displacement, this alternative mechanism still cannot explain why the stalk should become elongated in the first place. Nor can the mechanism account for the extremely fast downward motion, or for the correction of orientation.

6.4.2 cAMP signalling

In our model cAMP signalling is a prerequisite for normal stalk development and fruiting body formation (see Fig. 6.3). However, serious doubts have been expressed in the literature about whether chemotaxis continues to play a role during culmination, especially with respect to the prespore cells (Sternfeld, 1998). The alternative idea is that the growing stalk provides the force that carries the prespore cells aloft (Thomason *et al.*, 1999). However, Watts & Treffry (1976) found that mature spores are not visible until the fruiting body reaches its maximum height, and Kitami (1984) showed that during culmination both prestalk and prespore cells are still able to exhibit a chemotactic response to cAMP. Besides, Chen *et al.* (1995, 1998) showed that normal culmination is impaired when the rate of chemotactic motion is reduced. They showed that a chemotactic response by the prestalk cells only, or by the prespore cells only, is not sufficient for normal culmination. They conclude that prespore cells play a more active role than previously assumed.

Because the stalk tip is orientated by cAMP waves, the same processes that alter the cAMP waves should also alter the stalk orientation. The fact that culminants orientate away from each other (Feit & Sollitto, 1987) can therefore simply be due to their own NH_3 production and the effect it has on the cAMP dynamics (see Fig. 6.7). Moreover, because temperature and light conditions influence the NH_3 production, thermotactic and phototactic orientations can also be expected during the culmination stage (see chapters 3 and 4).

6.4.3 Model considerations

In our model a central role is reserved for cell-cell and cell-substratum adhesion. There is a vast amount of experimental evidence that supports differential adhesion between cell types and between the cells and the substratum in *Dictyostelium*, and stresses the importance of adhesion during development. For reviews on the role of adhesion in *Dictyostelium*, see Fontana (1995) and Bozzaro & Ponte (1995). Tuning our model has produced expected parameters for adhesion strengths between cell types. Hence we predict that the same relations between adhesion strengths will be found in experiments. However, one has to bear in mind that in the model the J_{τ_1,τ_2} values represent effective cell adhesions, in which several processes are lumped together. Hence it may prove difficult to relate them directly to experimental observations.

We have restricted the set of entities used in our model to the ones that are needed to obtain a good description of the reverse fountain. The pathfinder cells are essential in our model. If they are omitted, then the stiff tube mass will surround the stalk tip and no peristaltic motion will be possible; a stiff bag will be formed instead of an elongating stalk. This problem cannot be solved by simply using a more flexible stalk tube (or by implementing pathfinder cells only and no tube mass, which produces more or less the same results). First of all, the stiff stalk tube has to support the fruiting body: without it the culminant will collapse. Secondly, the stiffness is needed to prevent downward motion of the complete stalk, as well as to give the stalk tip its typical wedge-like shape (as described by Higuchi & Yamada, 1984), which allows it to penetrate easily through the upward moving cell mass.

In our model we assumed a clear distinction between the PstA and PstO cells. Jermyn & Williams (1991) however showed that there is no entirely distinct class of PstO cells, but there is a discontinuous gradient in gene expression, with cells in the top one-tenth expressing the PstA marker most strongly. Because the cell differentiation seems to be a gradual process, the excitability and adhesion strengths can also be expected to change more gradually. For reasons of convenience we have modelled the cell-type transition as an instantaneous process. However, we expect that the results will still hold even if the induction process is neither instantaneous nor local, as long as the properties connected with adhesion and excitability change together. This is important because the cAMP dynamics may not be disturbed too much during the time it takes for the newly formed PstA cells to sort out to the tip, which in the model is due to the interplay between the chemotaxis and differential adhesion (see chapter 3). Hence, if there is a co-regulation between adhesion strength and excitability, this would be strong support for the mechanism we propose.

The volume increase of the stalk cells occurring due to vacuolation is not very important for the model behaviour. In contrast, Higuchi & Yamada (1984) postulated that this process must be responsible for the downward elongation. We find, however, that the volume increase has a relatively small effect. The supply of stalk cells at the stalk tip is indeed greater when volume increase is larger, which helps to increase the downward velocity. However, in the model the vacuolation can be removed completely without causing a qualitative change in behaviour.

The stalk tube seems to become even more solid when exposed to the air (Higuchi & Yamada, 1984). But even before the stalk comes in contact with the air the tube is already stiff enough for it to be located by its resistance to the passage of a fine glass needle through the tissue (Sternfeld, 1992). No gradual change in stiffness is needed in the model, and therefore we have not implemented this feature.

Neither have we implemented any processes relating to the upper and lower cup, because they are not directly needed for either elevating the cell mass or preserving the final shape of the fruiting body. And we observe in the model that even if there is no specific cell type connected to the basal disc, something comparable is nevertheless created, with a core formed by the stalk tip, and an outer ring formed by 'rearguard' cells that are left behind.

However, some of the above processes that are not essential for the culmination as described above could play all kinds of other roles during the development. For example, it could very well be that the turgor pressure of the highly vacuolated cells contributes to the maintenance of the final stalk structure (Watts & Treffry, 1976).

In our simulations we do not find the typically observed extended shape of the tip. We expect that this specific form of the tip is a three-dimensional (3D) property, caused by 3D scroll waves, and hence cannot be depicted in our 2D simulations. Such scroll waves have been found to organize the tip region during the slug stage (Siegert & Weijer, 1992). Scroll waves may also explain the early formation of the stalk primordium, because in the core of the scroll wave one finds a permanently low cAMP concentration (Siegert & Weijer, 1992), and during the slug stage low cAMP levels are needed to induce differentiation into pathfinder cells (Berks & Kay, 1990).

Finally, there is also another consequence of performing 2D instead of 3D simulations. Because the stalk is much narrower than the prestalk area that forms it, the stalk can become very long. However, due to scaling properties, this effect is quadratically larger in 3D than in 2D. Hence, to produce a fruiting body of normal height in 2D, the culminant must be initially four times as broad.

6.4.4 Side-effects

The mechanisms described here not only generate the dynamics that are directly connected with the unfolding of the reverse fountain, but, as a side-effect, they can also give rise to a number of seemingly unrelated features. Nevertheless, many of these features are observed in experiments. Thus, in our model, no extra assumptions are needed to explain such features.

Harwood *et al.* (1992) showed that when the differentiation of PstA cells into stalk cells is blocked, and hence no stalk is formed, the culminant continues to extend. This process goes on and on, and eventually the culminant becomes an erratic hair-like structure, which collapses onto the substratum. In our model, we can perceive the same kind of behaviour because the upward motion is due to chemotaxis – not to stalk extension, as previously assumed (Thomason *et al.*, 1999) – and because the upward motion does not stop, due to the fact that the PstA cell pool is never emptied and hence cAMP waves keep on being produced.

Kitami (1985) showed that when a culminant is exposed to a centrifugal force of 40-50 G, hardly any cell mass can culminate (it remains shaped like a mound). When a cell mass did not culminate, it did not form a normal stalk. This one-to-one relation between upward motion of the cells and downward motion of the stalk (see Fig. 6.3) logically follows from the mechanism we propose.

In our model, the mechanism that corrects the direction of elongation does not work if we start with a small isolated cluster of cells: the cells form a rounded mass, show no efficient peristaltic motion and are pushed sideways by the upward moving cells. This corresponds to the description that Sternfeld (1992) gives of the small clusters of early stalk cells that are formed during the late slug stage: sometimes 25–50 cells separate, expand a little and attain a surface position before they finally reach the rear of the slug.

We also observe a constriction at the base of the prespore zone before the stalk reaches the substratum. In our model, this is simply due to the combination of adhesion and upward motion. Neither a spiralling motion nor a contractile event at the surface of the cell mass is required to produce this constriction (Chen *et al.*, 1998, suggested that these factors might be needed to explain the constriction).

After the stalk tip reaches the base, the stalk becomes slightly thickened, as observed by Higuchi & Yamada (1984). If we look at the final configuration, with the globule of spores on a slender stalk, we see that the spore head is still enclosed by the slime sheath, both in our simulations and *in vivo*. This may indeed be important for holding together the mass of spores (Watts & Treffry, 1976), but no 'new' features are needed. The stalk is surrounded by the stalk tube, but the tube mass neither envelops the spore head nor the cells that are left on the substratum, again as *in vivo* (Watts & Treffry, 1976).

And finally, Sternfeld (1992) found that the outer ring of the basal disc consists only of a single layer of rearguard cells: the major portion of the basal disc is formed by the downward moving stalk. In our simulations, a basal disc-like shape is formed, with an outer ring of cells that fail to move upwards with the mass of prespore cells. To obtain this behaviour we do not have to define basal-disc cells or rearguard cells.

6.4.5 Conclusions

In this study, we have largely ignored the genetics and detailed regulatory mechanisms of *Dictyostelium discoideum*. As a result, our model allows us to pinpoint those elements that are essential for the successful formation of a fruiting body: we have shown that the whole process can unfold in a minimal model with fixed parameters. Nevertheless, it is known that many genes are up and down regulated during culmination, and research in the near future is likely to reveal much more about the high number of genes involved. If one wants to relate gene knowledge to this model, it is important to take the following points into consideration. First of all, many of these genes are connected to processes not directly related to the cell movements, such as, for example, the maturation of spore cells. Nevertheless, a large set of genes is needed for each process that we have described in the model. And these processes must be fine-tuned, which again requires a number of genes. Moreover, all processes have to be operational under many different circumstances. Therefore, by evaluating the role of those genes that are involved in cell movement in the light of our model, one should be able to generate interesting insights into evolutionary refinements of the culmination process, as well as into genetic robustness and redundancy. Finally, because the model is completely defined at the (sub)cellular level, whereas the mechanisms at work are on larger scales, one can begin to understand how gene expression can govern macro-level phenomena. For example, using this model it should be feasible to interpret the aberrant phenotypes that are created by restriction enzyme-mediated integration (REMI) (Smith, 2000).

We have used the hybrid CA/PDE model-formalism, because this formalism can describe the interaction between signalling, adhesion, pressure, pushing and pulling in a very elegant way. Our explanation for the dynamics during culmination is based on the interactions of these processes. These processes are the same as those which play the central role during the earlier stages of the development: here we have described the culmination, but previously we have used the model-formalism to explain how single amoebae aggregate into a mound, which eventually leads to the formation of the slug (Savill & Hogeweg, 1997). Later on we used the same formalism to unravel the mechanisms behind the thermotactic and phototactic properties that direct a slug to a suitable site for culmination (see chapters 3 and 4). Thus, we now can describe all the stages of the morphogenesis with one formalism. In summary, our model of the culmination of *Dictyostelium discoideum* culminates the modelling of its development.

Acknowledgements

We are grateful to André Noest for helpful discussions. We would like to thank Dr. S. M. McNab for linguistic advice. A. F. M. Marée was financially supported by the Priority Program Nonlinear Systems of the Netherlands Organization for Scientific Research.

7

Summarising Discussion

Maynard Smith & Szathmáry (1995) pointed out that the development of a multicellular organism, with differentiated cells, requires that three problems be solved. The first problem is gene regulation. Only very sophisticated mechanisms for gene regulation can produce differentiated cell types. This problem is not addressed in this thesis. The second problem, cell heredity, is irrelevant as far as the slime mould is concerned. During morphogenesis no cell division takes place, and hence states of differentiation do not have to be (partly) heritable through cell division. The third problem, which we have focused on, is the emergence of morphogenesis: how morphs can be generated and how a multicellular creature can sense and response in a coordinated way to the environment.

With the model for *Dictyostelium discoideum* presented in this thesis we have demonstrated that it is possible to study morphogenesis in the widest sense of the word, and to identify the underlying mechanisms. These mechanisms will be reviewed in this final chapter; next we look in more detail at the modelling approach we have used; and finally we point to some omissions in our model, as well as to its potential as a basis for interesting further research. First of all, however, the main themes of the thesis are briefly reviewed.

7.1 A Short Review

Part I of the thesis is devoted to pattern formation in excitable media. In **chapter 2** we show the occurrence of lateral instability in excitable media, which leads either to propagating waves with ripples, or to spiral breakup. Lateral instability can develop when the inhibitor diffuses at a high rate, and is associated with a negative slope of the so-called eikonal-curvature relationship: when the inhibitor has a high diffusion rate, the velocity of a wave is restrained by the inhibitor ahead of the wavefront, and hence the wave moves faster when the wavefront is slightly curved. The slope of the eikonal-curvature relation could be measured using quasi one-dimensional computations, and is used as fitness measure in a genetic algorithm. In this way we were able to zoom in on the parameter region where lateral instability could be observed. We also found a number of other types of interesting dynamics, the most notable being a regime with diffusion-driven limit-cycle behaviour.

Our study, when combined with previous studies that used the same model (see, e.g. Panfilov & Hogeweg, 1993, 1996), shows that the model we use is well suited for investigating the very wide range of dynamics that occur in excitable media.

Part II of the thesis is devoted to *Dictyostelium discoideum* development. The above-mentioned model is used to describe the cyclic AMP (cAMP) dynamics; a stochastic two-scale cellular automata (CA) model, presented in detail in section 1.3 on page 6, is used to describe the individual amoebae. In the model, every cell is represented as a group of connected automata, i.e. the basic scale is subcellular.

Chapter 3 tackles problems connected with slug motion, such as shape conservation and cell sorting, as well as the mechanisms underlying thermotactic behaviour, which direct the slug to the surface (Dusenbery, 1988). We have implemented cell adhesion and cAMP signalling in such a way that they can interact, but it is still possible to unravel the mechanisms that emerge. We show that the interplay between differential adhesion and (non-differential) chemotaxis is sufficient to explain a number of aspects connected with normal slug motion, and also leads to fast and complete cell sorting, a phenomenon which cannot be due solely to cell adhesion or chemotaxis.

The whole slug is able to show an adequate response to a thermal gradient, by means of temperature-dependent differences in its excitability. Individual amoebae, on the other hand, can neither sense a temperature gradient, nor show temperature-dependent differentiation in motion velocity. The behaviour is achieved by a modification of the cAMP waves: differences in temperature alter the excitability of the cell, and thereby the shape of the cAMP wave. Chemotaxis towards cAMP causes the slug to turn. Furthermore, due to the fact that the wavefronts always keep a smooth shape because of the well-known curvature-effect, the waves of excitation function as spatiotemporal noise-filters. This spatiotemporal integration generates a very high sensitivity (even very small temperature gradients can be detected), as well as the ability to receive a signal in the presence of extreme noise.

In conclusion, the study demonstrates the importance of the interactions between different processes, and shows that precise sensing of the environment can result from the integration of spatiotemporal information.

Next, the model is extended with ammonia (NH_3) dynamics and light refraction. In **chapter 4** we show that the phototactic response, which leads the slug to the soil surface, can also unfold from the interactions between the different modules. Again the individual amoebae are unable to detect the signal (where does the light come from?), or to show an adequate response (move towards the light source). We have elucidated the following minimal mechanism for phototaxis: because the slug refracts the light and has a rounded shape, the light is focused on the side opposite the light source (the 'lens-effect'). Production of NH_3 increases with light intensity, and the NH_3 decreases the excitability. Hence waves move more slowly on the side opposite to the light source, they become slanted, and chemotaxis towards the waves causes the slug to turn.

This study illustrates how side-effects[1] can be important for validating the model, for generating new ideas, and for gathering together multiple aspects of the development: we did not set out to explain mutants which show bi-directional phototaxis or to interpret experiments that were done with these mutants, yet we are able to explain these as autonomous results (see also section 7.2).

Next, the model is extended with cell differentiation that stems from a local induction process, and with production and displacement of the extracellular matrices. We also introduce differences in stiffness. In **chapter 5** and **chapter 6** we move from the slug stage to the culmination stage. The 'textbook-view' of the culmination has always been that the stalk grows by the successive addition of prestalk cells at the top, and the prespore cells are carried aloft by the growing stalk (Thomason *et al.*, 1999). However, both our model and *in vivo* experiments performed by others rule out this possibility. We show that periodic upward movements, due to chemotactic motion towards cAMP, induce pressure waves, which squeeze the stalk downwards through the cell mass. These pressure waves result from cAMP dynamics and differential adhesion, i.e. they are themselves observables generated by the model. The mechanisms that we propose are in agreement with, and moreover, can explain many experimental observations. The mechanisms show a high amount of self-organisation and self-correction: an elongated stalk is formed which very rapidly moves downwards to the base; any deviation from downward elongation is corrected very efficiently; pathfinder cells always remain positioned along the tip of the stalk; the downward motion stops automatically when the stalk tip reaches the base and the same holds for the upward motion when the stalk formation is completed; a rounded spore head is formed on top of the stalk.

In conclusion, our study, when combined with the study by Savill & Hogeweg (1997), lets us describe within one model the entire process of morphogenesis from aggregation all the way to fruiting body formation (except for the initiation and termination of the slug stage). It can be said that our model of the culmination of *Dictyostelium discoideum* culminates the modelling of its development.

7.2 From Local Interactions towards Global Coordination

The two-scale stochastic CA model we used to describe the amoebae is ideal for studying the development of *Dictyostelium*, since the cooperative behaviour observed during the development is driven by the movements and responses of the individual cells. Besides, the formalism handles pressure, deformation and motion, i.e. the physical aspects of morphogenesis, in a very elegant way. Only local transition rules are involved in the description of these processes; there is, for example, no need to specifically calculate the global pressure distribution. In short, all update rules in the model are defined on two local scales, namely cellular and

[1]Obviously there is no strict definition of a side-effect, since side-effects are defined mainly by one's own expectations. In one way, all the surprising behaviour that emerged during these model studies could be (initially) called side-effects.

subcellular. Nevertheless, the behaviour that can be observed at the intermediate and global level is due to the collective behaviour of the cells: the multicellular organism that is formed by all the amoebae together can sense the environment much more precisely than an individual amoeba can, and can respond to it in a coordinated and accurate way, and surprisingly, even new observables emerge from the collective behaviour of the amoebae.

For example, an individual amoeba can neither respond to a slight temperature gradient, nor measure the direction of incidence of light. Both the very high sensitivity and the ability to filter the noise, as well as the ability to determine the light source, arise from the collective behaviour. The slime mould uses self-organising structures that are 'larger than life', i.e. larger than the individual amoebae, on order to make information integration, information processing and information transmission possible. The shape of the slug itself behaves as a lens, waves of excitation are formed in which many amoebae are involved at every moment in time, broad pressure waves generate peristalsis, lumps of cells move with different velocities because of the interplay between chemotaxis and adhesion, and so forth.

The mechanisms underlying thermotaxis and phototaxis are both related to slanted wavefronts. The chemotaxis then causes the slug to turn. Several properties of wave propagation play an important role. For example, in our *Dictyostelium* model the concave wavefronts move faster than plane waves, due to an increased influx of activator into the nearby region, and for the same reason convex wavefronts move more slowly (this is called the curvature-effect). It can easily be seen that due to this curvature-effect the short-wavelength noise can be averaged. This is why even very small temperature gradients can be measured and why even very high noise levels can be filtered: for example, the noise can be even more than 300 times as large as the signal (see Fig. 7.1).

The curvature-effect also explains why the wave becomes slanted when during phototaxis there are large differences between the concentrations of NH_3 on each side of the slug. When the slant becomes too large, the momentum of the force, created by the cells moving towards the cAMP wave, causes the side-effect of bi-directional phototaxis.

During culmination many self-organising and self-correcting phenomena occur, all of which are needed for successful fruiting body formation. A nice 'side-effect', however, is the orientation of nearby culminants: the default production of NH_3 alters the excitability, and therefore the waves again become slanted. As a consequence, the fruiting bodies end up orientated away from each other. This is often observed in experiments; whether or not this behaviour is functional, however, is still under debate.

7.3 Model Complexity

In general, theoreticians show a preference for keeping models as simple as possible. And for good reason. Nevertheless, the model we end up with is rather complex by theoretical standards, although much of the complexity of *Dicty-*

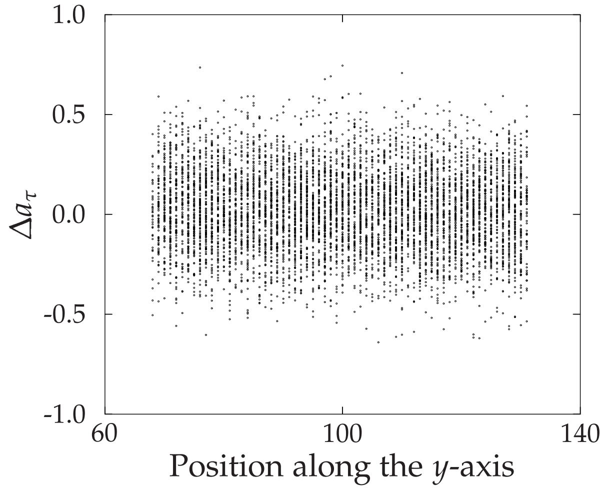

Figure 7.1. Plot of the highest noise level at which the model slugs can still detect and respond to a temperature gradient. Temperature variations cause variations in excitability, which can be expressed by Δa_τ (see section 3.4.2 on page 46). Here we plot the values of Δa_τ at $t = 0$ as a function of the y position, i.e. along the temperature gradient. The dots show the values of Δa_τ for all individual automata in the presence of noise that is added to the gradient. The slope of the gradient, a_{grad}, is 6×10^{-4}, the standard deviation of the added noise-term is 0.2, i.e. the noise is more than 300 times as large as the signal. With the naked eye, one can hardly see the gradient. Nevertheless, the slug is able to orientate itself.

ostelium is still ignored (e.g. there is no gene regulation in the model).

In this section we first re-emphasise the need to study the simplest models; then we discuss why we think we have struck a useful balance in our model; and finally we discuss ways in which we can extend our modelling approach so as to incorporate gene regulation, while still pursuing our aim of uncovering general principles.

7.3.1 From simple to simpler, to a little more complex

The usefulness of the simplest possible models is indisputable. First of all, one can understand the model thoroughly. Secondly, many aspects of a system under study, do not (or barely) influence specific phenomena of interest, and should be ignored. This allows us to consider models which are valid for many systems. A good example are the models of excitable media we discussed earlier; the concept of excitable media is in fact an abstraction which ignores irrelevant details. One should, however, bear in mind that, because of the generality of such representations, and because they are often used to study phenomena that occur generally, these models do not reveal details about the particular implementation. Thirdly, it is very useful to derive measures that are independent of much of the observed variation. A specific example that we would like to mention here demonstrates the derivation of such a measure for a particular case, namely the fitness of viral strains.

Fitness differences between viral variants are often estimated experimentally by means of pairwise competition experiments. As a fitness measure, one conventionally uses the slope of the logarithmic ratio of the genotype- or phenotype-frequencies plotted in time. This fitness measure, however, remains proportional to the actual replication rate realized in the particular experimental setup, and therefore cannot be extrapolated to other situations. We have developed a method of computing the relative fitness, which is independent of the actual replication rate (Marée *et al.*, 2000, not part of this thesis). By using generic competition models, we were able to derive a formula for the relative fitness, without having to make any assumptions about (changes in) the replication rate during the course of the experiment. This means that we obtained a general formula that is applicable not only when viruses grow exponentially, but also for (quasi) steady state conditions, as well as for any other growth regime.

Obviously, models should be simple, but not too simple. Recently we have developed a heuristic method which can help modellers to find sensible ways of extending very basic ordinary differential equation (ODE) models, in order to fit the data, yet can enable them to keep their models as simple as possible (Müller, Marée & de Boer, 2000b, not part of this thesis). In the latter study we first state that every parameter describes many underlying processes and that the value of a parameter in equilibrium is just a realization of the process function. Next we calculate parameter values from observed steady states, and replace the parameters with the highest variation by a more explicit description of the underlying processes. We have applied this method to HIV-1 set-points and obtained a model in which several factors collectively determine the steady-state viral burden. The model is unlike most ODE models, in which steady states of variables are usually determined by one process only. Our method gave a strong indication that the lymphoid tissue could play an important role in the viral dynamics. We have used this observation to extend the model further with such a compartment (Müller, Marée & de Boer, 2000a, not part of this thesis). Note, however, that this method can only be applied in systems in which the dynamics always reach a steady state. This imposes a strong limitation on the systems that can be studied, e.g. it precludes pattern formation.

7.3.2 Interaction of generic modules and interesting new observables

In part II of this thesis we address a different level of model complexity. We use a comprehensive model, in which we do not confine beforehand the set of phenomena we look at; instead we implement a number of experimentally established processes that occur during the morphogenesis of *Dictyostelium*, and we observe the consequences of their interactions. We implement these processes using different model-formalisms. They were chosen on the basis of what they could describe in the easiest way, which helped to maintain a certain level of simplicity in the model, and allowed us to filter out everything which does not influence the phenomena of interest. For example, in our hybrid model light was described in a CA, using a ray-tracing technique, whereas NH_3 was described in a partial differential equation, as a reaction diffusion equation; the tube mass could be very well described as one very large and stiff cell in the Glazier & Graner-model formalism. We have shown how many aspects of the morphogenesis emerge from the dynamic interactions on different scales between the generic behaviours of these different modules. Nowadays, several other research groups are also moving into this direction, and have also started to model phenomena 'beyond pattern formation' (see, e.g. Kerszberg & Wolpert, 1998; Murray & Swanson, 1999; Bretschneider, Vasiev & Weijer, 1999).

Whereas we emphasise the importance of the interactions between different processes, many studies have instead tried to explain a specific feature with one linear mechanism. For example, Clow *et al.* (2000) have tried to ascertain whether cell sorting in *Dictyostelium* is due to differential cell adhesion or chemotaxis. First they showed that there is a massive evidence in literature that both processes are important; next, however, they tried to find out which idea must be wrong. They concluded that differential adhesion could be ruled out, because they found that clumps of cells did not slowly increase and fuse; instead they observed directed motion, which did not agree with their intuitive idea about what kind of patterns were to be expected if differential adhesion were the only process at work. However, they could not explain the patterns with chemotaxis towards cAMP alone either, and therefore postulated that another process *precedes* chemotaxis towards cAMP. However, if we assume that both chemotaxis and differential adhesion are at work, their observations fit quite well to our picture of cell sorting. Having identified the first cells that show the prestalk cell-specific marker as the most excitable ones and therefore the ones that become the organising centre of cAMP signalling, we expect to observe directed cell motion towards this initial cluster if there is differential adhesion between the cell types. We know that this initial cell sorting changes the properties of the excitable medium itself; these changes strongly couple back to the cell dynamics. The model we have developed can be used as a tool to analyse such complex interactions and feedbacks and to link them to the observations in the above-mentioned experiments.

As indicated at the beginning of this section, we have completely ignored gene regulation in our model. We find that the whole development of *Dictyostelium* can unfold without the need to change the parameters of most processes: in our model the morphogenesis is mainly a self-organising process, and many interesting new observables emerge solely from the interactions between generic modules. This view, however, deviates from the general genetic way of looking at development in terms of gene regulation.

7.3.3 Gene regulation and morphogenesis

Although *Dictyostelium* is considered to be the most primitive eukaryote which has the basic features of multicellular development, it still has 8 000 – 10 000 genes, of which, for example, at least 3 000 are expressed during the slug stage (Loomis, 2000). The rapid increase in genetic knowledge challenges us to determine functional roles for all those genes. We are aware that many of these genes are involved in adhesion, induction, maturation, sensing of the environment, etc.; in our opinion, for a successful interpretation of the role of these genes, we need to understand the dynamics and mechanisms on the intermediate scale.

In this thesis we opted for a level of abstraction at which we did not implement the specific function of individual genes. Many models, however, have been developed to explain how the generic principles that we have used are implemented at the (sub)cellular level (although so far few models incorporate the level of the gene regulation). Interpreting gene expression in terms of our model presents a challenge; in particular, it may well prove possible to link distortions of (sub)cellular processes to aberrant phenotypes.

The technique of restriction enzyme-mediated integration (REMI) makes it possible to create many aberrant phenotypes (Smith, 2000). REMI allows both the production of mutants and the simultaneous tagging of the mutant gene. Flanking genomic sequences of significant mutants can be recovered, cloned and sequenced (Newell & Gross, 2000). Thus, information can be obtained about both the aberrant morphogenetic process and the gene involved, e.g. by searching for homologues. When the role of a gene at the (sub)cellular level can be elucidated, and its effect on the module can be determined, our modelling approach should be able to predict and explain the aberrations that can be observed during the morphogenesis. In conclusion, interpreting gene expression in terms of our model provides a heuristic method for assigning gene function in the light of the morphogenesis as a whole.

Recent studies have suggested that organisms may need complex gene networks in order to function robustly. Barkai & Leibler (1997) and Alon *et al.* (1999) have shown that in the biochemical network which organises chemotaxis in the bacteria *Escherichia coli*, the precision of adaptation is robust. In contrast, other properties, such as steady state behaviour, are less robust. They found that the precision of adaptation is a consequence of the network's connectivity and does not require 'fine-tuning' of the biochemical parameters. von Dassow *et al.* (2000) looked at the gene network which fixates the segment polarity pattern in the embryo of the fruitfly *Drosophila*, and also found the network to be robust, in the sense that correct patterning is relatively often found when parameters are varied randomly.

The question that then arises directly is whether our model also needs a complex gene network to ensure its robustness. Since the modules we use are very coarse descriptions of the underlying dynamics, our model behaviour is in some sense very robust with respect to particular implementations of the (sub)cellular processes. However, we had to zoom in on a very specific parameter space to find the phenomena we were seeking. Thus, the specific morphogenesis presented here is not a generic property of the model in the way that the spiral wave is a generic property of many models that describe excitable media. Nevertheless, once we found the right parameter region, it turned out that we could always vary parameters considerably, yet retain the model's qualitative behaviour;

we have found many self-organising and self-correcting properties, as a result of which the observed phenomena are not too sensitive to the specific parameter values. Nevertheless, because certain processes have to remain within this (relatively broad) range of admissible parameter settings, it is particularly the adaptation to various circumstances which has to be robust (cf. Alon *et al.*, 1999).

7.3.4 Evolving complexity

The previous section also raises the question of how such gene networks, connected to development, evolve. Indeed we started this chapter by stating that the development of a multicellular organism requires that besides the problems related to pattern formation, problems related to gene regulation and cell heredity have to be solved as well (Maynard Smith & Szathmáry, 1995). Evolutionary processes have not been taken into account in this thesis. Nevertheless, it is interesting to speculate on how these questions might be incorporated in our modelling approach.

Hogeweg (2000a,b) has taken up this challenge. She has made precisely the above-mentioned extensions to describe all the elements of the evolution of multicellularity (as indicated at the beginning of this chapter), while at the same time minimising the *a priori* assumptions. The problem tackled in these studies is multicellular development in general; no specific organism has been modelled. The first new element, i.e. gene regulation, was implemented as a boolean network defining genes that encode cell signalling, maternal factors and adhesion strengths. The second new element, i.e. cell heredity, was implemented by allowing for cell divisions during early development as well as when cell volumes are large. After cell division both daughter cells keep the same state of the network, i.e. there is cell heredity[2]. The gene networks can evolve; the only fitness measure that is used is simply cell differentiation. Now, with all four basic elements of the evolution of multicellularity implemented at (sub)cellular level, but with no direct solutions included (and with even fewer parameters than in our *Dictyostelium* model), we see the emergence, in many evolutionary runs, of cell differentiation, gene-regulation and a balance between cell heredity and positional signalling, as well as, most surprisingly, many types of morphogenesis: in the 'shadow' of the evolutionary run phenomena are observed which could be best described as engulfing, budding, elongation, intercalation, meristematic growth, and so forth. This means that this kind of modelling is able to generate morphogenesis, solely as a side-effect of the need for cell differentiation during the transition to multicellularity.

Research into systems in which the behaviour can be easily understood has made it simpler to focus on 'generic' properties occurring in many contexts. The above-mentioned study illustrates that it seems profitable not only to study generic properties of minimally defined systems, but also to derive general properties of relatively 'rare' and complicated systems while minimising the *a priori*

[2]Note, however, that heredity evolved to become limited, using the property that differences in the local neighbourhood can lead, via cell-to-cell signalling, to different gene expression, which can then influence the development; the development can then couple back to the gene-regulation.

assumptions. 'Special' systems derived in this way are able to reveal important mechanisms absent in most other systems (Hogeweg, 1998).

The model developed by Hogeweg (2000a,b) evolves highly non-generic and complex gene networks, which, due to the unfolding and feedback to multiple intermediate levels and different time-scales, are difficult to comprehend in terms of the observed morphogenesis. Nevertheless, we can still study this model system relatively easily, and uncover general principles that also apply to the complex gene networks found in nature.

7.4 Future Directions

Although this thesis ends with the culmination of *Dictyostelium discoideum* morphogenesis, there are still a number of gaps in our knowledge. Our model also points to directions for interesting further research. As indicated before, we have not yet shown how the transition takes place from the mound stage to the slug stage, or from the slug stage to the culmination stage. We have worked on this problem, but we still do not completely understand the mechanisms underlying these transitions and the way they are timed. As is known from experiments, NH_3 again plays an important role here, and hence we have focused mainly on this signalling molecule.

Another problem is related to phototaxis. Fisher (1997) tried to explain bi-directional phototaxis of certain mutant slime mould slugs as an actively turning towards and away from the light, so as to correct the deviation from the preferred direction of motion. We, however, found that the bi-directionality occurred simply as a side-effect of the turning mechanism, when the slug is too sensitive to NH_3. Thus, we have found a mechanism which brings together multiple aspects of the phototaxis; an extra validation of the model. A recent paper by Miura & Siegert (2000), however, has shown that, with respect to phototaxis, life is not so simple. They showed that a sudden increase in light intensity leads to a transient appearance of new cAMP waves, in between those that are already propagating. Moreover, provided there are no spiral or target waves, new target waves can appear. These effects last during 3-4 waves. The experiments show that light does indeed influence the cAMP waves; at first glance, however, in the opposite way to the way we assumed in chapter 4. However, to explain phototaxis, one cannot ignore, for example, the experimentally established lens-effect. Hence, these experiments have to be interpreted within the framework of our model, if we want to understand how the observed effects can contribute to the many features related to phototaxis.

Because multiple module simulations like the ones presented in this thesis consume a lot of computer time, all simulations were done using a two-dimensional (2D) grid (except for a number of small test simulations). To be able to simulate the development in 2D, we modelled different stages using different viewpoints, i.e. either top-view (e.g. to model phototaxis), or side-view (e.g. to model the culmination).

Since the simulations were done in 2D, we still do not know whether our results are affected by this large simplification. We expect that all identified mechanisms will still hold in three dimensions (3D). Nevertheless, a number of behaviours are assumed to be purely 3D phenomena, such as tip formation, or the occurrence of a scroll wave in the anterior part, which breaks up in plane waves posteriorly. This could be important for the initiation and termination of the slug stage.

It would also be interesting to make the model for spiral breakup studied in part I into a 3D model. In most models for spiral breakup, the breakup is connected to instabilities in the propagation of wave-trains in excitable media. When this is simulated in a 3D homogeneous excitable medium, with an initial scroll wave, one can observe that the spiral breaks up in an identical way in every cross section : no additional 3D behaviour can be observed. This new mechanism of ours, however, has the potential to bring about breakups that are truly 3D, since wavefronts are laterally unstable in all directions. In 3D this may lead to interesting new dynamics.

In part II we have used a model in which the properties of the excitable medium depend on the history of the excitation pattern. Thus, our model could simply be viewed as an excitable medium in motion. This more general problem is closely connected with the questions that arise concerning the modelling of other kinds of excitable tissue. For example, in cardiac tissue the excitation wave also initiates a wave of motion (cardiac contraction), which can also affect excitation.

Finally, in our opinion it would be very challenging to start modelling embryogenesis itself, using the approach we have presented in this thesis, combined with the ever-increasing store of knowledge on gene networks, (limited) heredity and cell-to-cell signalling. This provides a framework in which cells can differentiate and generate shape simultaneously, and in which detailed experimental findings can be linked to the observed development of the whole organism.

7.5 Conclusion

The emergence of multicellular organisms is regarded as one of the major transitions in evolution. The cellular slime mould *Dictyostelium discoideum* has shown itself to be an excellent paradigm for the study of various aspects of multicellular development. It is a unique 'model' organism, because it presents us within 48 hours with a complete transition to multicellularity, which is inevitably attended by multicellular coordination and morphogenesis. We have shown that the morphogenesis in the broadest sense of the word can emerge from the interactions and feedbacks between a few simple modules. We have presented a model consisting of a relatively small number of simple, well-defined and well understood building blocks, whose properties are in accordance with experimental findings, and which interact with each other only locally. This has given us an informative description of the *Dictyostelium* morphogenesis, from single cells all the way to the fruiting body. We have shown that in order to progress from (sub)cellular interactions towards a coordinated multicellular behaviour that is able to sense and respond to the environment in an appropriate way, the slime mould uses spatiotemporal patterns which are 'larger than life'. Such patterns are formed by interacting processes, and are used for feedback between different levels of organisation. Finally, we have shown that even when complex dynamics emerge, it is still feasible to unravel the underlying mechanisms by using this multiple-scale modelling approach and looking at the intermediate scales.

Bibliography

Akam, M. The molecular basis for metameric pattern in the *Drosophila* embryo. *Development* 101: 1–22 (1987).

Alcantara, F. & Monk, M. Signal propagation during aggregation in the slime mould *Dictyostelium discoideum*. *J. Gen. Microbiol.* 85: 321–334 (1974).

Allessie, M. A., Bonke, F. I. M. & Schopman, F. G. J. Circus movement in rabbit atrial muscle as a mechanism of trachycardia. *Circ. Res.* 33: 54–62 (1973).

Alon, U., Surette, M. G., Barkai, N. & Leibler, S. Robustness in bacterial chemotaxis. *Nature* 397: 168–171 (1999).

Amagai, A., Ishida, S. & Takeuchi, I. Cell differentiation in a temperature-sensitive stalkless mutant of *Dictyostelium discoideum*. *J. Embryol. Exp. Morphol.* 74: 235–243 (1983).

Bär, M. & Eiswirth, M. Turbulence due to spiral breakup in a continuous excitable medium. *Phys. Rev. E* 48: R1635–R1637 (1993).

Barkai, N. & Leibler, S. Robustness in simple biochemical networks. *Nature* 387: 913–917 (1997).

Barkley, D. S. Adenosine-3',5'-phosphate: identification as acrasin in a species of cellular slime mold. *Science* 165: 1133–1134 (1969).

Berks, M. & Kay, R. R. Combinatorial control of cell differentiation by cAMP and DIF-1 during development of *Dictyostelium discoideum*. *Development* 110: 977–984 (1990).

Boerlijst, M. & Hogeweg, P. Self-structuring and selection: spiral waves as a substrate for prebiotic evolution. In *Artificial life II*, edited by C. G. Langton, C. Taylor, J. D. Farmer & S. Rasmussen, volume 10 of *SFI studies in the sciences of complexity*, pp. 255–276. Addison-Wesley, Redwood City, California (1991).

Bonner, J. T. Evidence for the formation of aggregates by chemotaxis in the development of the slime mold *Dictyostelium discoideum*. *J. Exp. Zool.* 106: 1–26 (1947).

Bonner, J. T. The demonstration of acrasin in the later stages of the development of the slime mold *Dictyostelium discoideum*. *J. Exp. Zool.* 110: 259–271 (1949).

Bonner, J. T. Proteolysis and orientation in *Dictyostelium* slugs. *J. Gen. Microbiol.* 139: 2319–2322 (1993).

Bonner, J. T. A way of following individual cells in the migrating slugs of *Dictyostelium discoideum*. *Proc. Natl. Acad. Sci. U.S.A.* 95: 9355–9359 (1998).

Bonner, J. T., Chiang, A., Lee, J. & Suthers, H. B. The possible role of ammonia in phototaxis of migrating slugs of *Dictyostelium discoideum*. *Proc. Natl. Acad. Sci. U.S.A.* 85: 3885–3887 (1988).

Bonner, J. T., Compton, K. B., Cox, E. C., Fey, P. & Gregg, K. Y. Development in one dimension: the rapid differentiation of *Dictyostelium discoideum* in glass capillaries. *Proc. Natl. Acad. Sci. U.S.A.* 92: 8249–8253 (1995).

Bonner, J. T. & Dodd, M. R. Evidence for gas-induced orientation in the cellular slime molds. *Dev. Biol.* 5: 344–361 (1962).

Bonner, J. T., Har, D. & Suthers, H. B. Ammonia and thermotaxis: further evidence for a central role of ammonia in the directed cell mass movements of *Dictyostelium discoideum*. *Proc. Natl. Acad. Sci. U.S.A.* 86: 2733–2736 (1989).

Bonner, J. T., Hay, A., John, D. G. & Suthers, H. B. pH affects fruiting and slug orientation in *Dictyostelium discoideum*. *J. Embryol. Exp. Morphol.* 87: 207–213 (1985).

Bonner, J. T., Koontz, Jr, P. G. & Paton, D. Size in relation to the rate of migration in the slime mold *Dictyostelium discoideum*. *Mycologia* 45: 235–240 (1953).

Bonner, J. T., Suthers, H. B. & Odell, G. M. Ammonia orients cell masses and speeds up aggregating cells of slime moulds. *Nature* 323: 630–632 (1986).

Bonner, J. T. & Whitfield, F. E. The relation of sorocarp size to phototaxis in the cellular slime mold, *Dictyostelium purpureum*. *Biol. Bull.* 128: 51–57 (1965).

Bozzaro, S. & Ponte, E. Cell adhesion in the life cycle of *Dictyostelium*. *Experientia* 51: 1175–1188 (1995).

Bresenham, J. E. Algorithm for computer control of a digital plotter. *IBM Systems J.* 4: 25–30 (1965).

Bretschneider, T., Siegert, F. & Weijer, C. J. Three-dimensional scroll waves of cAMP could direct cell movement and gene expression in *Dictyostelium* slugs. *Proc. Natl. Acad. Sci. U.S.A.* 92: 4387–4391 (1995).

Bretschneider, T., Vasiev, B. & Weijer, C. J. A model for cell movement during *Dictyostelium* mound formation. *J. theor. Biol.* 189: 41–51 (1997).

Bretschneider, T., Vasiev, B. & Weijer, C. J. A model for *Dictyostelium* slug movement. *J. theor. Biol.* 199: 125–136 (1999).

Buder, J. Neue phototropische Fundamentalversuche. *Ber. Dtsch. Bot. Ges.* 38: 10–19 (1920).

Budrene, E. O. & Berg, H. C. Complex patterns formed by motile cells of *Escherichia coli*. *Nature* 349: 630–633 (1991).

Budrene, E. O. & Berg, H. C. Dynamics of formation of symmetrical patterns by chemotactic bacteria. *Nature* 376: 49–53 (1995).

Castets, V., Dulos, E., Boissonade, J. & de Kepper, P. Experimental evidence of a sustained standing Turing-type nonequilibrium chemical pattern. *Phys. Rev. Lett.* 64: 2953–2956 (1990).

Chaplain, M. A. J., Singh, G. D. & McLachlan, J. C. (editors). *On Growth and Form: Spatio-temporal Pattern Formation in Biology*. Wiley series in mathematical and computational biology. John Wiley & Sons, Chichester (1999).

Chen, T.-L. L., Kowalczyk, P. A., Ho, G. & Chisholm, R. L. Targeted disruption of the *Dictyostelium* myosin essential light chain gene produces cells defective in cytokinesis and morphogenesis. *J. Cell Sci.* 108: 3207–3218 (1995).

Chen, T.-L. L., Wolf, W. A. & Chisholm, R. L. Cell-type-specific rescue of myosin function during *Dictyostelium* development defines two distinct cell movements required for culmination. *Development* 125: 3895–3903 (1998).

Clow, P. A., Chen, T.-L. L., Chisholm, R. L. & McNally, J. G. Three-dimensional in vivo analysis of *Dictyostelium* mounds reveals directional sorting of prestalk cells and defines a role for the myosin II regulatory light chain in prestalk cell sorting and tip protrusion. *Development* 127: 2715–2728 (2000).

Cohen, M. H. & Robertson, A. Chemotaxis and the early stages of aggregation in cellular slime molds. *J. theor. Biol.* 31: 119–130 (1971a).

Cohen, M. H. & Robertson, A. Wave propagation in the early stages of aggregation of cellular slime molds. *J. theor. Biol.* 31: 101–118 (1971b).

Conway Morris, S. The Cambrian "explosion": slow-fuse or megatonnage? *Proc. Natl. Acad. Sci. U.S.A.* 97: 4426–4429 (2000).

Cotter, D. A., Sands, T. W., Virdy, K. J., North, M. J., Klein, G. & Satre, M. Patterning of development in *Dictyostelium discoideum*: factors regulating growth, differentiation, spore dormancy, and germination. *Biochem. Cell Biol.* 70: 892–919 (1992).

Courtemanche, M., Glass, L. & Keener, J. P. Instabilities of a propagating pulse in a ring of excitable media. *Phys. Rev. Lett.* 70: 2182–2185 (1993).

Courtemanche, M. & Winfree, A. T. Re-entrant rotating waves in a Beeler-Reuter based model of two-dimensional cardiac electrical activity. *Int. J. Bifurc. Chaos* 1: 431–444 (1991).

Dallon, J. C. & Othmer, H. G. A continuum analysis of the chemotactic signal seen by *Dictyostelium discoideum*. *J. theor. Biol.* 194: 461–483 (1998).

Darcy, P. K. & Fisher, P. R. Pharmacological evidence for a role for cyclic AMP signalling in *Dictyostelium discoideum* slug behaviour. *J. Cell Sci.* 96: 661–667 (1990).

von Dassow, G., Meir, E., Munro, E. M. & Odell, G. M. The segment polarity network is a robust developmental module. *Nature* 406: 188–192 (2000).

Davies, L., Satre, M., Martin, J.-B. & Gross, J. D. The target of ammonia action in *Dictyostelium*. *Cell* 75: 321–327 (1993).

Dormann, D., Siegert, F. & Weijer, C. J. Analysis of cell movement during the culmination phase of *Dictyostelium* development. *Development* 122: 761–769 (1996).

Dormann, D., Vasiev, B. & Weijer, C. J. Propagating waves control *Dictyostelium discoideum* morphogenesis. *Biophys. Chem.* 72: 21–35 (1998).

van Duijn, B. & Inouye, K. Regulation of movement speed by intracellular pH during *Dictyostelium discoideum* chemotaxis. *Proc. Natl. Acad. Sci. U.S.A.* 88: 4951–4955 (1991).

Dunbar, A. J. & Wheldrake, J. F. Analysis of mRNA levels for developmentally regulated prespore specific glutamine synthetase in *Dictyostelium discoideum*. *Dev. Growth Differ.* 39: 617–624 (1997).

Durston, A. J. *Dictyostelium discoideum* aggregation fields as excitable media. *J. theor. Biol.* 42: 483–504 (1973).

Durston, A. J., Cohen, M. H., Drage, D. J., Potel, M. J., Robertson, A. & Wonio, D. Periodic movements of *Dictyostelium discoideum* sorocarps. *Dev. Biol.* 52: 173–180 (1976).

Dusenbery, D. B. Avoided temterature leads to the surface: computer modeling of slime mold and nematode thermotaxis. *Behav. Ecol. Sociobiol.* 22: 219–223 (1988).

Dworkin, M. & Keller, K. H. Solubility and diffusion coefficient of adenosine 3':5'-monophosphate. *J. Biol. Chem.* 252: 864–865 (1977).

Feit, I. N. & Sollitto, R. B. Ammonia is the gas used for the spacing of fruiting bodies in the cellular slime mold, *Dictyostelium discoideum*. *Differentiation* 33: 193–196 (1987).

Fisher, P. R. The role of gaseous metabolites in phototaxis by *Dictyostelium discoideum* slugs. *FEMS Microbiol. Lett.* 77: 117–120 (1991).

Fisher, P. R. Genetics of phototaxis in a model eukaryote, *Dictyostelium discoideum*. *Bioessays* 19: 397–407 (1997).

Fisher, P. R., Häder, D.-P. & Williams, K. L. Multidirectional phototaxis by *Dictyostelium discoideum* amoebae. *FEMS Microbiol. Lett.* 29: 43–47 (1985).

Fisher, P. R. & Williams, K. L. Bidirectional phototaxis by *Dictyostelium discoideum* slugs. *FEMS Microbiol. Lett.* 12: 87–89 (1981).

FitzHugh, R. Thresholds and plateaus in the Hodgkin-Huxley nerve equations. *J. Gen. Physiol.* 43: 867–896 (1960).

FitzHugh, R. Impulses and physiological states in theoretical models of nerve membrane. *Biophys. J.* 1: 445–466 (1961).

Foerster, P., Müller, S. C. & Hess, B. Curvature and spiral geometry in aggregation patterns of *Dictyostelium discoideum*. *Development* 109: 11–16 (1990).

Fontana, D. R. *Dictyostelium discoideum* cohesion and adhesion. In *Principles of cell adhesion*, edited by P. D. Richardson & M. Steiner, pp. 63–86. CRC Press, Boca Raton (1995).

Francis, D. W. Some studies on phototaxis of *Dictyostelium*. *J. Cell. Comp. Physiol.* 64: 131–138 (1964).

Gerhardt, M., Schuster, H. & Tyson, J. J. A cellular automation model of excitable media including curvature and dispersion. *Science* 247: 1563–1566 (1990).

Ginger, R. S., Drury, L., Baader, C., Zhukovskaya, N. V. & Williams, J. G. A novel *Dictyostelium* cell surface protein important for both cell adhesion and cell sorting. *Development* 125: 3343–3352 (1998).

Glazier, J. A., Anderson, M. P. & Grest, G. S. Coarsening in the 2-dimensional soap froth and the large Q-Potts-model – a detailed comparison. *Phil. Mag. B* 62: 615–645 (1990).

Glazier, J. A. & Graner, F. Simulation of the differential adhesion driven rearrangement of biological cells. *Phys. Rev. E* 47: 2128–2154 (1993).

Graner, F. Can surface adhesion drive cell-rearrangement? Part I: Biological cell-sorting. *J. theor. Biol.* 164: 455–476 (1993).

Graner, F. & Glazier, J. A. Simulation of biological cell sorting using a two-dimensional extended Potts model. *Phys. Rev. Lett.* 69: 2013–2016 (1992).

Graner, F. & Sawada, Y. Can surface adhesion drive cell rearrangement? Part II: A geometrical model. *J. theor. Biol.* 164: 477–506 (1993).

Grimson, M. J., Haigler, C. H. & Blanton, R. L. Cellulose microfibrils, cell motility, and plasma membrane protein organization change in parallel during culmination in *Dictyostelium discoideum*. *J. Cell Sci.* 109: 3079–3087 (1996).

Grindrod, P. Plane waves. In *The theory and applications of reaction-diffusion equations: patterns and waves*, Oxford applied mathematics and computing science series, pp. 114–156. Clarendon Press, Oxford, 2nd edition (1996).

Häder, D.-P. & Burkart, U. Optical properties of *Dictyostelium discoideum* pseudoplasmodia responsible for phototactic orientation. *Exp. Mycol.* 7: 1–8 (1983).

Hagberg, A. & Meron, E. From labyrinthine patterns to spiral turbulence. *Phys. Rev. Lett.* 72: 2494–2497 (1994).

Harwood, A. J., Hopper, N. A., Simon, M.-N., Driscoll, D. M., Veron, M. & Williams, J. G. Culmination in *Dictyostelium* is regulated by the cAMP-dependent protein kinase. *Cell* 69: 615–624 (1992).

Haser, H. & Häder, D.-P. Orientation and phototaxis in pseudoplasmodia of an axenic strain of the cellular slime mold, *Dictyostelium discoideum*. *Exp. Mycol.* 16: 119–131 (1992).

Higuchi, G. & Yamada, T. A cinematographical study of cellular slime molds. I. Stalk and disk formation in *Dictyostelium discoideum*. *Cytologia* 49: 841–849 (1984).

Hodgkin, A. L. & Huxley, A. F. A quantitative description of membrane current and its application to conduction and excitation in nerve. *J. Physiol.* 117: 500–544 (1952).

Höfer, T., Sherratt, J. A. & Maini, P. K. Cellular pattern formation during *Dictyostelium* aggregation. *Physica D* 85: 425–444 (1995a).

Höfer, T., Sherratt, J. A. & Maini, P. K. *Dictyostelium discoideum*: cellular self-organization in an excitable biological medium. *Proc. R. Soc. Lond. Ser. B* 259: 249–257 (1995b).

Hogeweg, P. On searching generic properties of non generic phenomena: an approach to bioinformatic theory formation. In *Artificial Life VI: Proceedings of the Sixth International Conference on Artificial Life*, edited by C. Adami, R. K. Belew, H. Kitano & C. E. Taylor, pp. 285–294. MIT Press, Cambridge, MA (1998).

Hogeweg, P. Evolving mechanisms of morphogenesis: on the interplay between differential adhesion and cell differentiation. *J. theor. Biol.* 203: 317–333 (2000a).

Hogeweg, P. Shapes in the shadow: evolutionary dynamics of morphogenesis. *Artif. Life* 6: 85–101 (2000b).

Horváth, D., Petrov, V., Scott, S. K. & Showalter, K. Instabilities in propagating reaction-diffusion fronts. *J. Chem. Phys.* 98: 6332–6343 (1993).

Inouye, K. & Takeuchi, I. Analytical studies on migrating movement of the pseudoplasmodium of *Dictyostelium discoideum*. *Protoplasma* 99: 289–304 (1979).

Ising, E. Beitrag zur Theorie des Ferromagnetismus. *Zeitschr. f. Physik* 31: 235–258 (1925).

Ito, H. & Glass, L. Spiral breakup in a new model of discrete excitable media. *Phys. Rev. Lett.* 66: 671–674 (1991).

Jahnke, W., Henze, C. & Winfree, A. T. Chemical vortex dynamics in three-dimensional excitable media. *Nature* 336: 662–665 (1988).

Jermyn, K., Traynor, D. & Williams, J. The initiation of basal disc formation in *Dictyostelium discoideum* is an early event in culmination. *Development* 122: 753–760 (1996).

Jermyn, K. A. & Williams, J. G. An analysis of culmination in *Dictyostelium* using prestalk and stalk- specific cell autonomous markers. *Development* 111: 779–787 (1991).

Jiang, Y., Levine, H. & Glazier, J. Possible cooperation of differential adhesion and chemotaxis in mound formation of *Dictyostelium*. *Biophys. J.* 75: 2615–2625 (1998).

Karma, A. Spiral breakup in model equations of action potential propagation in cardiac tissue. *Phys. Rev. Lett.* 71: 1103–1106 (1993).

Karma, A. Electrical alternans and spiral wave breakup in cardiac tissue. *Chaos* 4: 461–472 (1994).

Kauffman, S. A. Pattern formation in the *Drosophila* embryo. *Phil. Trans. R. Soc. Lond. Ser. B* 295: 567–594 (1981).

Kauffman, S. A., Shymko, R. M. & Trabert, K. Control of sequential compartment formation in *Drosophila*. *Science* 199: 259–270 (1978).

Kawasaki, K., Mochizuki, A., Matsushita, M., Umeda, T. & Shigesada, N. Modeling spatio-temporal patterns generated by *Bacillus subtilis*. *J. theor. Biol.* 188: 177–185 (1997).

Kawasaki, Y., Kiryu, T., Usui, K. & Mizutani, H. Growth of the cellular slime mold, *Dictyostelium discoideum*, is gravity dependent. *Plant Physiol.* 93: 1568–1572 (1990).

Kay, R. R. DIF signalling. In *Dictyostelium: a model system for cell and developmental biology*, edited by Y. Maeda, K. Inouye & I. Takeuchi, pp. 279–292. Universal Academy Press, Tokyo (1997).

Keener, J. P. An eikonal-curvature equation for action potential propagation in myocardium. *J. Math. Biol.* 29: 629–651 (1991).

Keller, E. F. & Segel, L. A. Initiation of slime mold aggregation viewed as an instability. *J. theor. Biol.* 26: 399–415 (1970).

Kellerman, K. A. & McNally, J. G. Mound-cell movement and morphogenesis in *Dictyostelium*. *Dev. Biol.* 208: 416–429 (1999).

Kerszberg, M. & Wolpert, L. Mechanisms for positional signalling by morphogen transport: a theoretical study. *J. theor. Biol.* 191: 103–114 (1998).

Kessin, R. H. The evolution of the cellular slime molds. In *Dictyostelium: a model system for cell and developmental biology*, edited by Y. Maeda, K. Inouye & I. Takeuchi, pp. 3–13. Universal Academy Press, Tokyo (1997).

Kessin, R. H., Gundersen, G. G., Zaydfudim, V., Grimson, M. & Blanton, R. L. How cellular slime molds evade nematodes. *Proc. Natl. Acad. Sci. U.S.A.* 93: 4857–4861 (1996).

Kessler, D. A. & Levine, H. Stability of traveling waves in the Belousov-Zhabotinskii reaction. *Phys. Rev. A* 41: 5418–5430 (1990).

Kitami, M. Chemotactic response of *Dictyostelium discoideum* cell to c-AMP at the culmination stage. *Cytologia* 49: 257–264 (1984).

Kitami, M. Motive force of the culminating mass of cells in the developing fruiting body of *Dictyostelium discoideum*. *Cytologia* 50: 109–115 (1985).

Kosugi, T. & Inouye, K. Negative chemotaxis to ammonia and other weak bases by migrating slugs of the cellular slime moulds. *J. Gen. Microbiol.* 135: 1589–1598 (1989).

Kuramoto, Y. Instability and turbulence of wavefronts in reaction-diffusion systems. *Prog. Theor. Phys.* 63: 1885–1903 (1980).

Lauzeral, J., Halloy, J. & Goldbeter, A. Desynchronization of cells on the developmental path triggers the formation of spiral waves of cAMP during *Dictyostelium* aggregation. *Proc. Natl. Acad. Sci. U.S.A.* 94: 9153–9158 (1997).

Lechleiter, J., Girard, S., Peralta, E. & Clapham, D. Spiral calcium wave propagation and annihilation in *Xenopus laevis* oocytes. *Science* 252: 123–126 (1991).

Levine, H., Aranson, I., Tsimring, L. & Truong, T. V. Positive genetic feedback governs cAMP spiral wave formation in *Dictyostelium*. *Proc. Natl. Acad. Sci. U.S.A.* 93: 6382–6386 (1996).

Levine, H. & Reynolds, W. Streaming instability of aggregating slime mold amoebae. *Phys. Rev. Lett.* 66: 2400–2403 (1991).

Levine, H., Tsimring, L. & Kessler, D. Computational modeling of mound development in *Dictyostelium*. *Physica D* 106: 375–388 (1997).

Loomis, W. F. The *Dictyostelium* genome sequencing project [online] <dicty.cmb.nwu.edu/dicty/genomeseq.htm> (2000).

Ludwig, D., Aronson, D. G. & Weinberger, H. F. Spatial patterning of the spruce budworm. *J. Math. Biol.* . 8: 217–258 (1979).

MacKay, S. A. Computer simulation of aggregation in *Dictyostelium discoideum*. *J. Cell Sci.* 33: 1–16 (1978).

MacWilliams, H. K. Transplantation experiments and pattern mutants in cellular slime mold slugs. In *Developmental order: its origin and regulation*, edited by S. S. Subtelny & P. B. Green, pp. 463–483. A. R. Liss, New York (1982).

Maeda, M. Functional analysis [online] <www.csm.biol.tsukuba.ac.jp/function.html> (2000).

Maeda, Y., Inouye, K. & Takeuchi, I. (editors). *Dictyostelium: a model system for cell and developmental biology*. Number 21 in Frontiers science series. Universal Academy Press, Tokyo (1997).

Marée, A. F. M., Keulen, W., Boucher, C. A. B. & de Boer, R. J. Estimating relative fitness in viral competition experiments. accepted for publication in *J. Virol.*

Markus, M., Kloss, G. & Kusch, I. Disordered waves in a homogeneous, motionless excitable medium. *Nature* 371: 402–404 (1994).

Markus, M. & Stavridis, K. Observation of chemical turbulence in the Belousov-Zhabotinsky reaction. *Int. J. Bifurc. Chaos* 4: 1233–1243 (1994a).

Markus, M. & Stavridis, K. Wavefront deformations in excitable media: chemical lenses and ripples. *Phil. Trans. R. Soc. Lond. Ser. A* 347: 601–609 (1994b).

Martiel, J.-L. & Goldbeter, A. A model based on receptor desensitization for cyclic AMP signaling in *Dictyostelium* cells. *Biophys. J.* 52: 807–828 (1987).

Matsuyama, T., Takagi, Y., Nakagawa, Y., Itoh, H., Wakita, J. & Matsushita, M. Dynamic aspects of the structured cell population in a swarming colony of *Proteus mirabilis*. *J. Bacteriol.* 182: 385–393 (2000).

Maynard Smith, J. & Szathmáry, E. *The Major Transitions in Evolution*. W. H. Freeman Spektrum, Oxford (1995).

Meinhardt, H. A model for the prestalk/prespore patterning in the slug of the slime mold *Dictyostelium discoideum*. *Differentiation* 24: 191–202 (1983).

Miura, K. & Siegert, F. Light affects cAMP signaling and cell movement activity in *Dictyostelium discoideum*. *Proc. Natl. Acad. Sci. U.S.A.* 97: 2111–2116 (2000).

Mostow, G. D. (editor). *Mathematical models for cell rearrangement*. Yale University Press, London (1975).

Müller, V., Marée, A. F. M. & de Boer, R. J. Release of virus from lymphoid tissue affects HIV-1 and HCV kinetics in the blood. submitted.

Müller, V., Marée, A. F. M. & de Boer, R. J. Small variations in multiple parameters account for wide variations in HIV-1 set points: a novel modeling approach. submitted.

Murray, J. D. *Mathematical Biology*, volume 19 of *Biomathematics*. Springer-Verlag, Berlin, 2nd edition (1993).

Murray, J. D. & Swanson, K. R. On the mechanochemical theory of biological pattern formation with applications to wound healing and angiogenesis. In *On Growth and Form: Spatio-temporal Pattern Formation in Biology*, edited by M. A. J. Chaplain, G. D.

Singh & J. C. McLachlan, Wiley series in mathematical and computational biology, pp. 251–285. John Wiley & Sons, Chichester (1999).

Nagumo, J. S., Arimoto, S. & Yoshizawa, S. An active pulse transmission line simulating nerve axon. *Proc. IRE* 50: 2061–2071 (1962).

Nagy-Ungvarai, Zs. & Müller, S. C. Characterization of wave front instabilities in the Belousov-Zhabotinsky reaction: an overview. *Int. J. Bifurc. Chaos* 4: 1257–1264 (1994).

Nanjundiah, V. Chemotaxis, signal relaying and aggregation morphology. *J. theor. Biol.* 42: 63–105 (1973).

Nanjundiah, V. Models for pattern formation in the dictyostelid slime molds. In *Dictyostelium: a model system for cell and developmental biology*, edited by Y. Maeda, K. Inouye & I. Takeuchi, pp. 305–322. Universal Academy Press, Tokyo (1997).

Newell, P. C. & Gross, J. D. Restriction enzyme mediated integration in *Dictyostelium discoideum* [online] <www.bioch.ox.ac.uk/˜pcnlab/remi.html> (2000).

Nusslein-Volhard, C. Determination of the embryonic axes of *Drosophila*. *Development* Suppl: 1–10 (1991).

O'Day, D. Macrocyst world: the sexual cycle of *Dictyostelium* and other CSM species [online] <www.erin.utoronto.ca/˜w3oday/MACWORLD4.html> (2000).

Odell, G. M. & Bonner, J. T. How the *Dictyostelium discoideum* grex crawls. *Phil. Trans. R. Soc. Lond. Ser. B* 312: 487–525 (1986).

Ohta, T., Mimura, M. & Kobayashi, R. Higher-dimensional localized patterns in excitable media. *Physica D* 34: 115–144 (1989).

van Oss, C., Panfilov, A. V., Hogeweg, P., Siegert, F. & Weijer, C. J. Spatial pattern formation during aggregation of the slime mould *Dictyostelium discoideum*. *J. theor. Biol.* 181: 203–213 (1996).

Othmer, H. G. & Schaap, P. Oscillatory cAMP signaling in the development of *Dictyostelium discoideum*. *Comments Theor. Biol.* 5: 175–282 (1998).

Ouyang, Q. & Flesselles, J.-M. Transition from spirals to defect turbulence driven by a convective instability. *Nature* 379: 143–146 (1996).

Palková, Z., Janderová, B., Gabriel, J., Zikánová, B., Pospíšek, M. & Forstová, J. Ammonia mediates communication between yeast colonies. *Nature* 390: 532–536 (1997).

Pálsson, E. & Cox, E. C. Origin and evolution of circular waves and spirals in *Dictyostelium discoideum* territories. *Proc. Natl. Acad. Sci. U.S.A.* 93: 1151–1155 (1996).

Panfilov, A. V. Three dimensional vortices in active media. In *Nonlinear wave processes in excitable media*, edited by A. V. Holden, M. Markus & H. G. Othmer, volume 244 of *NATO ASI series B: physics*, pp. 361–381. Plenum Press, New York (1991).

Panfilov, A. V. & Hogeweg, P. Spiral breakup in a modified FitzHugh-Nagumo model. *Phys. Lett. A* 176: 295–299 (1993).

Panfilov, A. V. & Hogeweg, P. Mechanisms of cardiac fibrillation. *Science* 270: 1223–1224 (1995), and response by A. T. Winfree, *ibid.* 270: 1224–1225 (1995).

Panfilov, A. V. & Hogeweg, P. Scroll breakup in a three-dimensional excitable medium. *Phys. Rev. E* 53: 1740–1743 (1996).

Panfilov, A. V. & Holden, A. V. Self-generation of turbulent vortices in a two-dimensional model of cardiac tissue. *Phys. Lett. A* 151: 23–26 (1990).

Panfilov, A. V. & Holden, A. V. (editors). *Computational biology of the heart*. John Wiley & Sons, Chichester (1997).

Panfilov, A. V. & Pertsov, A. M. Vortex ring in a three-dimensional active medium described by reaction-diffusion equations. *Dokl. Akad. Nauk SSSR* 274: 1500–1503 (1984).

Parnas, H. & Segel, L. A. Computer evidence concerning the chemotactic signal in *Dictyostelium discoideum*. *J. Cell Sci.* 25: 191–204 (1977).

Parnas, H. & Segel, L. A. A computer simulation of pulsatile aggregation in *Dictyostelium* *discoideum*. *J. theor. Biol.* 71: 185–207 (1978).

Poff, K. L., Fontana, D. R., Häder, D.-P. & Schneider, M. J. An optical model for phototactic orientation in *Dictyostelium discoideum* slugs. *Plant Cell Physiol.* 27: 533–539 (1986).

Potts, R. B. Some generalized order-disorder transformations. *Proc. Camb. Phil. Soc.* 48: 106–109 (1952).

Raper, K. B. Pseudoplasmodium formation and organization in *Dictyostelium discoideum*. *J. Elisha Mitchell Sci. Soc.* 56: 241–282 (1940).

Rubinow, S. I., Segel, L. A. & Ebel, W. A mathematical framework for the study of morphogenetic development in the slime mold. *J. theor. Biol.* 91: 99–113 (1981).

Savill, N. J. & Hogeweg, P. Modeling morphogenesis: from single cells to crawling slugs. *J. theor. Biol.* 184: 229–235 (1997).

Savill, N. J. & Hogeweg, P. Competition and dispersal in predator-prey waves. *Theor. Popul. Biol.* 56: 243–263 (1999).

Schaap, P., Tang, Y. & Othmer, H. G. A model for pattern formation in *Dictyostelium discoideum*. *Differentiation* 60: 1–16 (1996).

Schindler, J. & Sussman, M. Inhibition by ammonia of intracellular cAMP accumulation in *Dictyostelium discoideum*: its significance for the regulation of morphogenesis. *Dev. Genet.* 1: 13–20 (1979).

Segel, L. A., Goldbeter, A., Devreotes, P. N. & Knox, B. E. A mechanism for exact sensory adaptation based on receptor modification. *J. theor. Biol.* 120: 151–179 (1986).

Sekimura, T. & Kobuchi, Y. A spatial pattern formation model for *Dictyostelium discoideum*. *J. theor. Biol.* 122: 325–338 (1986).

Shibata, M. & Bures, J. Reverberation of cortical spreading depression along closed-loop pathways in rat cerebral cortex. *J. Neurophysiol.* 35: 381–388 (1972).

Siegert, F. & Weijer, C. Digital image processing of optical density wave propagation in *Dictyostelium discoideum* and analysis of the effects of caffeine and ammonia. *J. Cell Sci.* 93: 325–335 (1989).

Siegert, F. & Weijer, C. J. Analysis of optical density wave propagation and cell movement in the cellular slime mould *Dictyostelium discoideum*. *Physica D* 49: 224–232 (1991).

Siegert, F. & Weijer, C. J. Three-dimensional scroll waves organize *Dictyostelium* slugs. *Proc. Natl. Acad. Sci. U.S.A.* 89: 6433–6437 (1992).

Smith, D. Completed and near-complete 80 REMI genes [online] <glamdring.ucsd.edu/others/dsmith/REMIgenes2000.html> (2000).

Smith, E., Fisher, P. R., Grant, W. N. & Williams, K. L. Sensory behaviour in *Dictyostelium discoideum* slugs: phototaxis and thermotaxis are not mediated by a change in slug speed. *J. Cell Sci.* 54: 329–339 (1982).

Smith, E. & Williams, K. L. Preparation of slime sheath from *Dictyostelium discoideum*. *FEMS Microbiol. Lett.* 6: 119–122 (1979).

Stavroudis, O. N. Ray tracing. In *The optics of rays, wavefronts, and caustics*, volume 38 of *Pure and applied physics*, pp. 81–103. Academic Press, New York (1972).

Steinberg, M. Reconstruction of tissues by dissociated cells. *Science* 141: 401–408 (1963).

Steinbock, O., Siegert, F., Müller, S. C. & Weijer, C. J. Three-dimensional waves of excitation during *Dictyostelium* morphogenesis. *Proc. Natl. Acad. Sci. U.S.A.* 90: 7332–7335 (1993).

Sternfeld, J. Evidence for differential cellular adhesion as the mechanism of sorting-out of various cellular slime mold species. *J. Embryol. Exp. Morph.* 53: 163–178 (1979).

Sternfeld, J. A study of PstB cells during *Dictyostelium* migration and culmination reveals a unidirectional cell type conversion process. *Roux's Arch. Dev. Biol.* 201: 354–363 (1992).

Sternfeld, J. The anterior-like cells in *Dictyostelium* are required for the elevation of the

spores during culmination. *Dev. Genes Evol.* 208: 487–494 (1998).
Sternfeld, J. & David, C. N. Cell sorting during pattern formation in *Dictyostelium*. *Differentiation* 20: 10–21 (1981).
Takeuchi, I., Kakutani, T. & Tasaka, M. Cell behavior during formation of prestalk/prespore pattern in submerged agglomerates of *Dictyostelium discoideum*. *Dev. Genet.* 9: 607–614 (1988).
Tang, Y. & Othmer, H. G. A G protein-based model of adaptation in *Dictyostelium discoideum*. *Math. Biosci.* 120: 25–76 (1994).
Tasaka, M. & Takeuchi, I. Role of cell sorting in pattern formation in *Dictyostelium discoideum*. *Differentiation* 18: 191–196 (1981).
Thomason, P., Traynor, D. & Kay, R. Taking the plunge. Terminal differentiation in *Dictyostelium*. *Trends Genet.* 15: 15–19 (1999).
Tsyganov, I. M., Tsyganov, M. A., Medvinsky, A. B. & Ivanitsky, G. R. Processes of selforganization in highly excitable media: open catalog of new structures. *Dokl. Akad. Nauk* 346: 825–832 (1996).
Turing, A. M. The chemical basis of morphogenesis. *Phil. Trans. Roy. Soc. Lond. B* 237: 37–72 (1952).
Tyson, J. J., Alexander, K. A., Manoranjan, V. S. & Murray, J. D. Spiral waves of cyclic AMP in a model of slime mold aggregation. *Physica D* 34: 193–207 (1989).
Tyson, J. J. & Murray, J. D. Cyclic AMP waves during aggregation of *Dictyostelium* amoebae. *Development* 106: 421–426 (1989).
Umeda, T. A mathematical model for cell sorting, migration and shape in the slug stage of *Dictyostelium discoideum*. *Bull. Math. Biol.* 51: 485–500 (1989).
Vaessen, E. P. B. *Calcium waves: a(nother) way of looking at calcium waves*. Master's thesis, University of Utrecht (1999).
Vasiev, B. N., Hogeweg, P. & Panfilov, A. V. Simulation of *Dictyostelium discoideum* aggregation via reaction-diffusion model. *Phys. Rev. Lett.* 73: 3173–3176 (1994).
Verkerke-van Wijk, I & Schaap, P. cAMP, a signal for survival. In *Dictyostelium: a model system for cell and developmental biology*, edited by Y. Maeda, K. Inouye & I. Takeuchi, pp. 145–162. Universal Academy Press, Tokyo (1997).
Wang, B. & Kuspa, A. *Dictyostelium* development in the absence of cAMP. *Science* 277: 251–254 (1997).
Watts, D. J. & Treffry, T. E. Culmination in the slime mould *Dictyostelium discoideum* studied with a scanning electron microscope. *J. Embryol. Exp. Morphol.* 35: 323–333 (1976).
Weijer, C. J., McDonald, S. A. & Durston, A. J. A frequency difference in optical-density oscillations of early *Dictyostelium discoideum* density classes and its implications for development. *Differentiation* 28: 9–12 (1984).
Whitaker, B. D. & Poff, K. L. Thermal adaptation of thermosensing and negative thermotaxis in *Dictyostelium*. *Exp. Cell Res.* 128: 87–93 (1980).
Wilkins, M. R. & Williams, K. L. The extracellular matrix of the *Dictyostelium discoideum* slug. *Experientia* 51: 1189–1196 (1995).
Williams, G. B., Elder, E. M. & Sussman, M. Modulation of the cAMP relay in *Dictyostelium discoideum* by ammonia and other metabolites: possible morphogenetic consequences. *Dev. Biol.* 105: 377–388 (1984).
Williams, J. Prestalk and stalk cell heterogeneity in *Dictyostelium*. In *Dictyostelium: a model system for cell and developmental biology*, edited by Y. Maeda, K. Inouye & I. Takeuchi, pp. 293–304. Universal Academy Press, Tokyo (1997).
Williams, J., Hopper, N., Early, A., Traynor, D., Harwood, A., Abe, T., Simon, M. N. & Véron, M. Interacting signalling pathways regulating prestalk cell differentiation and movement during the morphogenesis of *Dictyostelium*. *Development* Suppl: 1–7 (1993).

Williams, J. G. The role of diffusible molecules in regulating the cellular differentiation of *Dictyostelium discoideum*. *Development* 103: 1–16 (1988).

Williams, J. G., Jermyn, K. A. & Duffy, K. T. Formation and anatomy of the prestalk zone of *Dictyostelium*. *Development* Suppl: 91–97 (1989).

Williams, K. L., Vardy, P. H. & Segel, L. A. Cell migrations during morphogenesis: some clues from the slug of *Dictyostelium discoideum*. *Bioessays* 5: 148–152 (1986).

Winfree, A. T. Spiral waves of chemical activity. *Science* 175: 634–636 (1972).

Winfree, A. T. Electrical instability in cardiac muscle: phase singularities and rotors. *J. theor. Biol.* 138: 353–405 (1989).

Winfree, A. T. Electrical turbulence in three-dimensional heart muscle. *Science* 266: 1003–1006 (1994).

Winfree, A. T. & Strogatz, S. H. Organizing centres for three-dimensional chemical waves. *Nature* 311: 611–615 (1984).

Wolpert, L. Positional information and the spatial pattern of cellular differentiation. *J. theor. Biol.* 25: 1–47 (1969).

Yumura, S., Kurata, K. & Kitanishi-Yumura, T. Concerted movement of prestalk cells in migrating slugs of *Dictyostelium* revealed by the localization of myosin. *Dev. Growth Differ.* 34: 319–328 (1992).

Zeeman, E. C. Slime mold culmination. In *Catastrophe theory: selected papers*, pp. 216–233. Addison-Wesley, Reading, Massachusetts (1977).

Samenvatting

Het ontstaan van meercellige organismen wordt beschouwd als één van de belangrijkste stappen in de evolutie van het leven. Om de overgang te kunnen maken van onafhankelijke eencelligen naar functionele eenheden van meercellige organismen moesten manieren ontwikkeld worden om samen te werken en te communiceren over grotere afstanden. In dit proefschrift proberen we te ontrafelen hoe zulke samenwerking en communicatie tot stand gebracht kan worden.

De drie belangrijkste groepen van meercellige organismen, namelijk de planten, de dieren en de schimmels, ontstonden zo'n 540 miljoen jaar geleden, aan het begin van het Cambrium. Deze groepen bestuderen we in dit proefschrift echter niet; in plaats daarvan richten we ons op de slijmschimmel (*Dictyostelium discoideum*). Deze eencellige verandert namelijk ook af en toe in een meercellig organisme, en doordat dit proces zeer gedetailleerd bestudeerd kan worden, is er veel over deze overgang bekend. De slijmschimmel komt algemeen voor in de bossen, waar hij als een eencellige amoebe rondkruipt en leeft van de bacterien die de gevallen bladeren verteren. Wanneer echter alle bacteriën verorberd zijn, verandert het gedrag drastisch: rond de 100.000 cellen verzamelen zich en vormen een soort slakje, circa 1 mm lang. Dit slakje baant zich een weg naar de oppervlakte, door gebruik te maken van informatie uit de omgeving, zoals bijvoorbeeld lichtinval en temperatuurverschillen. Eenmaal aan de oppervlakte transformeert het slakje zich in een een soort van paddestoeltje, dat circa 6 mm hoog wordt. Dit vruchtlichaampje bestaat uit een een sporeknopje bovenop een lang en smal toelopend steeltje.

De belangrijkste manier waarop de cellen met elkaar communiceren is door middel van het molecuul cyclisch adenosinemonofosfaat (cAMP). Sommige van de amoeben stoten cAMP uit, en de amoeben die zich in hun nabijheid bevinden reageren op deze stimulatie door cAMP door middel van (i) een toename in cAMP productie en een daarop volgende uitstoot van cAMP, en (ii) een beweging in de richting van een hogere concentratie cAMP. De cAMP receptoren, die zich in het membraan van de amoeben bevinden, worden na stimulatie ongevoelig, waardoor deze reacties worden beëindigd. De cAMP wordt vervolgens afgebroken, waarna de amoeben opnieuw gestimuleerd kunnen worden. Op deze manier kunnen de cellen het cAMP signaal doorgeven, waardoor golven van cAMP worden gevormd waarmee over grotere afstand gecommuniceerd kan worden. Deze manier van doorgeven van signalen valt onder de klasse der exciteerbare media. Het concept 'exciteerbare media' is een belangrijk concept in de theoretische biologie. Het beschrijft ruimtelijke systemen die aan twee voorwaarden voldoen en als gevolg daarvan bepaalde patronen opleveren. Die voorwaarden zijn het vermogen om prikkels door te geven, en het vermogen om zich na een korte tijd van het doorgeven van deze prikkels te herstellen. Gedurende deze herstelperiode is het medium ongevoelig voor prikkels. Vaak wordt een exciteerbaar medium beschreven in termen van een activerende en een remmende substantie. Exciteerbare media produceren een enorme verscheidenheid aan patronen. De twee meest elementaire patronen zijn golven die zich vanuit een puntbron uitbreiden (zoals bijvoorbeeld de golven die het samentrekken van het hart aansturen), en golven die de vorm aannemen van een spiraal die zichzelf in stand kan houden (zulke spiralen worden bijvoorbeeld vaak waargenomen wanneer de amoeben van de slijmschimmel zich verzamelen).

In **deel I** van dit proefschrift onderzoeken we het algemene probleem van complexe patroonvorming in exciteerbare media. In **hoofdstuk 2** onderzoeken we een mechanisme waardoor spiralen kunnen uiteenvallen. Het wordt algemeen aangenomen dat hartfibrillatie en hartstilstand worden veroorzaakt door het ontstaan en uiteenvallen van spiralen. Het uiteenvallen van spiralen wordt ook bestudeerd in de Belousov-Zhabotinsky (BZ) reactie, een chemisch proces dat zich gedraagt als een exciteerbaar medium.

We gebruiken een partieel differentiaalvergelijkingen (PDE) model voor exciteerbare media, zoals ontwikkeld door Panfilov & Pertsov (1984). In het algemeen beweegt een hol golffront zich sneller voort dan een bol golffront, doordat in het geval van een hol golffront de hoeveelheid activerende substantie vlak voor de golf sneller toeneemt. Daardoor wordt dit stukje medium sneller geactiveerd. Deze relatie tussen voortbewegingssnelheid en kromming wordt de 'eikonal-curvature' relatie genoemd. Door de invloed van de kromming hebben golffronten de neiging een gladde vorm te behouden: ze zijn, zoals dat dat heet, lateraal stabiel. Wij onderzoeken de situatie waarbij de remmende substantie harder diffundeert dan de activerende substantie. Bij ons onderzoek kan het effect dat een grotere hoeveelheid activator vlak voor een hol golffront heeft, teniet worden gedaan door de aanwezigheid van een nog grotere hoeveelheid inhibitor. In deze studie laten wij zien dat door een snelle diffusie van de inhibitor de 'eikonal-curvature' relatie inderdaad negatief kan worden, wat betekent dat het golffront lateraal instabiel wordt en kleine rimpelingen worden opgeblazen. De spiraal kan hierdoor uiteindelijk uiteenvallen in vele spiraaltjes. Ons model kan zeer goed de patronen beschrijven die worden waargenomen in de BZ reactie, maar de resultaten zijn hoogstwaarschijnlijk veel breder toepasbaar.

In **deel II** van dit proefschrift ontwikkelen we een model dat de gehele levenscyclus van de slijmschimmel beschrijft en verklaart. Hiertoe gebruiken we in ons model verschillende modules, die elk een ander aspect van de ontwikkeling weergeven, en die op elkaar inwerken. De twee belangrijkste modules zijn het model voor exciteerbare media dat in deel I is geïntroduceerd, en het zogenaamde Glazier en Graner model, dat celverplaatsingen beschrijft ten gevolge van verschillen in adhesie tussen de cellen. Dit tweede model is een cellulaire automaat (CA), waarin een verzameling hokjes tezamen één amoebe beschrijft. Een amoebe verplaatst zichzelf langzaam over de CA, door zich steeds in een ander hokje uit te breiden. Of een amoebe zich uitbreidt of niet, wordt bepaald door een energieminimalisatie regel, die niet alleen de adhesie tussen cellen in beschouwing neemt, maar ook het totale volume van de cel, en de energie die het kost om een cel een beetje te verplaatsen. De twee bovenstaande modules zijn aan elkaar gekoppeld door aan de CA chemotaxis toe te voegen, en daarvoor de locale cAMP gradiënt uit de desbetreffende PDE te gebruiken.

In de **hoofdstukken 3** en **4** onderzoeken we hoe de slijmschimmel zich als een slak voortbeweegt en hoe deze zich oriënteert aan de hand van temperatuurgradiënten en lichtinval, om zo de oppervlakte van de bodem te bereiken. **Hoofdstuk 3** valt uiteen in twee delen. Het eerste deel beschrijft het voortbewegen van het slakje. Door middel van cAMP golven, die ontstaan aan de voorkant van de slak en vervolgens door het slakje heen bewegen, en de daarmee gepaard gaande chemotaxis naar cAMP toe, weten de modelslakjes voort te kruipen, met een snelheid die afhankelijk is van de grootte van het slakje. Tijdens dit voortbewegen behouden ze bovendien min of meer hun vorm. Deze resultaten zijn in overeenstemming met wat wordt waargenomen in *in vivo* experimenten. Daarnaast laten we zien dat, hoewel alle amoeben een even sterke chemotaxis vertonen, de cellen die uiteindelijk het steeltje zullen vormen naar voren uitsorteren, terwijl de uiteindelijke sporecellen daarachter terechtkomen. Hoewel dit verschil in gedrag veroorzaakt wordt door verschillen in adhesie, blijkt toch ook de chemotaxis essentieel voor het uitsorteren van de celtypen: aangezien beide processen afzonderlijk niet toereikend zijn om het uitsorteren van de celtypen te verklaren, is een combinatie van chemotaxis en differentiële adhesie nodig. Dit resultaat toont aan dat het belangrijk is om juist de interacties tussen verschillende processen in beschouwing te nemen.

In het tweede deel van dit hoofdstuk onderzoeken we hoe het slakje zich oriënteert volgens een temperatuurgradiënt. We laten zien dat dit gedrag van het slakje door ons model opgeleverd kan worden, ondanks dat de individuele amoeben niet in staat zijn om een temperatuurgradiënt te meten, en bovendien hun loopsnelheid niet afhangt van de temperatuur. In plaats daarvan veroorzaken temperatuurverschillen verschillen in de exciteerbaarheid van de cellen, wat vervolgens de vorm van de cAMP golf doet veranderen. Uiteindelijk draait het slakje naar de temperatuurgradiënt toe, als een gevolg van de chemotaxis naar de scheve cAMP golven. Het is erg frappant dat dit mechanisme zelfs blijft functioneren wanneer er extreem veel ruis door het signaal heen zit (de ruis kan zelfs 300 maal zo groot zijn als de gradiënt zelf). Dit komt doordat de golffronten als een gevolg van de hierboven beschreven invloed van de kromming hun gladde vorm neigen te behouden. Daardoor functioneren de golffronten als spatiaal-temporele ruisfilters, wat het mogelijk maakt om zowel zeer zwakke als zeer onregelmatige temperatuurgradiënten op te pikken.

In **hoofdstuk 4** kijken we naar een andere eigenschap die het slakje naar de oppervlakte leidt, namelijk fototaxis. Om dit te kunnen onderzoeken voegen we een module toe die, door middel van de zogenaamde 'ray-tracing' techniek, beschrijft hoe lichtstralen door het slakje worden verbogen. Bovendien beschrijven we het effect dat ammonia (NH_3) heeft op de cAMP dynamica. We vinden dat als gevolg van de interacties tussen de verschillende modules, en tussen de individuele cellen, het slakje zich naar de lichtbron toekeert, terwijl de individuele cellen ook nu weer noch in staat zijn het signaal te detecteren (waar komt het licht vandaan?), noch een adequate reactie kunnen vertonen (bewegen richting de lichtbron).

Ons onderzoek heeft het volgende minimale mechanisme opgeleverd: doordat het slakje de lichtstralen breekt, en bovendien een min of meer ronde vorm heeft, verenigen de lichtstralen zich in een brandpunt dat zich bevindt aan de kant van het slakje dat van de lichtbron is afgericht. NH_3 productie is hoger bij een hogere lichtintensiteit, en op zijn beurt vermindert NH_3 de exciteerbaarheid van de cellen. Hierdoor lopen langs de zijde die van het licht is afgericht de cAMP golven langzamer, en worden de golven dus schreef getrokken. Wederom laat uiteindelijk de chemotaxis naar de cAMP toe het slakje draaien.

Dit model levert een interessant bijverschijnsel op, dat een extra validatie van ons model is: wanneer het slakje te gevoelig is voor NH_3 kunnen de golven te schreef komen te liggen, en ontstaat er een torsiekracht die het slakje juist wegduwt uit de juiste richting. Daardoor gaat het slakje onder een bepaalde hoek ten opzichte van de lichtbron voortbewegen. Nu zijn er inderdaad mutanten beschreven die, net als onze modelslakjes, onder een bepaalde hoek ten opzichte van de lichtbron voortkruipen. Net zoals in ons model kan dit gedrag van deze zogenaamde 'bi-directionele' mutanten verminderd of opgeheven worden door de NH_3 rond het slakje te absorberen of de lichtintensiteit te verlagen.

De laatste twee hoofdstukken bestuderen het laatste stadium van de slijmschimmel, namelijk de culminatie, welke leidt tot de vorming van het het vruchtlichaampje. De celbewegingen tijdens de culminatie worden vergeleken met een "omgekeerde fontein": de uiteindelijke steelcellen, die zich in eerste instantie juist bovenaan bevinden, vormen een steeltje dat naar beneden beweegt en zich aan de bodem verankert, terwijl de uiteindelijke sporecellen daaromheen naar boven bewegen om het sporehoofdje te gaan vormen. In 'leerboeken' wordt verondersteld dat het steeltje naar beneden wordt gedrukt doordat bovenaan nieuwe steelcellen worden toegevoegd, en dat de sporecellen de lucht in worden getild door het groeiende steeltje. Echter, zowel ons model als verscheidene *in vivo* experimenten blijken deze mogelijkheid uit te sluiten.

Om de culminatie te onderzoeken breiden we in **hoofdstuk 5** het model verder uit, met slijmmassa die de slijmschimmel omgeeft en met een stijve extracellulaire matrix die het steeltje omgeeft, de zogenaamde steelbuis. Ook voegen we celdifferentiatie toe, die onder invloed staat van een bepaald soort inductieproces. We laten zien dat het gehele proces van culminatie zich wél kan ontvouwen als een gevolg van de interacties tussen cAMP communicatie, variaties in adhesie, celdifferentiatie en de productie van extracellulaire matrices. We denken het proces op de volgende manier te kunnen verklaren: de periodieke opwaartse bewegingen naar de cAMP golven toe veroorzaken drukgolven, die op hun beurt weer peristaltische bewegingen in de punt van het steeltje veroorzaken. De peristaltische bewegingen 'knijpen' het steeltje door de celmassa heen. Dit mechanisme leidt tot een lange, dunne steel, en bovendien stopt de neergaande beweging van het steeltje automatisch wanneer de bodem wordt bereikt, net zoals de omhooggaande beweging van de sporecellen automatisch stopt wanneer het steeltje af is. Nadat deze laatste beweging is gestopt, neemt het sporehoofdje een ronde vorm aan.

Dit mechanisme wat wij voorstellen heeft vele zelf-corrigerende eigenschappen; elke afwijking in de neerwaartse beweging van het steeltje wordt bijvoorbeeld direct gecorrigeerd. Ook zijn er veel *in vivo* experimenten in overeenstemming met ons mechanisme; het verklaart bijvoorbeeld waarom twee nabije vruchtlichaampjes zich altijd van elkaar africhten.

In **hoofdstuk 6** kijken we nog gedetailleerder naar de mechanismen die leiden tot het vormen van het vruchtlichaampje. We onderzoeken de exacte voorwaarden waaraan de verschillende deelprocessen moeten voldoen, en hoe zij op elkaar inwerken. Om het steeltje te laten afdalen blijkt het niet voldoende te zijn om simpelweg een stijve steelbuis te hebben of, in plaats daarvan, een groep van zogenaamde padvindercellen rondom de punt van het steeltje. In plaats daarvan blijken beide nodig te zijn, omdat slechts door de interactie tussen de steelbuis en de padvindercellen een lange en smalle steel kan worden gevormd en de weerstand, veroorzaakt door de cellen die massaal omhoog bewegen, efficiënt verminderd kan worden, wat noodzakelijk is voor een snelle afdaling door de celmassa.

In dit hoofdstuk onderzoeken we ook alle voorwaarden voor de oppervlaktespanningen tussen de verschillende celtypen. Deze geven een indicatie voor de relatieve bindingssterktes die men verwacht aan te treffen in *in vivo* experimenten. Aan het einde van dit hoofdstuk proberen we een verband te leggen tussen bijverschijnselen van het model en experimentele observaties. Het lijkt daarnaast mogelijk om ons model te gebruiken om verklaringen te vinden voor de reeks van afwijkende fenotypen van mutanten, die tegenwoordig op grote schaal gecreëerd kunnen worden.

Ten slotte, de slijmschimmel *Dictyostelium discoideum* heeft bewezen een uitstekend paradigma te zijn voor het bestuderen van allerhande aspecten van de ontwikkeling van meercelligheid. Het is een uniek ‘model’ organisme, dat ons in 48 uur de volledige overgang van eencelligheid naar meercelligheid kan laten zien. Een overgang die onvermijdelijk gepaard gaat met meercellige coördinatie en morfogenese. We hebben laten zien dat morfogenese in de breedste zin van het woord kan ontstaan uit de interacties en terugkoppelingen tussen een relatief klein aantal simpele bouwstenen, die duidelijk gedefinieerd zijn en goed begrepen worden. De eigenschappen van de bouwstenen die we gebruikt hebben zijn altijd in overeenstemming met wat in experimenten is gevonden, en de interacties die we hebben beschreven zijn altijd lokaal. We hebben laten zien dat om van (sub)cellulaire interacties tot een gecoördineerd meercellig gedrag te komen, dat in staat is tot het waarnemen van en het reageren op de omgeving, de slijmschimmel gebruik maakt van patronen in ruimte en tijd. Zulke patronen zijn, vergeleken met de kleine individuele amoeben, meer dan levensgroot. Ze worden gevormd door de interacties tussen de verschillende processen en gebruikt voor de terugkoppeling tussen de verschillende organisatieniveaus. Hoewel daardoor echter uiteindelijk zeer complexe processen plaatsvinden, is het toch nog mogelijk om de onderliggende mechanismen te ontrafelen. Ons model staat dat toe, doordat we kunnen kijken naar het gedrag op niveaus die liggen tussen het (sub)cellulaire niveau en het niveau van het volledige organisme in.

Curriculum Vitæ

De schrijver van dit proefschrift, Athanasius Franciscus Maria Marée, of kortweg Stan, werd geboren op 7 mei 1971 te Oosterbeek, gemeente Renkum. Vanaf augustus 1983 was hij leerling aan het Stedelijk Gymnasium te Arnhem, waar hij in juni 1989 het Gymnasium diploma behaalde. In datzelfde jaar begon hij aan de studie biologie aan de Universiteit Utrecht. Het propædeutisch examen werd behaald in juli 1990 met het predikaat cum laude. In augustus 1995 behaalde hij zijn doctoraal examen, eveneens met het predikaat cum laude. Zijn specialisaties waren Vergelijkende Fysiologie/Neuro-ethologie en Theoretische Biologie. Van oktober 1995 tot oktober 2000 was hij als onderzoeker in opleiding (OIO) werkzaam bij de vakgoep Theoretische Biologie en Bioinformatica aan de Universiteit Utrecht. Zijn voornaamste werkzaamheden aldaar bestonden uit het verrichten van wetenschappelijk onderzoek en het begeleiden van onderwijs. Voor een deel van de tijd werd onderzoek verricht aan virusdynamica, begeleid door Dr. R. J. de Boer. Het grootste deel van de onderzoekstijd werd echter besteed aan het modelleren van de morfogenese van de slijmschimmel *Dictyostelium discoideum*. Dit onderzoek, waarvan de belangrijkste resultaten staan beschreven in dit proefschrift, werd verricht onder begeleiding van Dr. A. V. Panfilov en Prof. P. Hogeweg.

The author of this thesis, Athanasius Franciscus Maria Marée, or shortly Stan, was born on May 7th, 1971 in Oosterbeek, municipality of Renkum, The Netherlands. In August 1983 he attended the Stedelijk Gymnasium in Arnhem where he gained his Gymnasium diploma in June 1989. In the same year he commenced his studies at the faculty of biology of the Utrecht University. In July 1990 he obtained his propædeutic diploma *cum laude*; in augustus 1995 he obtained a Master's degree, *cum laude* as well, with specializations in Comparative Physiology/Neuro-ethology and Theoretical Biology. From October 1995 until October 2000 he worked as a a postgraduate student (OIO) in the Theoretical Biology and Bioinformatics group at the Utrecht University. His main activities were doing reseach and assisting in teaching. Part of the time he worked on viral dynamics, supervised by Dr. R. J. de Boer. Most of the time, however, he worked on the modelling of the mophogenesis of the celllular slime mould *Dictyostelium discoideum*. The latter studies were supervised by Dr. A. V. Panfilov en Prof. P. Hogeweg, and the main results of these studies are described in this thesis.

List of Publications

Marée, A. F. M., van Wezel, R. J. A., Verstraten, F. A. J. & van de Grind, W. A. Processing of transparent motion information in area 17 complex cells of the cat. *Perception (suppl.)* 23: 57–58 (1994).

van Wezel, R. J. A., Verstraten, F. A. J., Marée, A. F. M. & van de Grind, W. A. Responses of complex cells in area 17 of the cat to transparent motion. *Invest. Ophthalmol. Vis. Sci. (suppl.)* 35: 1973 (1994).

van Wezel, R. J. A., Lankheet, M. J. M., Verstraten, F. A. J., Marée, A. F. M. & van de Grind, W. A. Responses of complex cells in area 17 of the cat to bi-vectorial transparent motion. *Vision Res.* 36: 2805–2813 (1996).

Marée, A. F. M. & Panfilov, A. V. Spiral breakup in excitable tissue due to lateral instability. *Phys. Rev. Lett.* 78: 1819–1822 (1997).

Marée, A. F. M., Panfilov, A. V. & Hogeweg, P. Migration and thermotaxis of *Dictyostelium discoideum* slugs, a model study. *J. theor. Biol.* 199: 297–309 (1999a).

Marée, A. F. M., Panfilov, A. V. & Hogeweg, P. Phototaxis during the slug stage of *Dictyostelium discoideum*: a model study. *Proc. R. Soc. Lond. Ser. B* 266: 1351–1360 (1999b).

Marée, A. F. M., Keulen, W., Boucher, C. A. B. & de Boer, R. J. Estimating relative fitness in viral competition experiments. accepted for publication in *J. Virol.*

Müller, V., Marée, A. F. M. & de Boer, R. J. Small variations in multiple parameters account for wide variations in HIV-1 set points: a novel modeling approach. submitted.

Müller, V., Marée, A. F. M. & de Boer, R. J. Release of virus from lymphoid tissue affects HIV-1 and HCV kinetics in the blood. submitted.

Marée, A. F. M. & Hogeweg, P. How slime moulds self-organize into a fruiting body: the "reverse fountain" explained. submitted.

Marée, A. F. M. & Hogeweg, P. Modelling *Dictyostelium discoideum* morphogenesis: the culmination. submitted.

Karma police
arrest this man
he talks in maths…

Uit: *Karma police*, Radiohead

Dankwoord

Op deze laatste twee bladzijden wil ik graag alle mensen bedanken die me de afgelopen jaren direct of indirect hebben geholpen met het tot stand brengen van dit proefschrift.

Ten eerste wil ik mijn promotor, Paulien Hogeweg, bedanken. Jouw enthousiasme en creatieve kijk op de wetenschap heeft me altijd weten te inspireren. Je wist me enorm te motiveren door steeds weer nieuwe ideeën aan te dragen, maar me tegelijkertijd veel ruimte te geven voor eigen ontplooiing. Ook mijn copromotor, Sasha Panfilov, wil ik hartelijk bedanken voor alle samenwerking in de afgelopen jaren. Ik kon altijd bij jou aankloppen met alle mogelijke vragen over exciteerbare media. Bovendien wil ik Rob de Boer graag bedanken. Ik vond het erg leuk als je me betrok in allerhande boeiende discussies en problemen, waarop ik dan mijn brede wetenschappelijke interesse mocht botvieren.

Ook gaat mijn dank uit naar iedereen in de groep die een min of meer tijdelijke aanstelling heeft of had. Bij onze Club Tijdelijk bijeenkomsten heb ik met jullie vele avonden lekker gegeten en eindeloos gediscussieerd. Ik denk hierbij aan Katsuhisa, José, Catelijne, Michiel, Erik, Martijn en Can. En natuurlijk aan Nick, zeker aan het begin heb je me veel geleerd over het modelleren van de slijmschimmel. Ook Ludo wil ik niet vergeten; jij stond altijd klaar met goede hulp en slimme ideeën (en jouw taarten waren echt het lekkerst). En Roeland, jouw inzichten in het modelformalisme waren voor mij erg belangrijk; ik vond het altijd leuk om mijn resultaten met jou te bespreken. En Bas, ik vind het erg handig dat ik jou immer kan lastig vallen met moeilijke webvragen. En ten slotte denk ik aan André. Het was nooit erg moeilijk om jou een discussie binnen te lokken. Vooral van jouw wiskundige en natuurkundige kennis heb ik dankbaar gebruik gemaakt.

Ik heb bovendien vaak mee mogen discussiëren met de studenten die in onze groep hun afstudeeronderzoek deden. Ik ga jullie niet allemaal opsommen, maar houd jullie wel in mijn gedachten. Voor een drietal studenten wil ik echter een uitzondering maken: Eltica, ik denk graag terug aan de liftreis van Ludo, jou en mij naar Jorge in Portugal; Jelle, ik vind het altijd erg leuk om met jou de hele wereld te bediscussiëren; en Eric, ik heb met veel plezier jouw Calciumonderzoek begeleid.

I am very grateful to the members of my reading committee: Tony Durston, James Glazier, Lee Segel and Kees Weijer. And I really would like to thank Sheila NcNab for improving my English, which has not been an easy job.

There are a number of foreign guests that I keep in memory: Viktor, it was nice working with you on viral dynamics; Christian, I really enjoy it when you are visiting Utrecht; and Jorge, you have learned our group to enjoy wine and to talk about non-science, by establishing the Wineclub.

Claudia en Leonoor, bedankt voor het voorbereiden en ontwerpen van de geweldige voorkant. Mijn moeder, broers, zussen en aanhang wil ik bedanken voor

de bijzondere wijze waarop we met elkaar door de afgelopen zware tijd heen zijn gekomen. Zonder deze steun zou ik nooit dit proefschrift hebben kunnen afronden. Bovendien heb ik alle belangstelling die jullie de afgelopen jaren voor mijn onderzoek hebben getoond erg kunnen waarderen. Tom, ik wil jou hier speciaal bedanken, vanwege alle hulp die je me de afgelopen maanden hebt gegeven. Het was erg fijn dat je me hebt 'geleerd' hoe je zoiets als promoveren moet doen. Joris, jou wil ik bedanken voor het helpen mijn Nederlands te ont-Engelsen.

Jan Kees, als systeembeheerder heb je mij enorm veel werk uit handen genomen. Maar belangrijker nog zijn de vele uurtjes die ik samen met jou en Ilse in Springhaver heb doorgebracht, in goede tijden en slechte tijden. Bedankt voor al jullie steun, alsmede voor het feit dat jullie mijn paranimfen willen zijn.

Daarnaast wil ik nog een paar vrienden bedanken die ervoor gezorgd hebben dat ik me bleef herinneren dat er naast het doen van onderzoek ook van andere zaken te genieten valt. Jiří en Barbara, Paul, Edwin en Liesbeth, bedankt dat jullie mij bij tijd en wijle wegsleepten uit Utrecht, om ergens ver weg lekker uit te blazen. En dan natuurlijk ook dank aan mijn huisgenoten, die mij thuis gesteund hebben. Iedereen die ik nu nog vergeten mocht zijn, nodig ik hierbij van harte uit om bij mij langs te komen voor een persoonlijk bedankje.

Claudia, ten slotte, bedankt voor de vele goede momenten die we in de afgelopen jaren samen gehad hebben.